INDC(NDS)-0785
Distr. IN

IAEA
International Atomic Energy Agency

INDC International Nuclear Data Committee

MCNP modelling of the TIARA SINBAD shielding benchmark

Bor Kos

and

Ivan A. Kodeli

Jožef Stefan Institute
Ljubljana, Slovenia

May 2019

IAEA Nuclear Data Section
Vienna International Centre, P.O. Box 100, 1400 Vienna, Austria

Selected INDC documents may be downloaded in electronic form from
http://www-nds.iaea.org/publications
or sent as an e-mail attachment.
Requests for hardcopy or e-mail transmittal should be directed to
NDS.Contact-Point@iaea.org
or to:
Nuclear Data Section
International Atomic Energy Agency
Vienna International Centre
PO Box 100
1400 Vienna
Austria

Printed by the IAEA in Austria

May 2019

INDC(NDS)-0785
Distr. IN

MCNP modelling of the TIARA SINBAD shielding benchmark

Bor Kos

and

Ivan A. Kodeli

Jožef Stefan Institute
Ljubljana, Slovenia

POVZETEK
V poročilu je opisan postopek modeliranja referenčnega eksperimenta TIARA z baze podatkov SINBAD za potrebe simuliranja transporta nevtronov s pomočjo programa MCNP. V prvem delu je predstavljena motivacija za modeliranje. Poročilo se nadaljuje z opisom modeliranja geometrije eksperimenta v CAD programu Rhinoceros, transformacija v geometrijski zapis formata MCNP. Podrobno je opisan tudi postopek modeliranja materialov, izvora in posameznih cenilk detektorjev. Sledi opis določevanja parametrov redukcije variance s pomočjo programa ADVANTG. V zadnjem delu poročila so navedeni rezultati primerjave eksperimentalnih rezultatov s simulacijami za tri različne detektorje (tekoči scintilatorski detektor, fisijske celice in Bonnerjeve sfere) s štirimi (ENDF/BVII. 1, ENDF/B-VIII, JEFF-3.3 and JENDL-4.0u) knjižnicami jedrskih podatkov.
Ključne Besede: MCNP, TIARA, ŽELEZO, BETON, ADVANTG, SINBAD

ABSTRACT
The report describes the modeling procedure for MCNP of the TIARA shielding benchmark experiment form the SINBAD database. In the first part of the report motivation behind the modeling is given. The report continues with a detailed description of the geometrical properties of the benchmark with the Rhinoceros CAD program and the transformation procedure of the CAD model in to MCNP format. In the next part of the report details are given on the material, source and detector (tally) modelling of the benchmark experiment. Furthermore the variance reduction procedure using ADVANTG is described. Finally the results of the comparison of the experimental results to the calculation results for three different detectors (liquid scintillator, fission cells, Bonner spheres) and with four different nuclear data libraries (ENDF/B-VII.1, ENDF/B-VIII, JEFF-3.3 and JENDL-4.0u) is given.
Keywords: MCNP, TIARA, IRON, CONCRETE, ADVANTG, SINBAD

September 2018

Definition of Symbols, Terms and Abbreviations

IAEA	International Atomic Energy Agency
TIARA	Takasaki Ion Accelerator for Advanced Radiation Application
SINBAD	Shielding Integral Benchmark Archive and Database
CIELO	Collaborative International Evaluated Library Organisation
MCNP	General purpose **M**onte **C**arlo **N**-**P**article transport code
ADVANTG	**A**utomate**D** **VA**ria**N**ce reduc**T**ion **G**enerator
CPU	Central Processing Unit
CAD	Computer Assisted Design
Rhino	Rhinoceros CAD software program
JSI	"Jožef Stefan" Institute
NIST	National Institute of Standards and Technology
ORNL	Oak Ridge National Laboratory
WW	Weight Window variance reduction parameters
FW-CADIS	Forward-Weighted Consistent Adjoint Driven Importance Sampling method

List of Tables

List of Figures

Contents

1 Introduction

The TIARA [1, 2] (Takasaki Ion Accelerator for Advanced Radiation Application) iron shielding experiment is one of several high quality experiments included in the SINBAD (Shielding Integral Benchmark Archive and Database) database [3]. It includes experimental results with three shielding materials, iron, concrete and polyethylene. The neutron source was produced by bombarding a 99.9 % ^{7}Li target with a high energy proton beam from a cyclotron. Two quasi-monoenergitic neutron sources resulted from the bombardment with peak energies at 43 MeV and 68 MeV.

The motivation behind the development of new MCNP [4] (General purpose **M**onte **C**arlo **N**-**P**article) models of the TIARA shielding benchmark experiment arises from the CIELO (Collaborative International Evaluated Library Organisation) project. The success and the controversy of the project was largely based on the fact that the benchmarking was an integral part of the evaluation process. In order for the benchmarks to be suitable for the validation and, eventually, evaluation processes they have to be of a high order of quality. The TIARA experiments are of interest for nuclear data validation because of their high energy neutron spectra and deep penetration examples with several different differential and integral detectors but detailed and complete models which include all of the detectors did not exist before.

In this report two shielding materials were analysed - iron and concrete. The iron shielding thickness ranged from 0 cm to 130 cm. The concrete shielding thickness ranged from 0 cm to 200 cm. Three different detectors were modelled - the BC501A liquid scintillation detector, a series of Bonner sphere detectors and finally ^{238}U and ^{232}Th fission cells.

Because this is a deep penetration shielding problem effective variance reduction parameters were needed for CPU (Central Processing Unit) time-wise effective calculations. The source was geometrically biased and space and energy dependant weight window variance reduction parameters were produced using the ADVANTG [5] hybrid deterministic/Monte Carlo code.

In Section 1.1 of the report the contract details with IAEA (International Atomic Energy Agency) are given. Section 2 contains all of the modelling details, from the initial CAD (Computer Assisted Design) modelling (2.1), to the MCNP geometrical modelling (2.2), material (2.2.1) and source definition (2.2.2) to the detector/tally modelling (2.2.3). A separate Section 3 of the report is dedicated to the variance reduction techniques implemented. Open issues of the models are described in Section 4. References for the computer codes used for each of the modelling steps are given in appropriate sections of the report. Finally results, including neutron energy spectra, reaction rates for the two fission cells and count rates for the different Bonner spheres for the iron (5.1.1, 5.1.3, 5.1.2) and concrete (5.2.1, 5.2.3, 5.2.2) shield cases are given in Section 5.

1.1 Deliverables according to contract

The deliverables according to the IAEA special service agreement (Requisition No: TAL-NAPC20180606-001) are:

"*MCNP input model for the TIARA benchmark with* 43 MeV *and* 68 MeV *protons incident on Li target to produce neutrons, passing through different thicknesses of iron and concrete, respectively. Some form of variance reduction must be employed that will allow execution of the test problems in reasonable time. Tallies for all types of detectors used in the experiment should be provided. - Document describing the model, the variance reduction technique, and notes on any deficiencies in the specifications that might influence the results. - The reports must include at least the results of sample calculations with the ENDF/B-VII.1 and ENDF/B-VIII libraries. Acceptance criterion for the deliverables is successful execution of the calculations for the benchmarks with MCNP-6.1 on the IAEA computers by the staff at the IAEA.*"

The deliverables can be broken in-to the following items:

- MCNP models including geometrical, source and tally definitions for the iron and concrete shielding cases
- Effective variance reduction parameters
- Document with detailed description of the modelling procedure
- Sample calculations with ENDF/B-VII.1 and ENDF/B-VIII nuclear data libraries

Items 1 and 2 will be delivered separately as MCNP input files (*.i) and external weight window files (*.wwinp). The list of all MCNP input files and weight window files is given in Appendix C. Sample input files are given in Appendix A and B. Items 3 and 4 are addressed in this report.

2 TIARA

The shielding experiment was performed at the TIARA (Takasaki Ion Accelerator for Advanced Radiation Application) at JAERI (Japan Atomic Energy Research Institute). The neutron source for the iron benchmark experiment was produced by 43 MeV and 68 MeV protons incident on a 99.9 % enriched ^{7}Li target. The generated neutrons in the target were passed through a 225 cm long iron collimator placed in a thick concrete wall which surrounds the accelerator. The neutron source spectra were measured 14 m from the target with an organic scintillator by the time-of-flight measurement technique and was normalized per 1 μC (micro-coulomb) of source proton charge. The absolute fluxes of the neutron source in the peak region were measured using a proton-recoil-telescope.

For the simulations performed in the scope of this work the neutrons were generated at the target location with a spectrum reported in the SINBAD documentation.

Transmission measurements through the various thicknesses of the iron slab were measured using several detection systems. Energy spectra were obtained by unfolding the resulting recoil spectra produced in a 12.7 cm by 12.7 cm BC 501A scintillator. The unfolding of the spectra was performed by the experimental team and is reported in the benchmark documentation.

Additionally to the on and off axis spectra measurements with the BC 501A scintillator, measurements with a series of Bonner sphere counters were performed. On and off axis measurements of reaction rates were also performed with ^{238}U fission cell and ^{232}Th fission cell.

The models developed in the scope of this report were developed from scratch, they are not based on any other models available for other transport codes or other, simplified, models for MCNP. In the first step CAD models (2.1) were produced for each of the material-source-detector combinations reported in the SINBAD documentation. The CAD models were used as the base for MCNP geometrical modelling (2.2). The material (2.2.1), source (2.2.2) and tally (2.2.3) modelling was based on the SINBAD documentation. Finally optimal variance reduction parameters were produced after several iteration of the ADVANTG input parameters (3).

2.1 CAD modelling

CAD model were developed with the Rhinoceros 5 (Rhino) software [6]. The CAD models can be used in further neutron transport analysis with other transport codes. The CAD models also contain all of the dimensions crucial for development of other models. They are also extremely useful for visualization purposes.

The dimension for the CAD models were mainly taken form the SINBAD documentation, specifically the following reports:

- JAERI-Data/Code 97-020 EXPERIMENTAL DATA ON CONCRETE SHIELD TRANSMISSION OF QUASI – MONOENERGETIC NEUTRONS GENERATED BY 43 - AND 68 – MeV PROTONS VIA THE ^{7}Li (p,n) REACTION (JOINT RESEARCH) (page 15 of 52)

- JAERI-Data/Code 96-005 EXPERIMENTS ON IRON SHIELD TRANSMISSION OF QUASI – MONOENERGETIC NEUTRONS GENERATED BY 43 - AND 68 – MeV PROTONS VIA THE ^{7}Li (p,n) REACTION (JOINT RESEARCH) (page 41 of 53)

- JAERI-Data/Code 96-029 NEUTRON TRANSMISSION BENCHMARK PROBLEMS FOR IRON AND CONCRETE SHIELDS IN LOW, INTERMEDIATE AND HIGH ENERGY PROTON ACCELERATOR FACILITIES (page 11 of 86)

- JAERI-Data/Code 98-013 EXPERIMENTAL DATA ON POLYETHLYENE SHIELD TRANSMISSION ON QUASI-MONOERGETIC NEUTRONS GENERATED BY 43- AND 68 MeV PROTONS VIA 7Li(P,N) REACATION (page 40 of 54)

All of the reports mentioned are available in the SINBAD database.

Some of the dimensions such as the surrounding room concrete structure, detector stand and specifics of the fission cell detectors were not included in the available documentation. The dimension in these cases are best estimates derived from the included figures and descriptions.

The CAD models with the major dimensions are presented in Figures 2.1, 2.2 and 2.3. The CAD models are available from the author on demand.

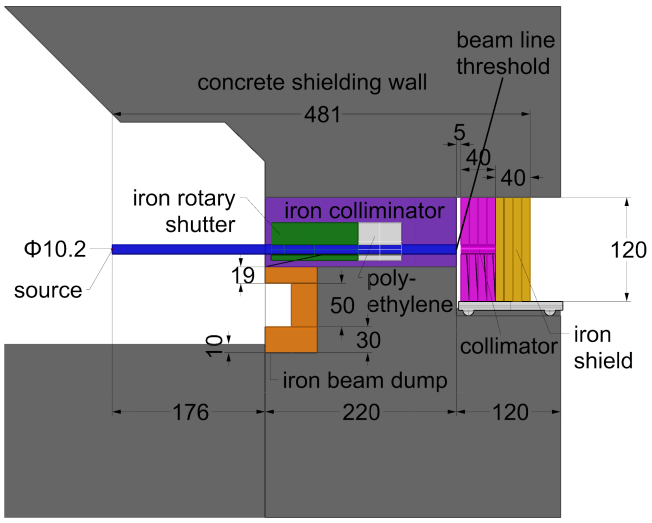

Figure 2.1: CAD model, side view at y=0, 40 cm iron shield, 40 cm collimator, BC 501A detectors at 20 cm and 40 cm off-axis, 68 MeV. All dimensions are in centimetres.

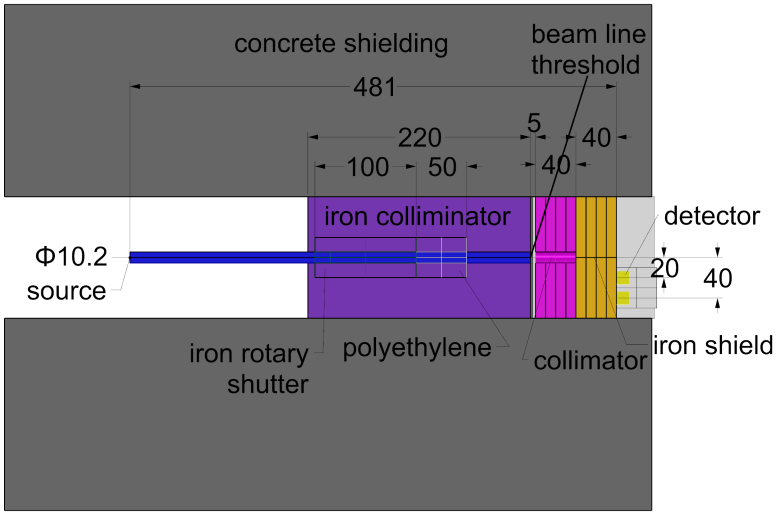

Figure 2.2: CAD model, top view at z=0, 40 cm iron shield, 40 cm collimator, BC 501A detectors at 20 cm and 40 cm off-axis, 68 MeV. All dimensions are in centimetres.

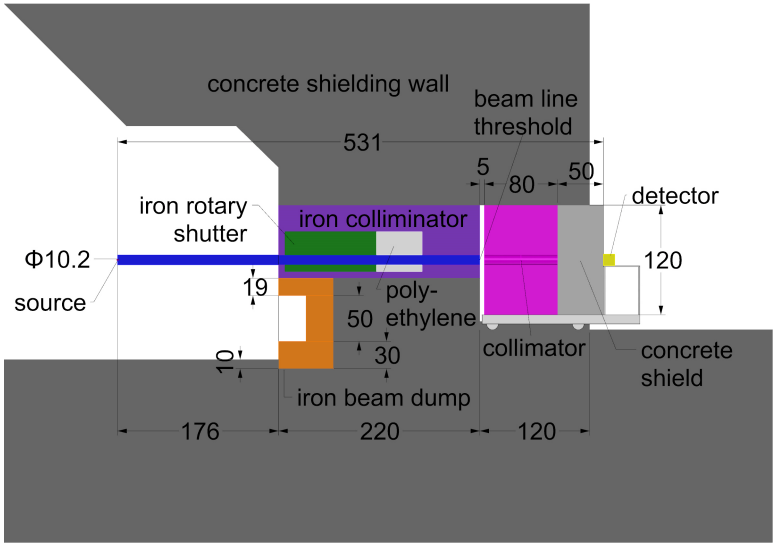

Figure 2.3: CAD model, side view at y=0, 50 cm concrete shield, 80 cm collimator, BC 501A detectors on axis and at 20 cm and 40 cm off-axis, 68 MeV. All dimensions are in centimetres.

2.2 MCNP modelling

The geometrical modelling in MCNP was done using the GRASP [7] CAD to MCNP conversion tool developed at JSI ("Jožef Stefan" Institute) by the author of the report. The MCNP models dimension correspond directly to those in the CAD models. Geometrical modelling based on pre-developed CAD models has proven to be straight forward and fast. As mention in the previous section of the report (2.1) some

of the dimensions, specifically fission chamber geometry, dimension of the surrounding concrete structure and detector support structures, were deducted from the Figures included in the SINBAD database. The effect of the derived dimensions on the final MCNP transport calculation was determined to be negligible.

Selected MCNP models which correspond to the CAD models shown in Figures 2.1, 2.2 and 2.3 are presented as Figures 2.4, 2.5 and 2.6. The MCNP models where visualized with the MCNP Visual Editor [8]. The different colours correspond to different materials used in the model. The definition of material is described in the next section of the report (2.2.1). The geometrical characteristics are converted from CAD format in-to MCNP format without any loss of detail using the GRASP tool.

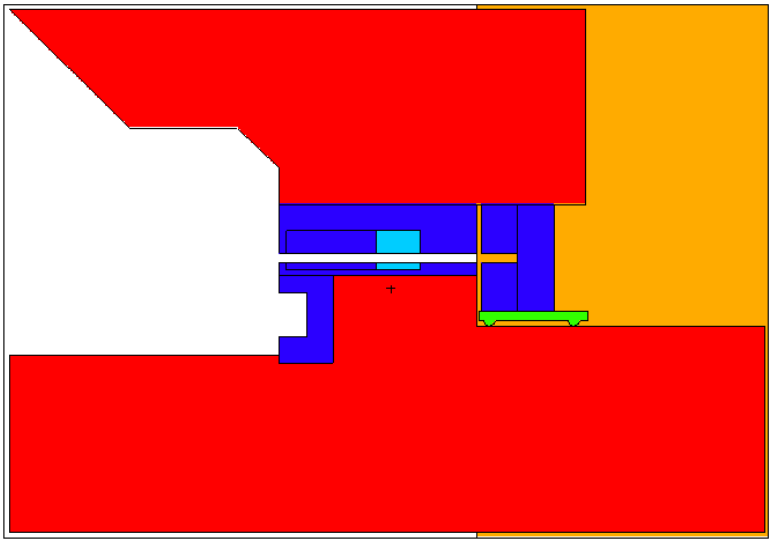

Figure 2.4: MCNP model, side view at y=0, 40 cm iron shield, 40 cm collimator, BC 501A detectors at 20 cm and 40 cm off-axis, 68 MeV. All dimensions are in centimetres.

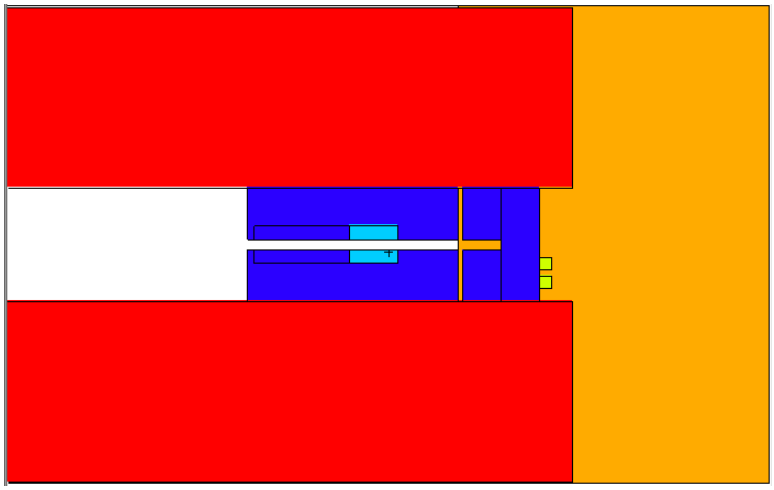

Figure 2.5: MCNP model, top view at z=0, 40 cm iron shield, 40 cm collimator, BC 501A detectors at 20 cm and 40 cm off-axis, 68 MeV. All dimensions are in centimetres.

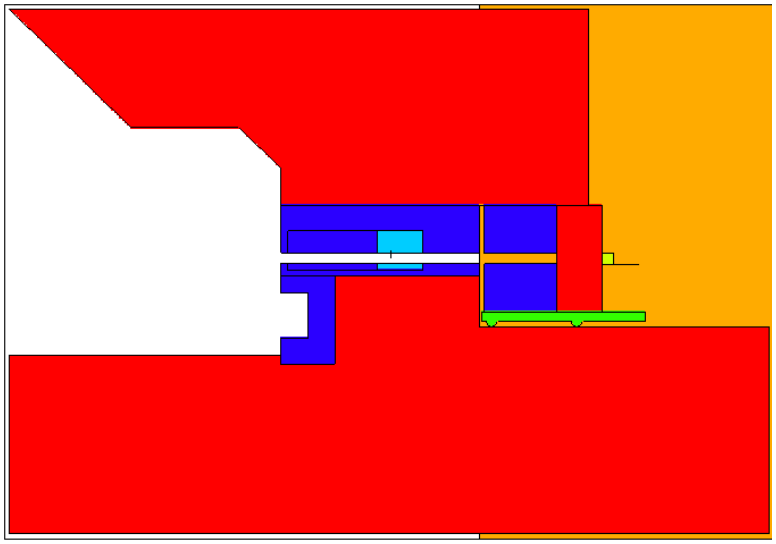

Figure 2.6: MCNP model, side view at y=0, 50 cm concrete shield, 80 cm collimator, BC 501A detectors on axis and at 20 cm and 40 cm off-axis, 68 MeV. All dimensions are in centimetres.

2.2.1 Materials

The materials for the MCNP input files were defined based on the information in the SINBAD documentation. 6 materials were defined. The information for the iron shield material and the concrete shield material came from the JAERI-Data/Code 96-029 (j96-029.pdf) document, Table 1.2 on page 13. The materials are given per element, but for MCNP calculations per nuclide definitions of the materials were needed. The

MATSSF code [9] was used to calculate the per nuclide atomic densities. The concrete shielding material was also used for the surrounding structures. Other materials included in the models are as follows:

- Polyethylene for the inside of the first collimator/chopper assembly. The composition was taken from NIST. (http://physics.nist.gov/PhysRefData/XrayMassCoef/tab2.html)
- Aluminium for the detector support structures. Natural aluminium was used with the a density of $2.6989\,\mathrm{g\,cm^{-3}}$.
- Liquid scintillator for the inside of the BC 501A detectors was taken from the specification data sheet of the detector. (https://www.crystals.saint-gobain.com/sites/imdf.crystals.com/files/documents/sgc-bc501-501a-519-data-sheet_69711.pdf)
- Dry air. The compostion was taken from the Compendium of Material Composition Data for Radiation Transport Modeling (https://www.pnnl.gov/main/publications/external/technical_reports/PNNL-15870Rev1.pdf).

The exact material definitions and densities used can be found in the appended MCNP input files in Appendix A and B.

2.2.2 Source

Because of the lack of detailed information on the ^{7}Li target, the proton beam and surrounding structures it was decided to use the measured neutron energy spectrum as reported in the SINBAD documentation. The original JAERI documentations gives different energy boundaries for the source spectrum to the ones provided in the SINBAD documentation. It is assumed that the JAERI boundaries are middle of the bin energies. These assumption is also supported by plots of the source spectra in the original JAERI documentation e.g. Fig 1.5 on page 15 of 86 in j96-029.pdf or Fig.3 on page 16 of 52 in j97-020.pdf. For the modelling purposes of this work the energy spectrum was taken from Table 3 for the 43 MeV case and from Table 4 of the SINBAD HTML file for the 68 MeV case and the energy bin boundaries are assumed to be upper bin boundaries.

The source was modelled as a point 396 cm from the beam line threshold at the MCNP coordinate system origin. Because the actual source spectra was measured at the end of the beam line we neglected the effects of the beam line on our source. To ensure this the beam line was modelled as a vacuum, neutrons do not undergo any interactions between the source point and the end of the beam line.The source was also limited to a conical shape. The cone base corresponds directly to the opening of the beam line at x = 396 cm with a diameter of $\phi = 10.2$ cm, if the coordinate system origin is at the source location. Such a source definition is also an effective variance reduction technique - more on that in Section 3. One might ask why even model the surrounding structures, but the measured source spectra does not take in to account

scatterings which might occur after the source neutron exits the beam line threshold at x = 396 cm. The reason for modelling the environment is to describe more realistically the surface area and flux angular distribution in the front of the block, as well as for future extensions of the model to study different source modelling options.

2.2.3 Detectors/tallies

As mentioned in the introduction three different detectors were modelled including the BC 501A liquid scintillator, Bonner sphere counters of various sizes and two different fission counters (^{238}U and ^{232}Th fission cells).

The BC 501A liquid scintillator tally was modelled as a F4 volume tally with the actual detector modelled as a cylinder with a height of h = 12.7 cm and a diameter of d = 12.7 cm. The cylinder was filled with a liquid scintillator material defined in the detector manufacturers' technical documentation. The tally results (Φ^{F4}_{MCNP}) are normalized according to the SINBAD documentation. The normalization factor is calculated with the following equation:

$$\Phi_{normalized} = \Phi^{F4}_{MCNP} * PtC * PF * 4 * \pi \tag{2.1}$$

where the factors in the equation are:

- PtC = Peak to continuum normalization factor (2.17 for the 43 MeV neutron source and 2.61 for the 43 MeV neutron source. These wo values are given in the captions of Table 3 and Table 4 of the SINBAD tia-exp.htm file)
- PF = peak flux of source neutrons which differs from case to case (The values are given in Table 1 of the SINBAD tia-exp.htm file)
- solid angle (4 * π)

Finally tally is divided in the energy domain according to the experimental results for easier comparison to the experimental results. The results for the BC 501A liquid scintillator are given in Section 5.2.1 and 5.1.1.

The Bonner sphere detectors were modelled as simple spheres with diameters which correspond to the diameters of the different polyethylene moderators (bare, 15 mm, 30 mm, 50 mm, 90 mm). The F4 tallies have volumes which correspond to the volumes of the spheres. Spheres are filled with air but the responses are modified with linearly interpolated response functions taken from Table 26 of the SINBAD tia-exp.htm file. The results are also absolutely normalized with the normalization factor given in Equation 2.1. For convenience the normalization factors and all experimental results are given in the MCNP input files so direct comparison to the calculation results are easy.

An analysis was performed where the Bonner spheres were modelled in detail according to the available geometrical and material information. The results differed by a large margin, consequently it was decided to use a simplified geometrical mode and the response functions provided in the documentation.

The fission cells were modelled similarly to the Bonner spheres. The cells were modelled as cylinders (h = 10.1 cm and a diameter of d = 3.81 cm). The cylinders are filled with air but the responses are modified with linearly interpolated fission cross sections taken from Table 45 of the SINBAD tia-exp.htm file. The results are also absolutely normalized with the normalization factor given in Equation 2.1. For convenience all of the experimental results, taken from the original JAERI documents (j96-029.pdf Table 1.29, 1.30, 1.31 and 1.32) are given in the MCNP input files so direct comparison to the calculation results are easy.

3 Variance reduction

Because this is a deep shielding problem variance reduction was needed to perform effective and fast simulations. The variance reduction was performed at the source, with limiting the physical properties of the transport problem and finally with energy dependant weight windows determined by the ADVANTG hybrid deterministic/Monte Carlo code.

As mentioned in Section 2.2.2 the geometry of the source was limited to a conical shape. This geometrical restriction reduces the time needed for the code to simulate neutrons travelling from the source point away from the detector locations. The directionally limited source was defined using the *vec* and *dir* keywords in the fixed source definition (*SDEF*) of the MCNP source. As mentioned in Section 2.2.2 the angle of the cone is calculated with the appropriate ratio (cosine), where the adjacent is the distance between the source point and the beam line threshold (396 cm) and the hypotenuse is calculated from the radius of the collimator and the distance between the source point and the beam line threshold (39.037 501 cm) $cos\phi = \frac{396}{\sqrt{396^2 + 5.45^2}} = 0.99990531$. The fractions of the solid angle for the bins are calculated as the ratio of the cosine to the full solid angle $bin_{ratio} = \frac{\left(1 - \frac{0.99990531}{2}\right)}{2} = 4.735e-05$.

The next step of the variance reduction was to limit the physics of the problem. This was done using the *cut* card to stop the neutron transport at a certain energy threshold. This variance reduction technique was implemented only for the BC 501A detector cases, where we are only interested in the neutron energy spectra above 4 MeV for the 43 MeV source and above 5 MeV for the 68 MeV source.

The final step was to produce energy and space dependant weight windows with ADVANTG. The procedure is described in the following Section (3.1).

3.1 ADVANTG

The **A**utomate**D** **VA**ria**N**ce reduc**T**ion [5] (ADVANTG) hybrid deterministic/Monte Carlo transport code developed at ORNL was used to determine energy and space dependant weight window (WW) variance reduction parameters. WW were only

determined for the cases where it was beneficial. In the first iteration step WW for all cases were developed, except for the thinnest shielding cases. In most cases it was beneficial to use WW for the cases with shield thickness higher than 40 cm.

The Forward-Weighted Consistent Adjoint Driven Importance Sampling [10] (FW-CADIS) method was used to determine the WW windows for multiple detector (tally) locations and with uniform uncertainties in each energy bin in the case of the BC 501A liquid scintillator detectors. FW-CADIS response weighting was turned of in the case of the BC 501A liquid scintillator detector. The hilo2k multigroup nuclear data library included with the ADVANTG distribution was used for all cases for the initial deterministic calculation. A detailed quadrature set was defined along with a high order of expansion of the scattering angle. A detailed Cartesian mesh used for the deterministic calculation was defined for each case, taking in to account the mean free paths of neutron at appropriate energies for each shielding and structural material.

When we compare the Figure-of-merit (FOM) statistical test of the analog[1] MCNP calculation to a ADVANTG accelerated MCNP calculation for the case of the 100 cm thick iron shield with the 43 MeV neutron source and the BC 501A liquid scintillator detector, the speed-up factor or relative FOM ($FOM_{rel} = \frac{FOM_{ADVANTG}}{FOM_{analog}}$) is 300. A comparison of a long analog MCNP calculation with 10^9 neutron particle histories simulated to an ADVANTG accelerated calculation, with 10^6 neutron particle histories is shown in 3.1. The $C_{ADVANTG}/C_{Analog}$ value is 1 within the combined 1σ statistical uncertainty which shows no bias is introduced in to the calculation with ADVANTG produced variance reduction parameters.

[1] A MCNP calculation where WW were not used.

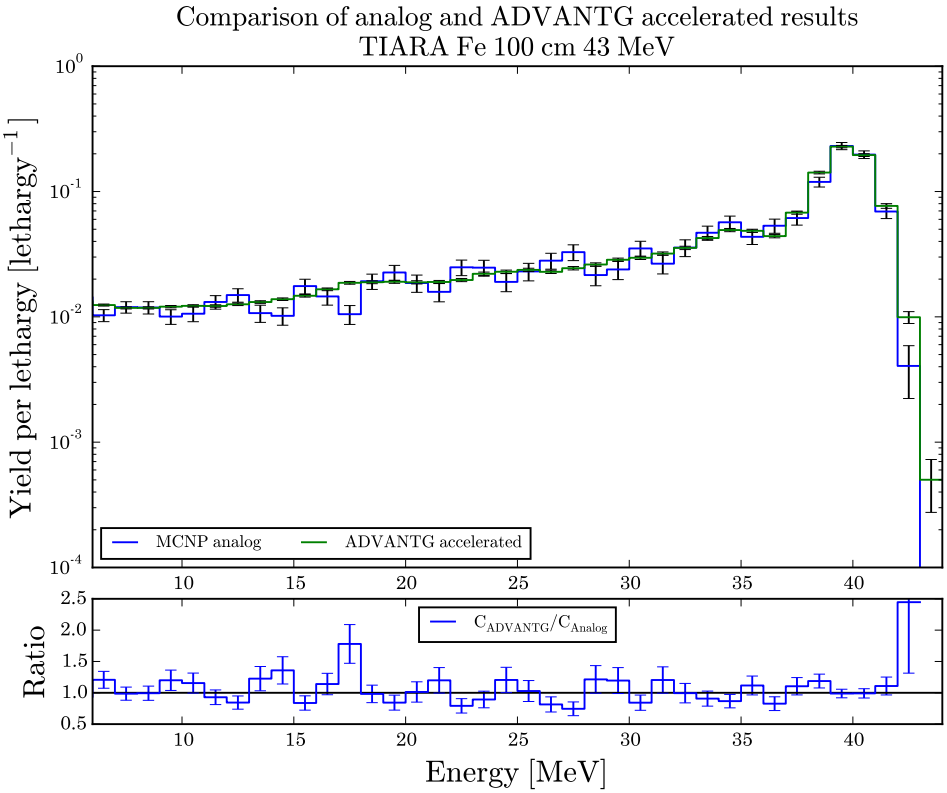

Figure 3.1: $C_{ADVANTG}/C_{Analog}$ (Calculation-over-calculation) comparison of ADVANTG accelerated MCNP calculation to an analog MCNP calculation of the spectra measured with a BC 501A liquid scintillator for the case of the 100 cm thick iron shield with a 43 MeV neutron source.

Using all of the above mentioned variance reduction parameters statistical uncertainties bellow 5 % (in most cases bellow 2 %) for all tallies or energy bins are achieved in under 5 min on a local computer cluster with 40 threads (Intel Xeon E5-2680 v2).

It should be noted that all of the simulations were done using MCNP5 version 1.6. ADVANTG was designed using this version of MCNP. The produced WW are compatible with MCNP6, but in some cases MCNP6 is slower. It has also been reported that in some cases MCNP6 reports failed statistical tests on the tallies where MCNP5 ver. 1.6 does not. But the mean values between the two releases doesn't differ. All of the WW produced in the scope of this work were also testes with MCNP6 and no significant difference between the mean results of the two MCNP releases was noted.

4 Open issues in the modelling

The models produced are to our knowledge the most complete set of MCNP input files for the TIARA iron and concrete shielding benchmarks. Previous models were

simplified version of the problem which did not include the surrounding structures and more importantly other detector tallies besides the BC 501A liquid scintillator detectors. Despite this several issues remain open which will have to be addressed in further evaluations. The following issues remain:

- Uncertainty in the geometrical modelling of the actual detectors (BC 501A, fission cells, Bonner spheres) surrounding concrete structure, detector stands and detectors support platforms because of lack of data in the original benchmark documentation.

- Source definition - comparison to a full proton induced neutron simulation should be performed. But the lack of detailed geometrical data prevents such a undertaking in the scope of this study. Further studies will be needed.

- A possible error in the experimental values or the original and SINBAD documentation can be observed when analysing the results for the 15 mm Bonner sphere with a Cadmium coating in the case of the 100 cm and 150 cm concrete shield with the 68 MeV source.

5 Results

Results simulated using MCNP5 ver 1.6 with the ENDF/B-VII.1, ENDF/B-VIII, JEFF-3.3 and JENDL-4.0u nuclear data libraries are given in this Section. The results for three different detectors are presented, the BC 501A liquid scintillator detectors, Bonner sphere detectors and Fission cells. Generally the agreement for the BC 501A detectors are good for the ENDF/B-VII.1, ENDF/B-VIII and JEFF-3.3 libraries, whereas the JENDL-4.0u library performs worse, especially for the off axis detectors.

The simulations with the Bonner sphere detectors generally overestimate the counts with the less moderated spheres (Bare, 15 mm, 30 mm) and underestimate with the more moderated spheres (50 mm, 90 mm). This trend is observed for both shield materials and thicknesses. A possible error in the experimental values or the original and SINBAD documentation can be observed when analysing the results for the 15 mm Bonner sphere with a Cadmium coating in the case of the 100 cm and 150 cm concrete shield with the 68 MeV source. The results are an order of magnitude higher than the results with the other Bonner spheres.

Generally good agreement between the calculation and experimental results can be seen for the Fission cells behind thinner iron shields with a slight under prediction of the calculations when using the 43 MeV source. The under prediction is even more obvious when looking at the results with the 68 MeV source. A systematic under-prediction is observed when looking at the Fission cell results for the concrete test shields, especially for the thicker shields.

5.1 Iron

The following chapters contain results for the iron shield cases for the BC 501A liquid scintillator detectors (5.1.2), Bonner sphere detectors (5.1.2) and Fission cells (5.1.3). The sample calculation were performed with the ENDF/B-VII.1, ENDF/B-VIII, JEFF-3.3 and JENDL-4.0u nuclear data libraries.

5.1.1 BC501A liquid scintillation detector

5.1.1.1 ENDF/B-VII.1

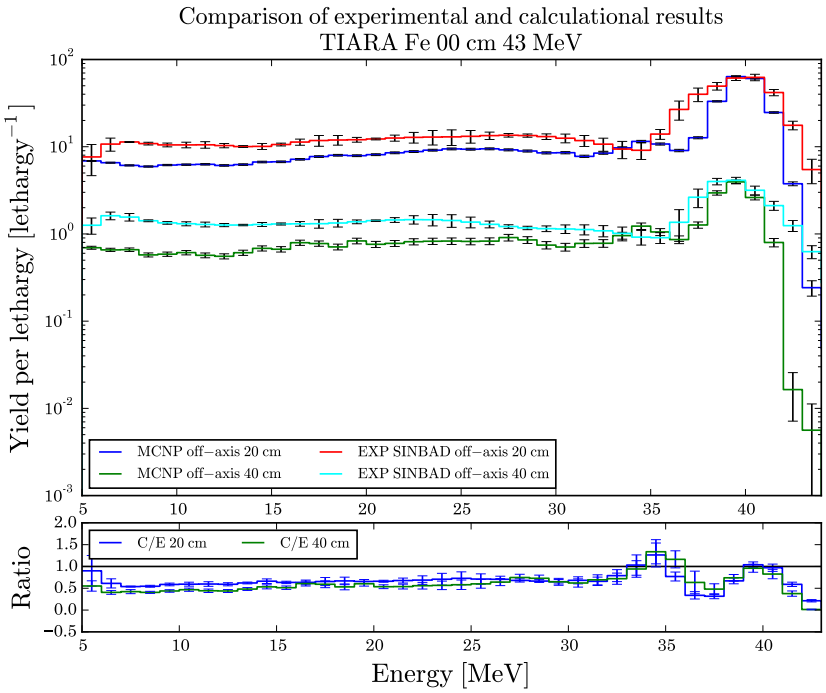

Figure 5.1: 0 cm iron shield, 43 MeV, ENDF/B-VII.1

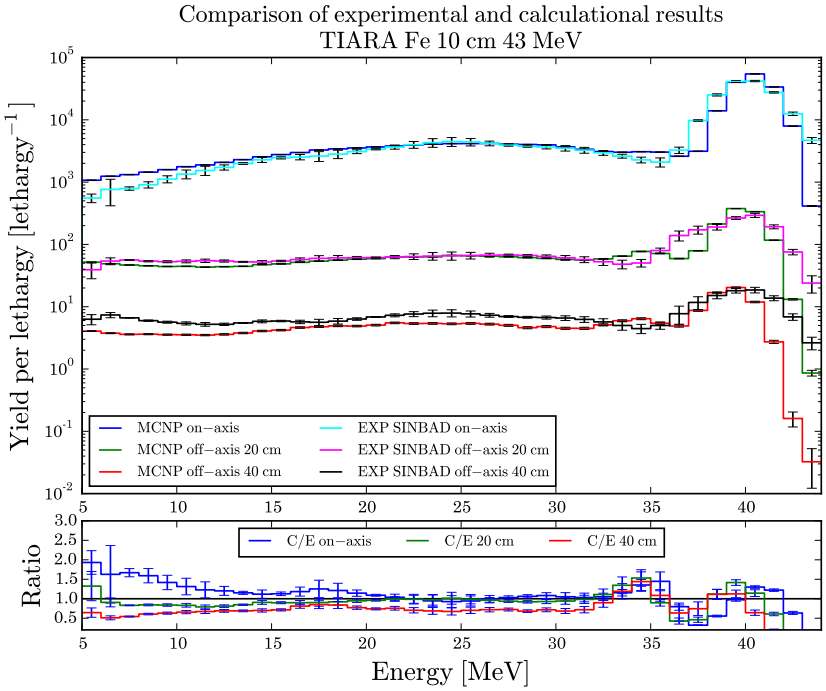

Figure 5.2: 10 cm iron shield, 43 MeV, ENDF/B-VII.1

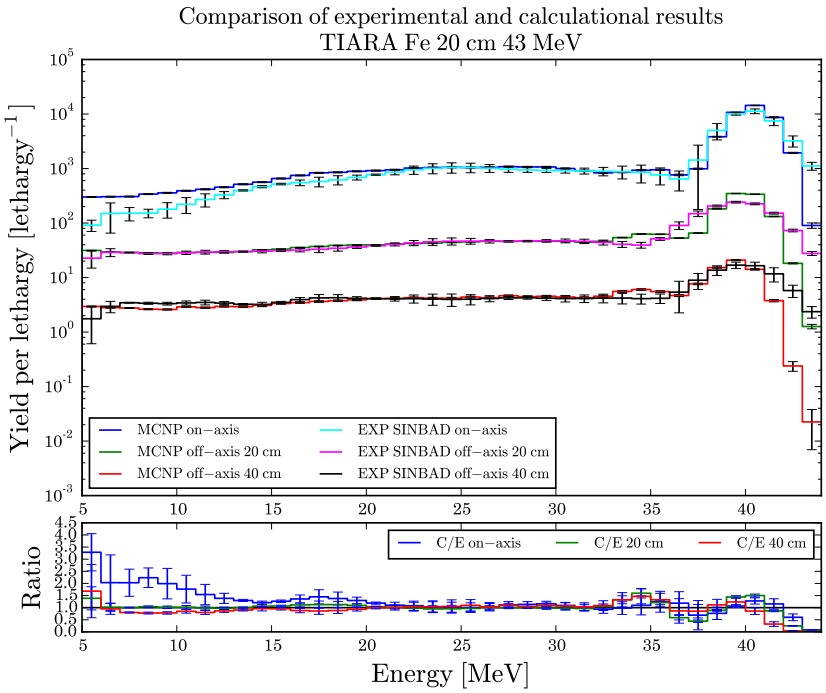

Figure 5.3: 20 cm iron shield, 43 MeV, ENDF/B-VII.1

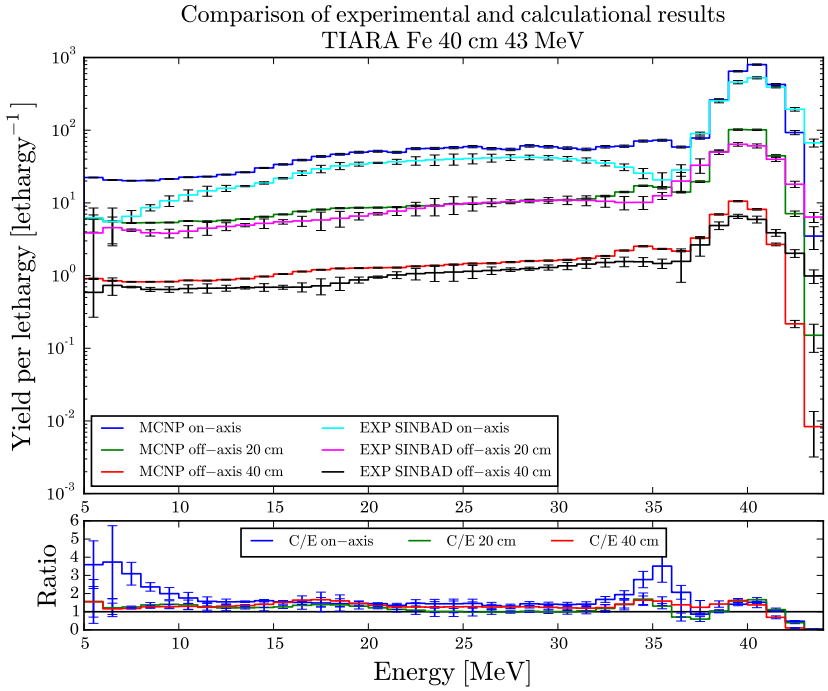

Figure 5.4: 40 cm iron shield, 43 MeV, ENDF/B-VII.1

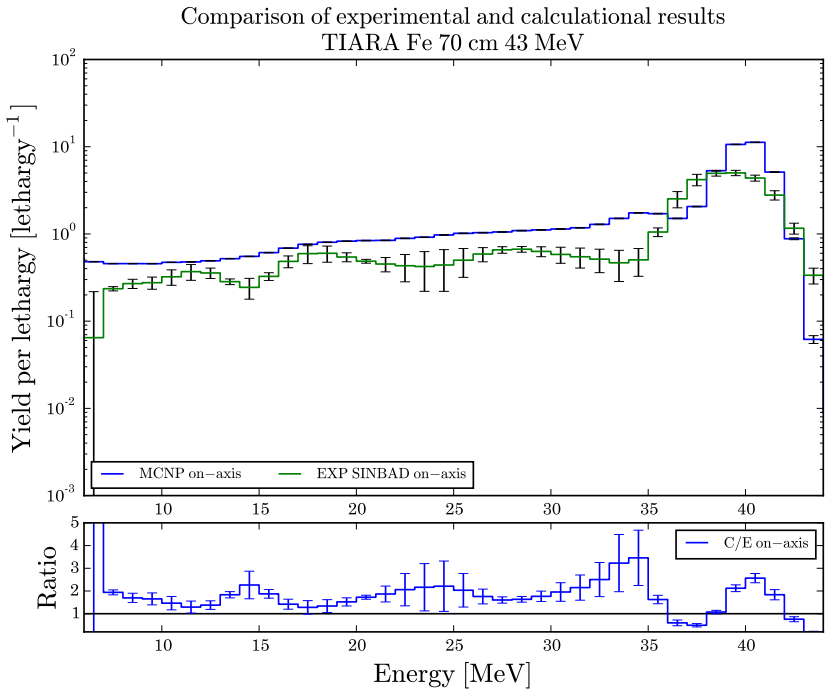

Figure 5.5: 70 cm iron shield, 43 MeV, ENDF/B-VII.1

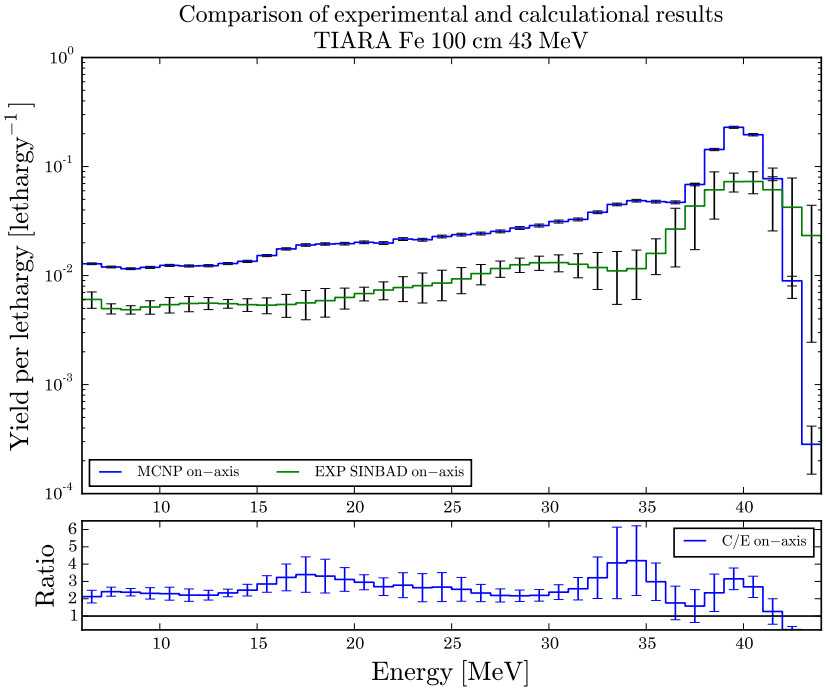

Figure 5.6: 100 cm iron shield, 43 MeV, ENDF/B-VII.1

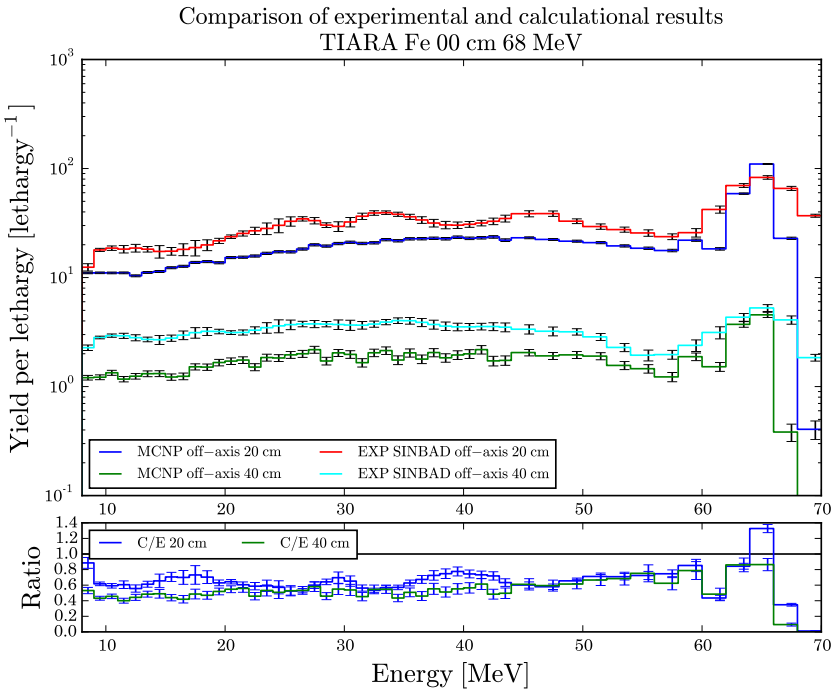

Figure 5.7: 0 cm iron shield, 68 MeV, ENDF/B-VII.1

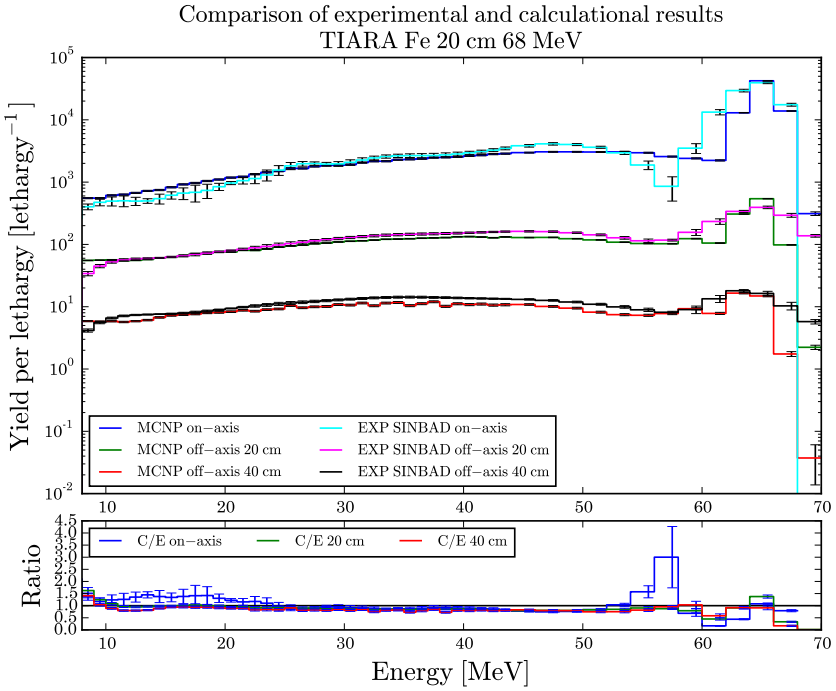

Figure 5.8: 20 cm iron shield, 68 MeV, ENDF/B-VII.1

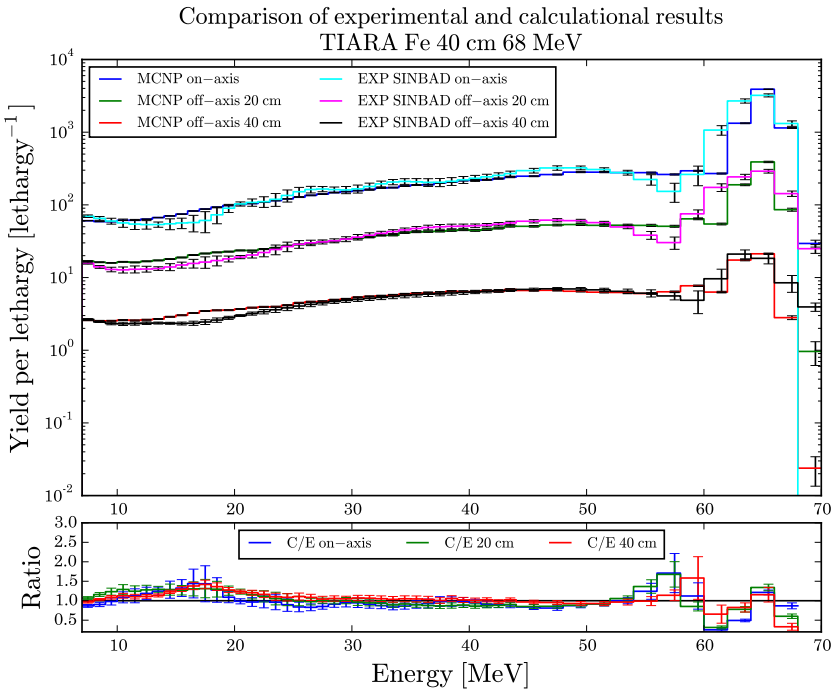

Figure 5.9: 40 cm iron shield, 68 MeV, ENDF/B-VII.1

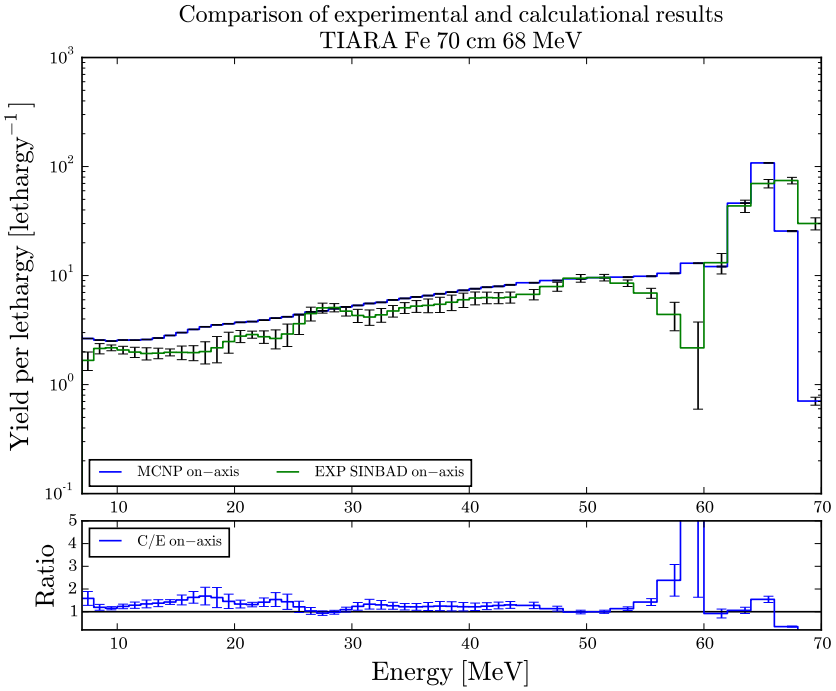

Figure 5.10: 70 cm iron shield, 68 MeV, ENDF/B-VII.1

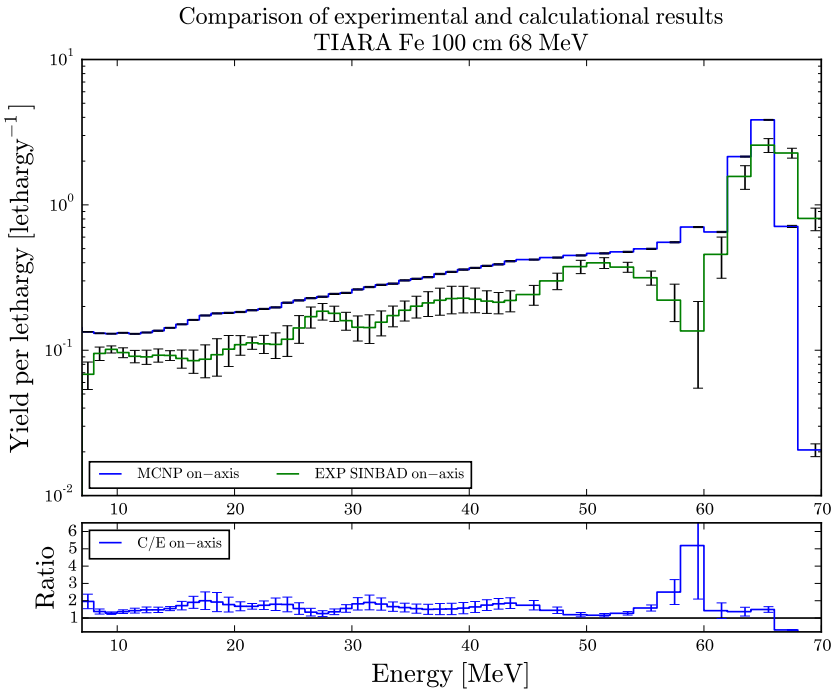

Figure 5.11: 100 cm iron shield, 68 MeV, ENDF/B-VII.1

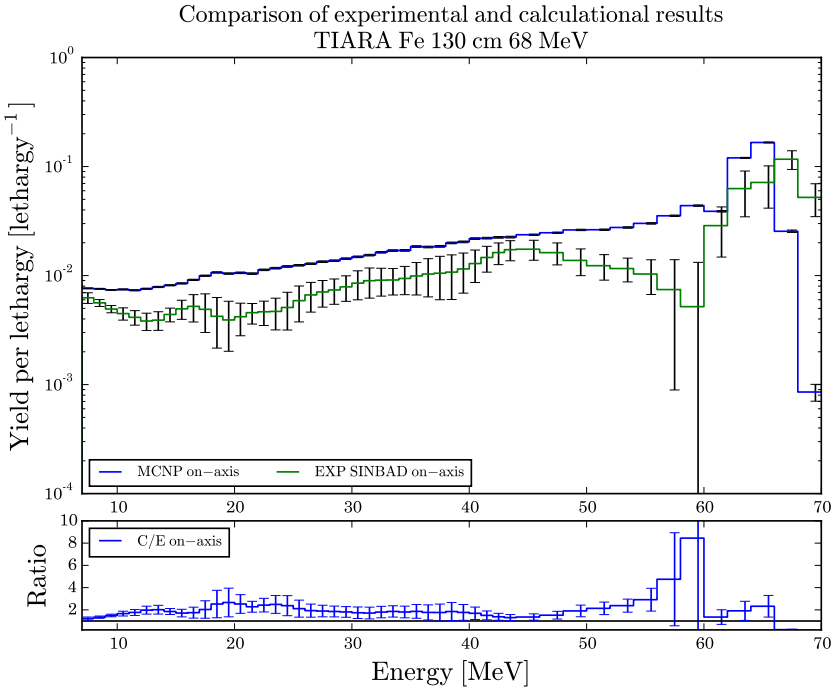

Figure 5.12: 130 cm iron shield, 68 MeV, ENDF/B-VII.1

5.1.1.2 ENDF/B-VIII

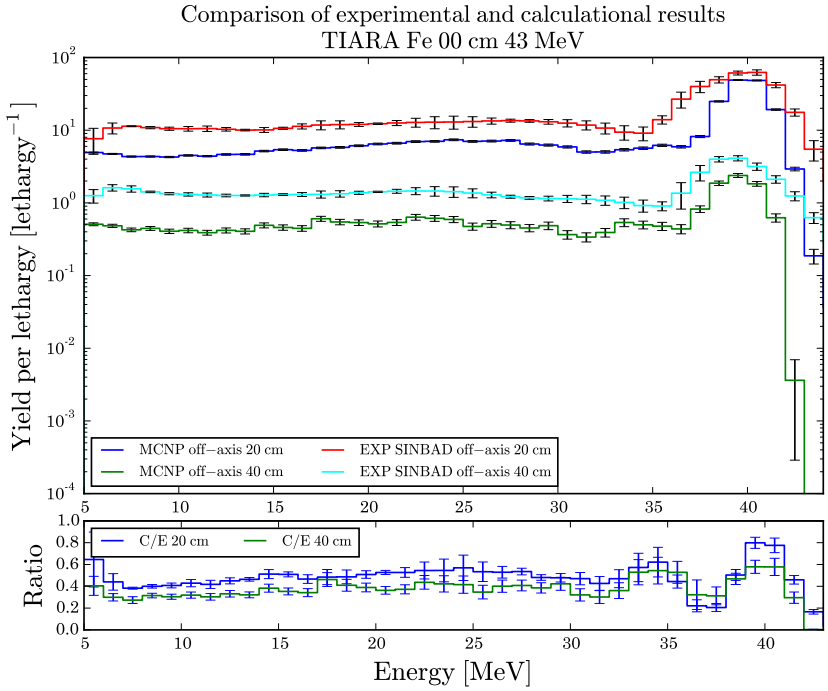

Figure 5.13: 0 cm iron shield, 43 MeV, ENDF/B-VIII

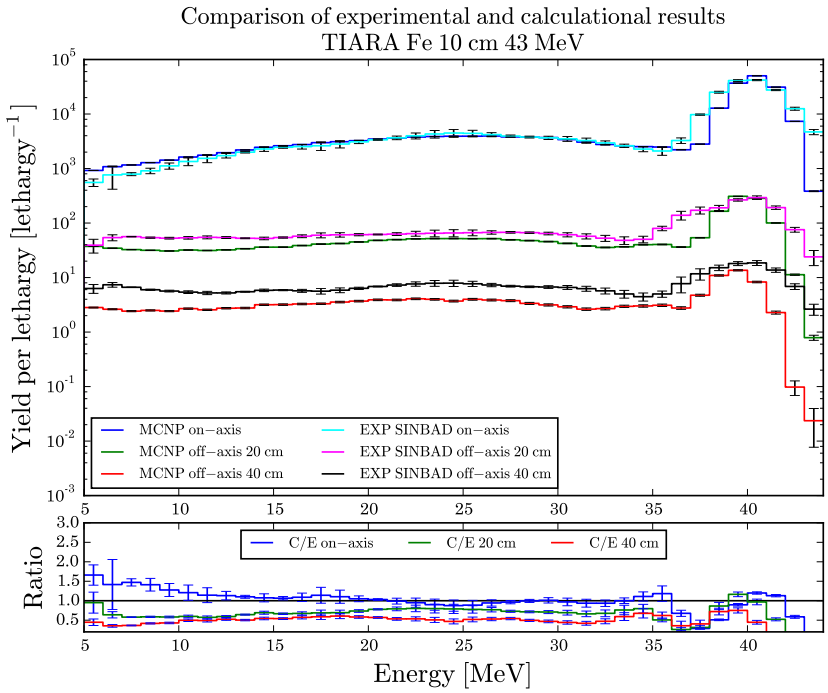

Figure 5.14: 10 cm iron shield, 43 MeV, ENDF/B-VIII

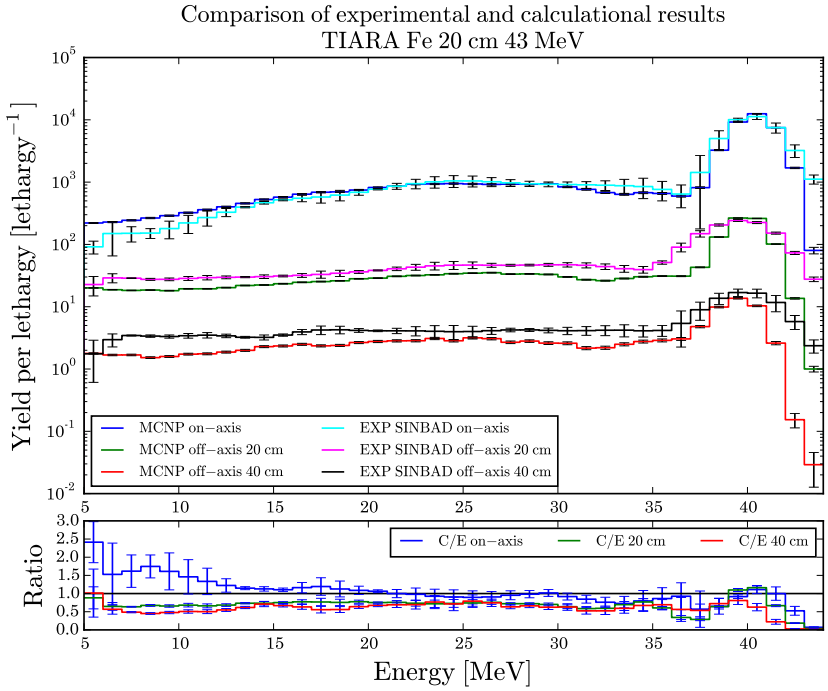

Figure 5.15: 20 cm iron shield, 43 MeV, ENDF/B-VIII

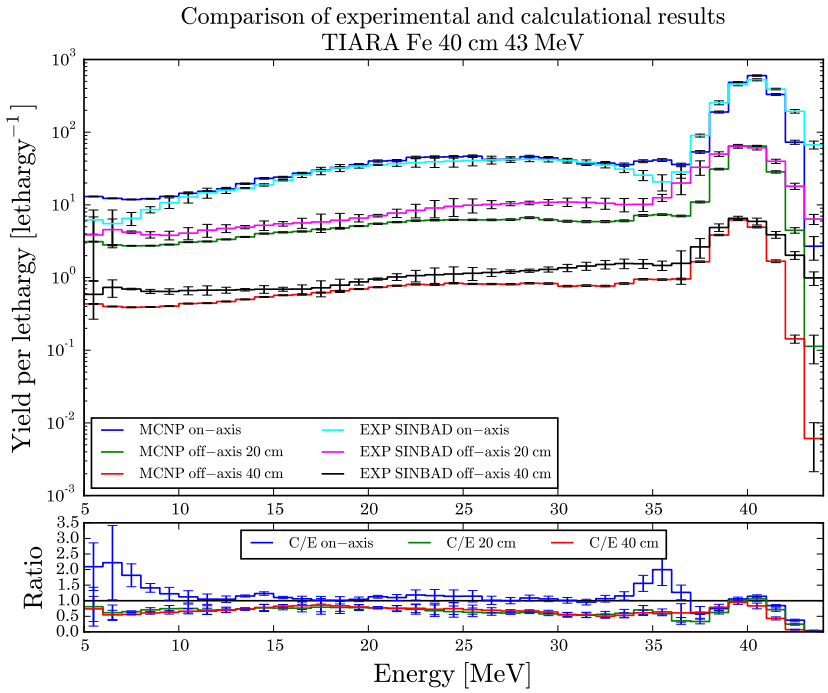

Figure 5.16: 40 cm iron shield, 43 MeV, ENDF/B-VIII

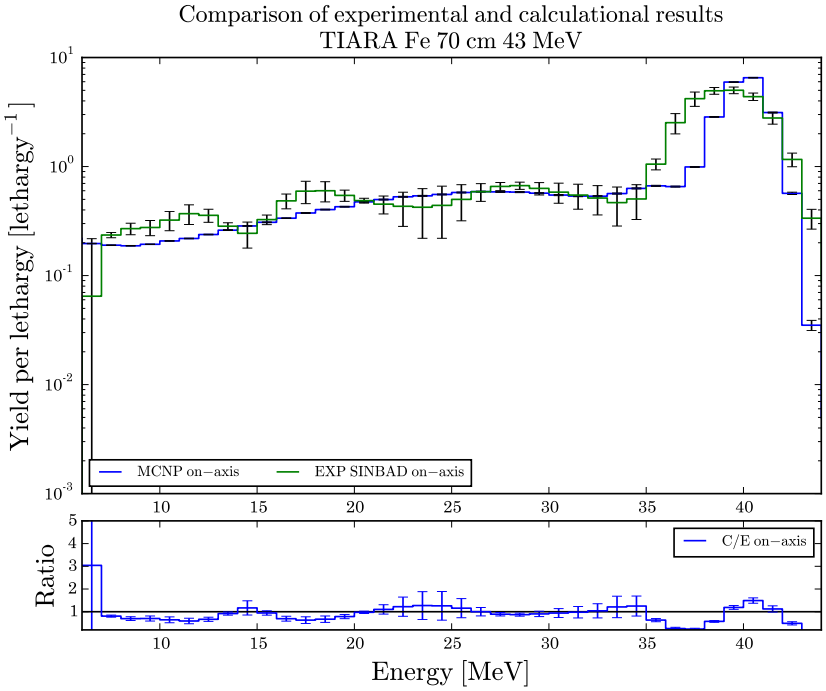

Figure 5.17: 70 cm iron shield, 43 MeV, ENDF/B-VIII

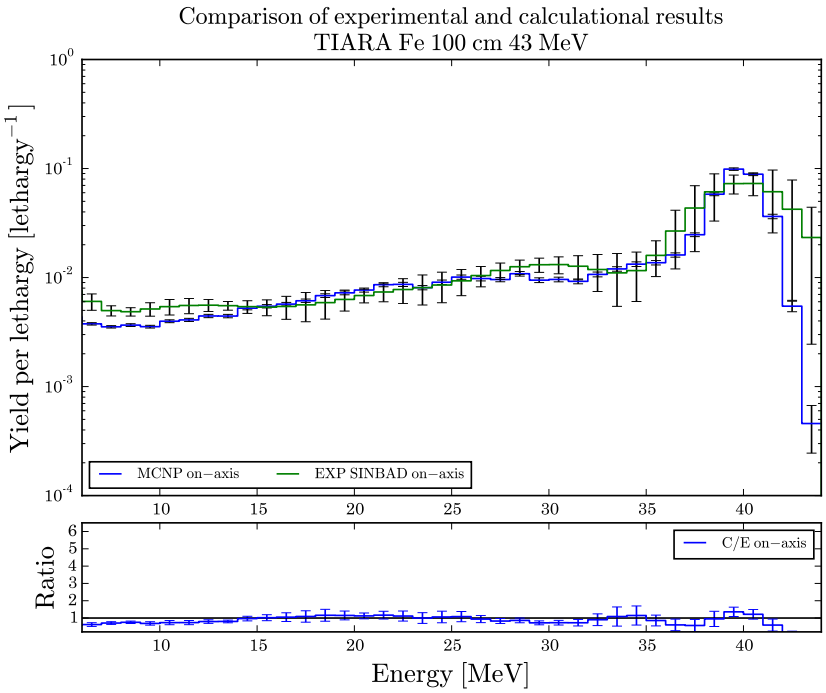

Figure 5.18: 100 cm iron shield, 43 MeV, ENDF/B-VIII

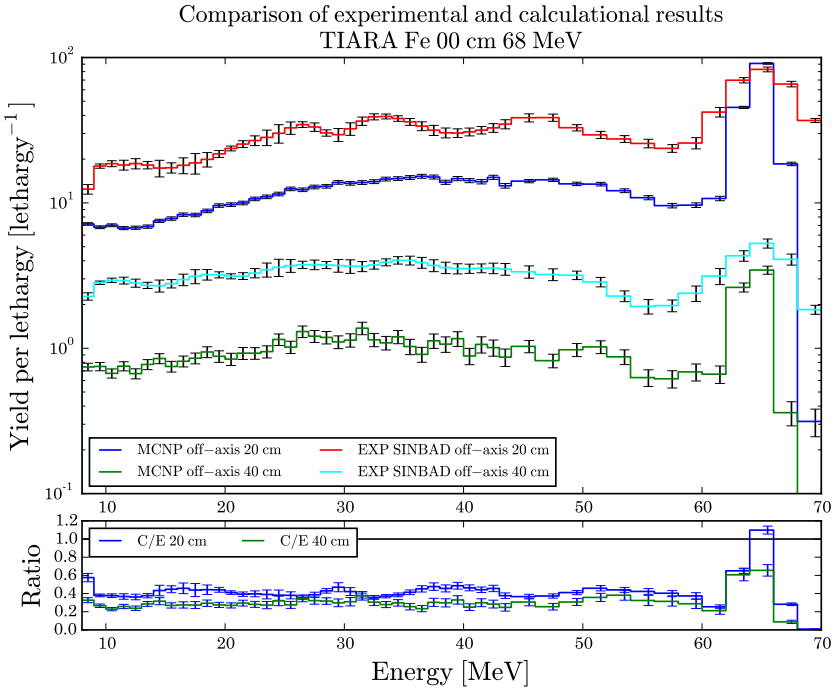

Figure 5.19: 0 cm iron shield, 68 MeV, ENDF/B-VIII

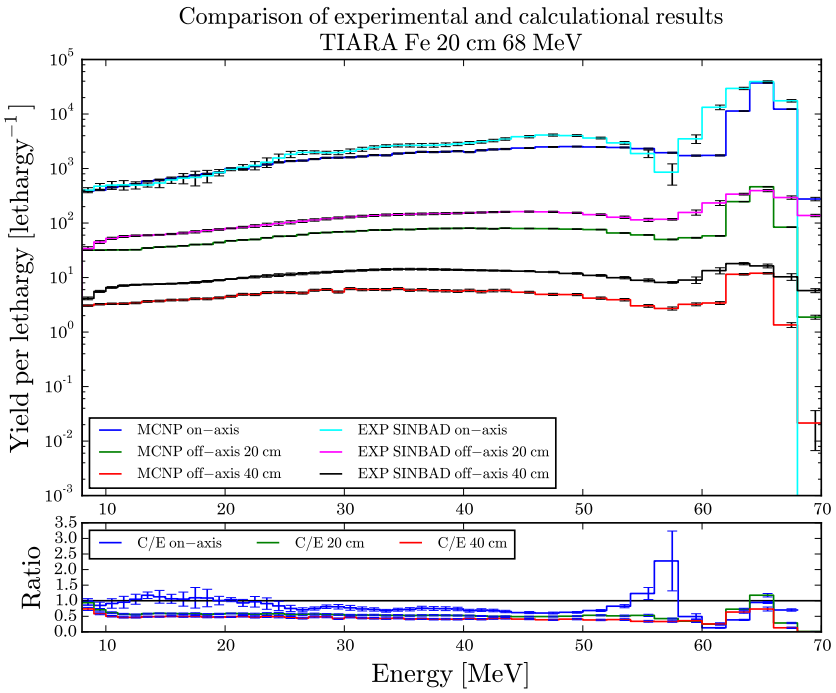

Figure 5.20: 20 cm iron shield, 68 MeV, ENDF/B-VIII

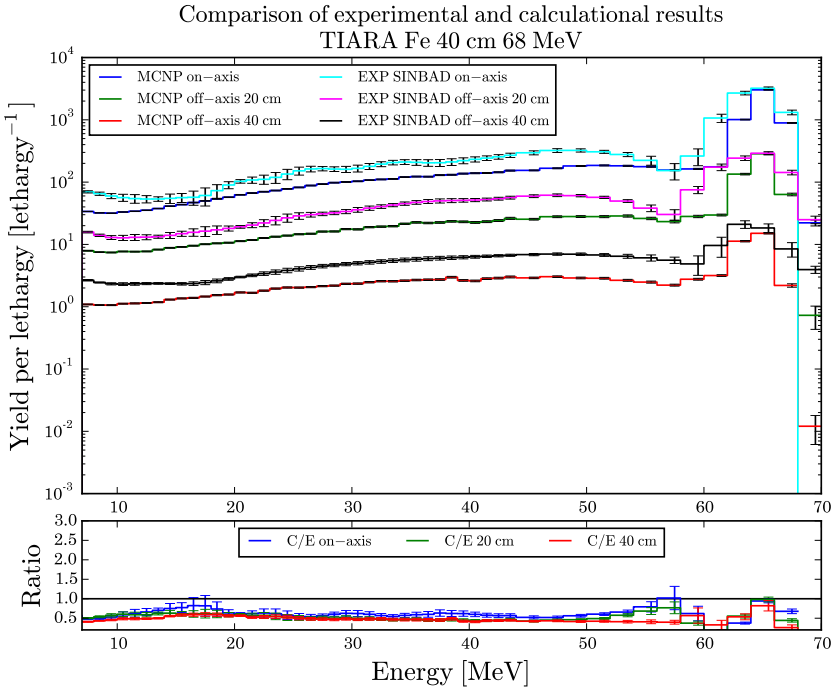

Figure 5.21: 40 cm iron shield, 68 MeV, ENDF/B-VIII

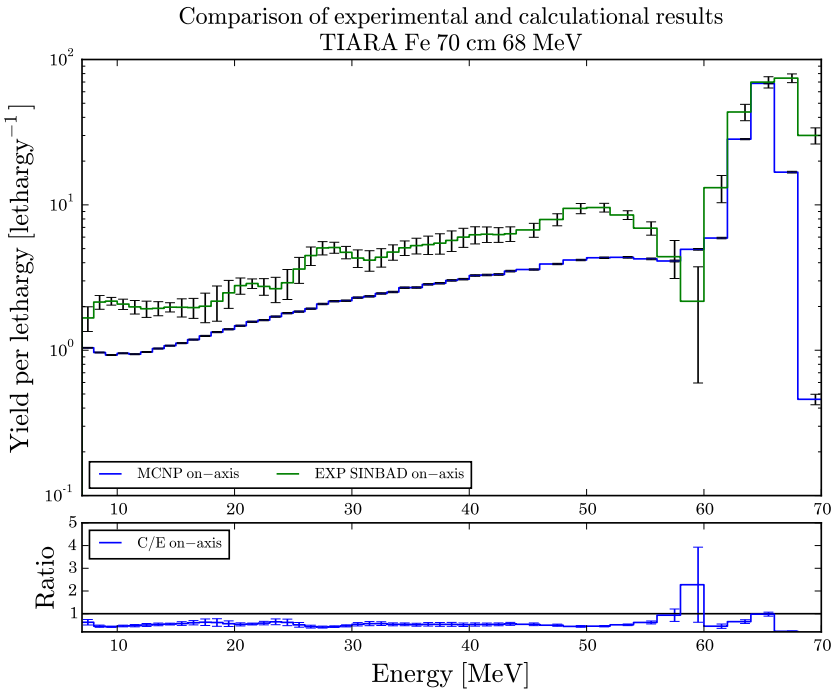

Figure 5.22: 70 cm iron shield, 68 MeV, ENDF/B-VIII

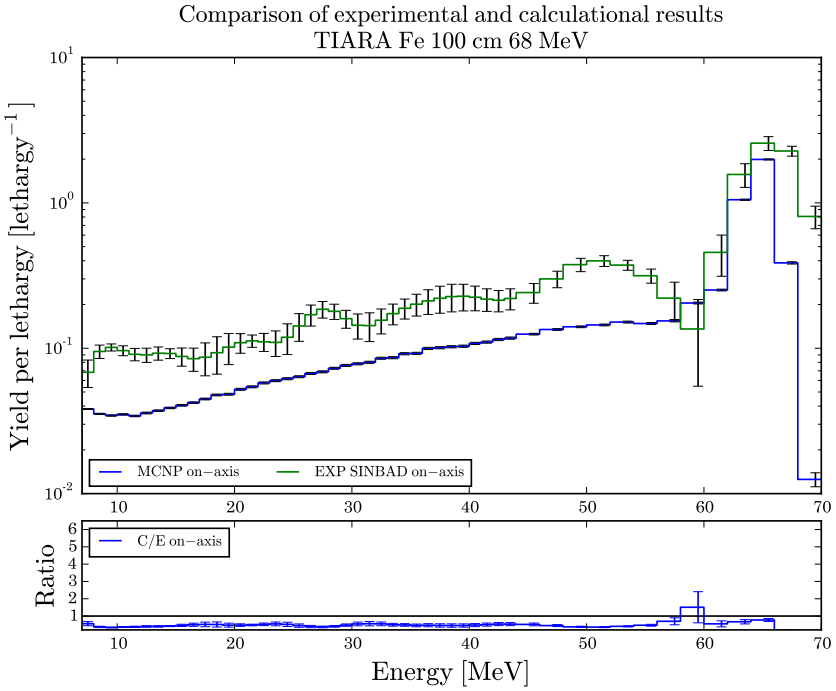

Figure 5.23: 100 cm iron shield, 68 MeV, ENDF/B-VIII

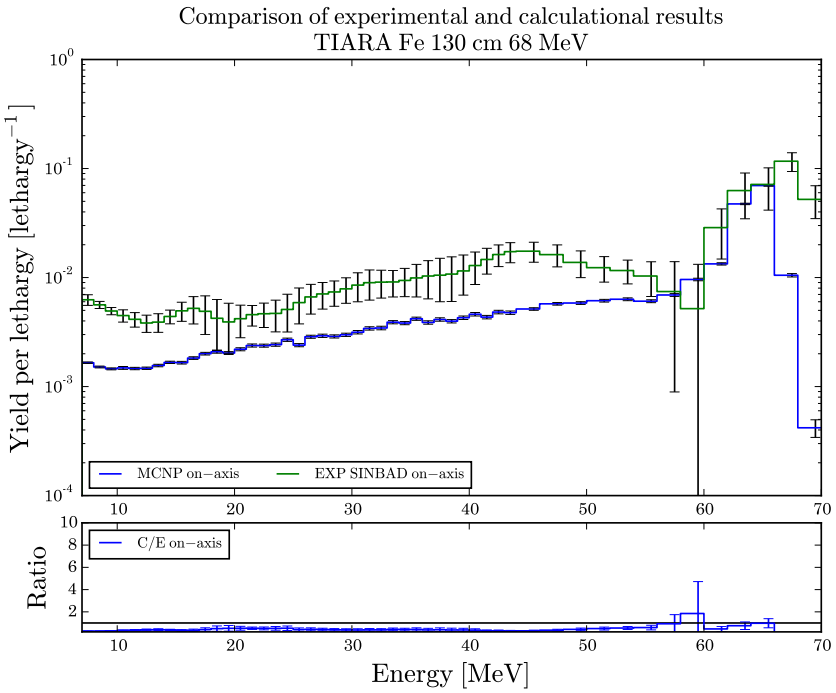

Figure 5.24: 130 cm iron shield, 68 MeV, ENDF/B-VIII

5.1.1.3 JEFF-3.3

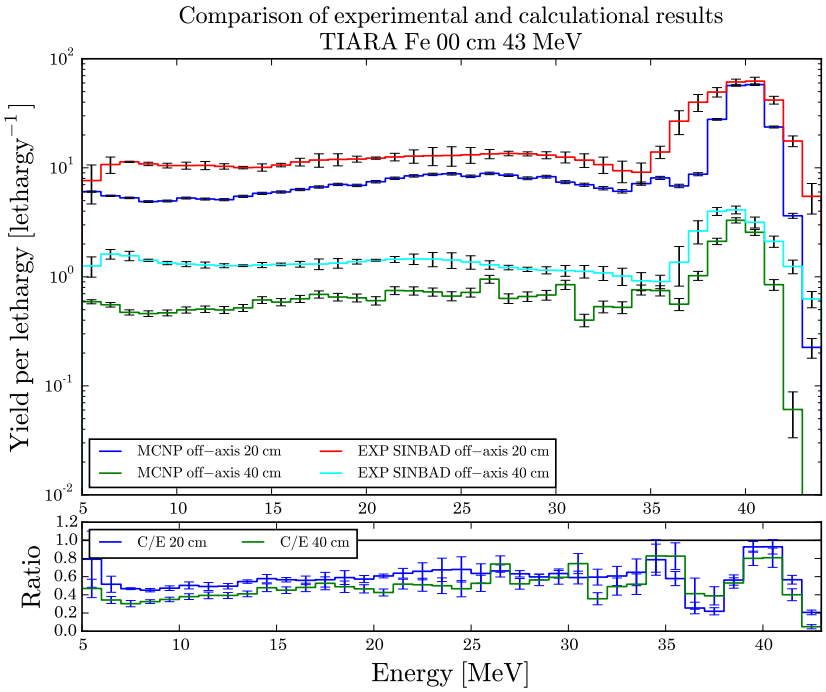

Figure 5.25: 0 cm iron shield, 43 MeV, JEFF-3.3

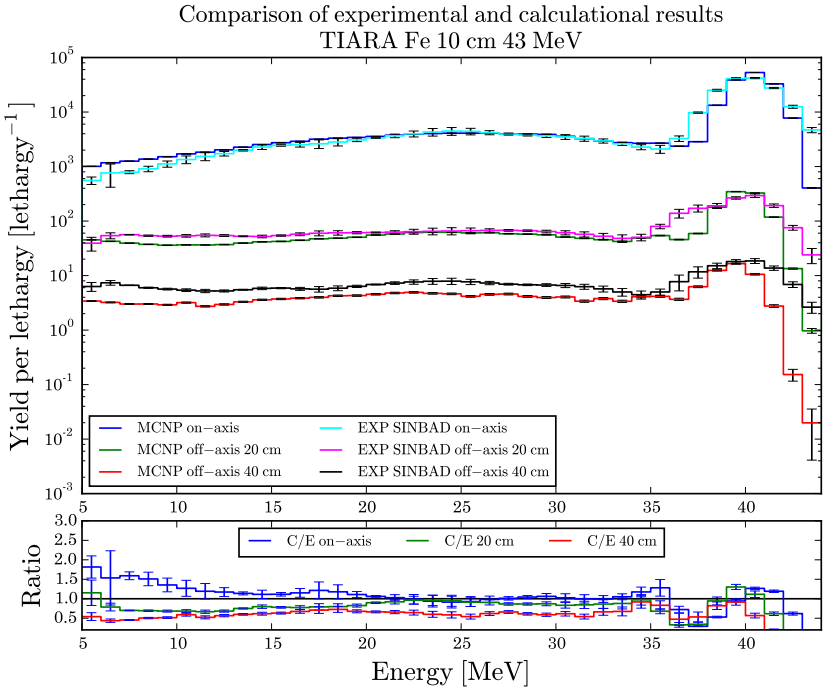

Figure 5.26: 10 cm iron shield, 43 MeV, JEFF-3.3

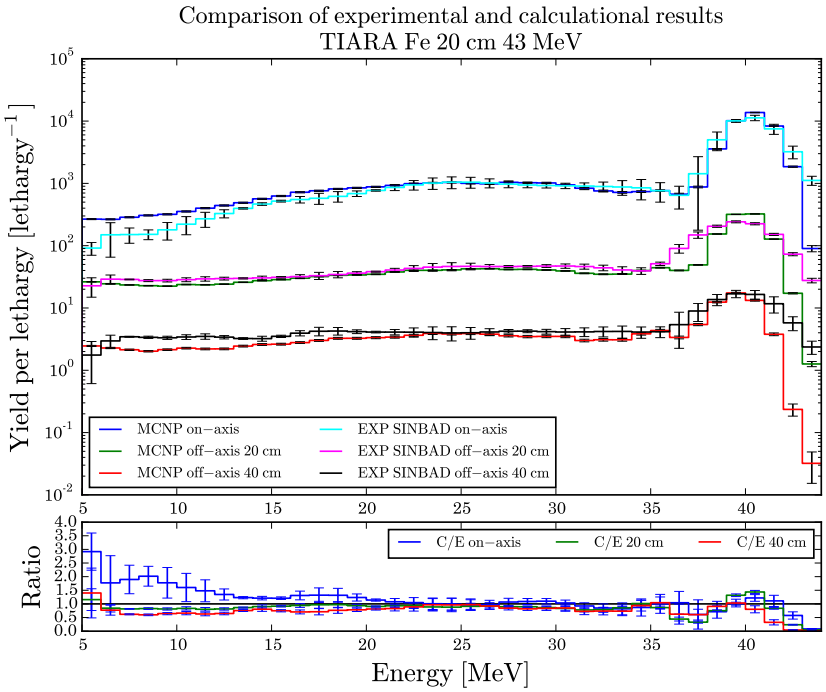

Figure 5.27: 20 cm iron shield, 43 MeV, JEFF-3.3

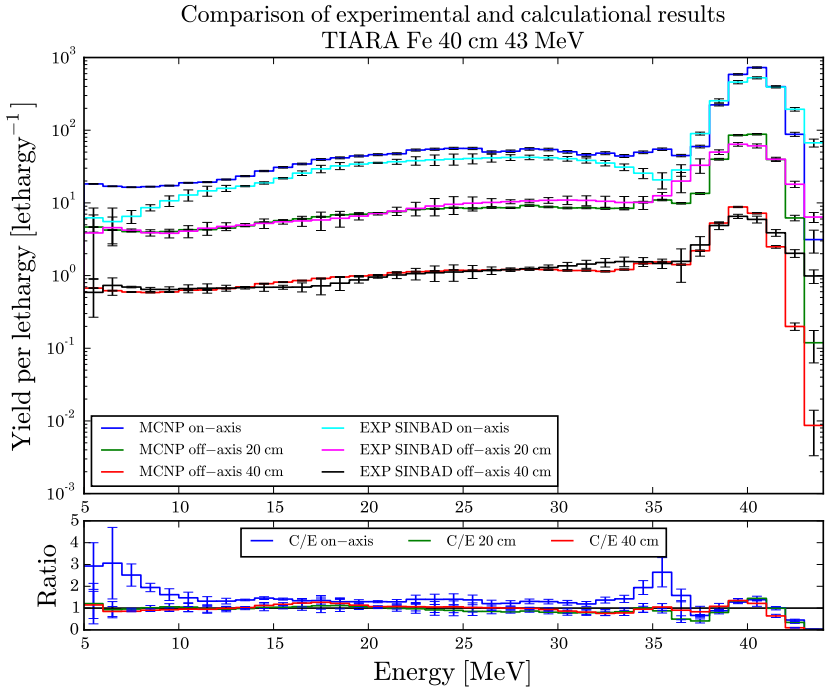

Figure 5.28: 40 cm iron shield, 43 MeV, JEFF-3.3

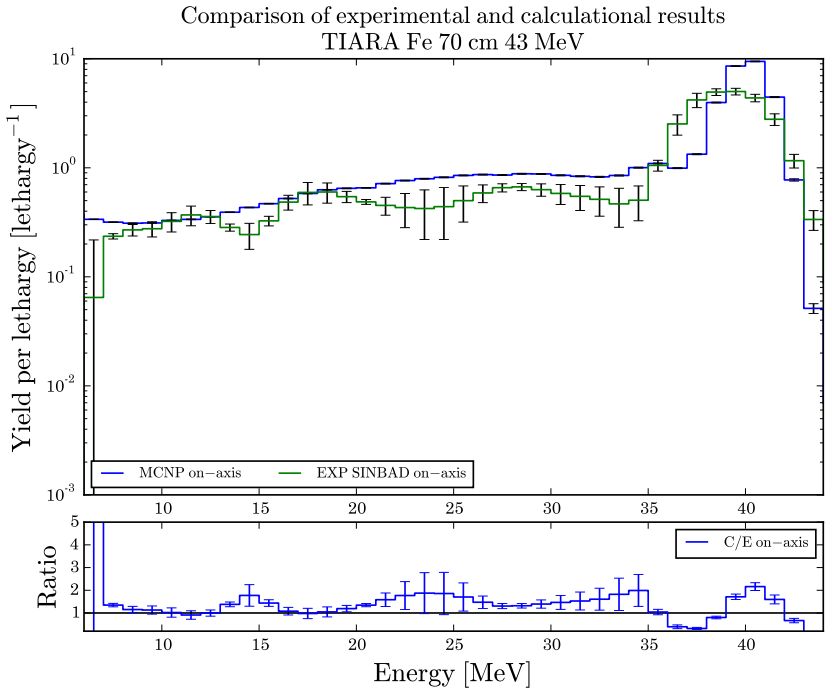

Figure 5.29: 70 cm iron shield, 43 MeV, JEFF-3.3

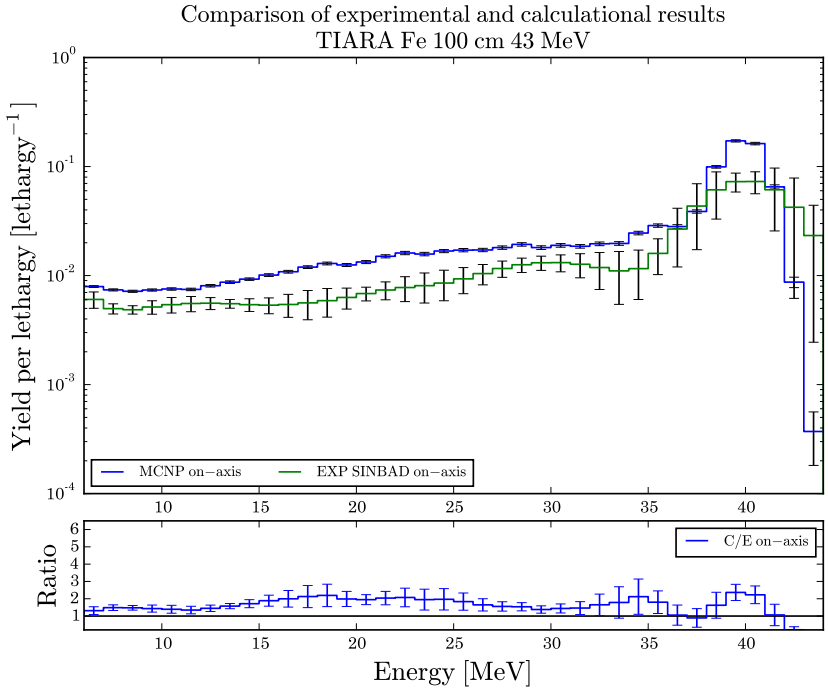

Figure 5.30: 100 cm iron shield, 43 MeV, JEFF-3.3

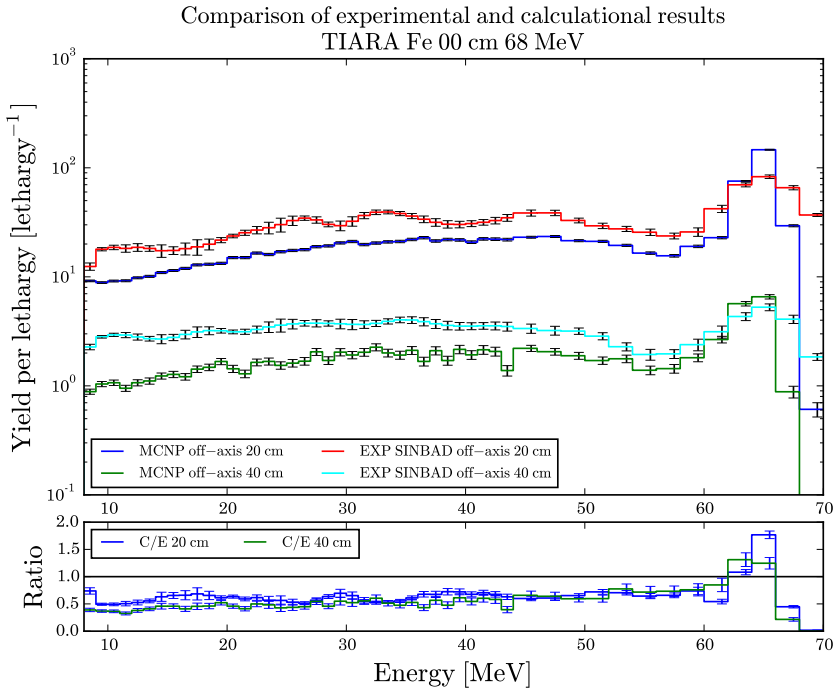

Figure 5.31: 0 cm iron shield, 68 MeV, JEFF-3.3

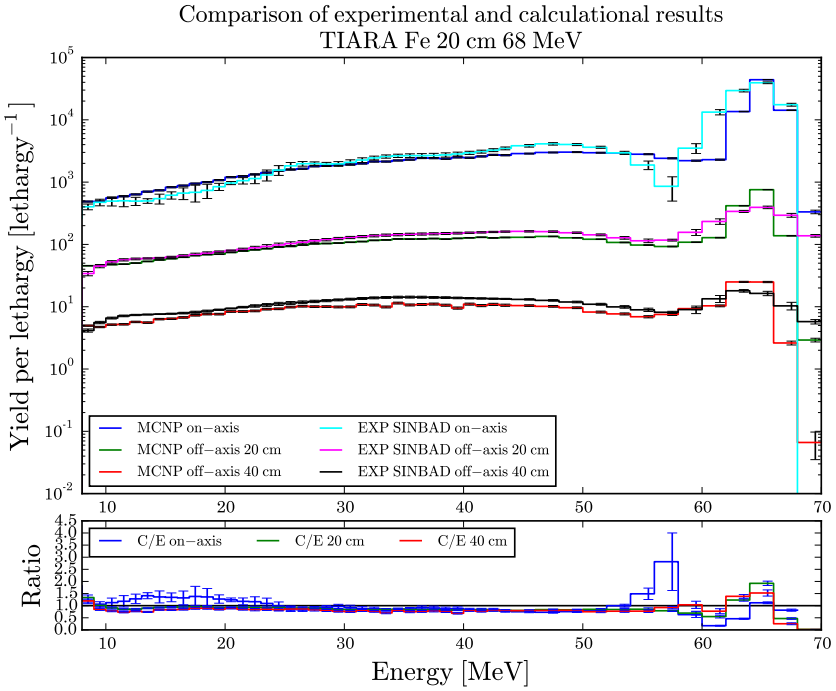

Figure 5.32: 20 cm iron shield, 68 MeV, JEFF-3.3

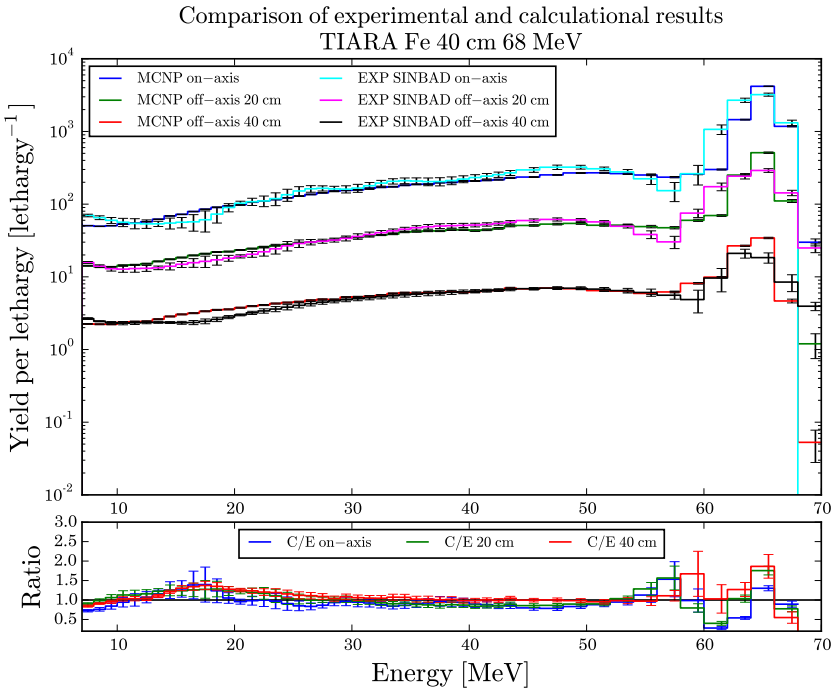

Figure 5.33: 40 cm iron shield, 68 MeV, JEFF-3.3

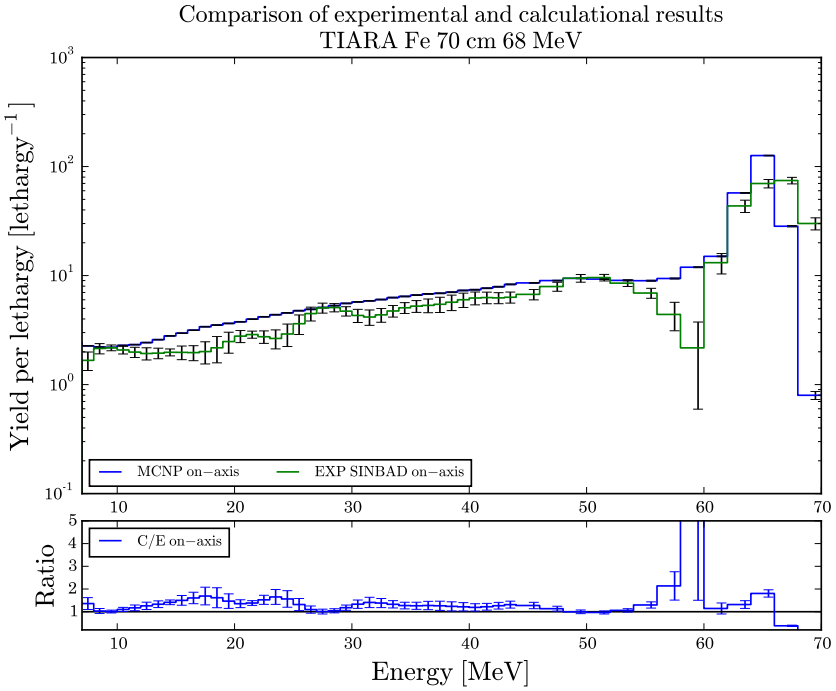

Figure 5.34: 70 cm iron shield, 68 MeV, JEFF-3.3

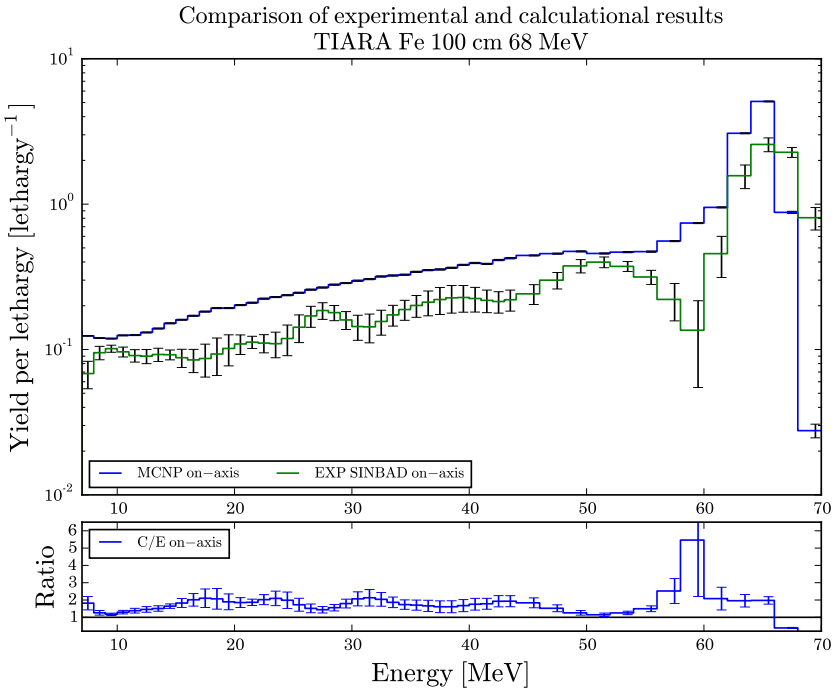

Figure 5.35: 100 cm iron shield, 68 MeV, JEFF-3.3

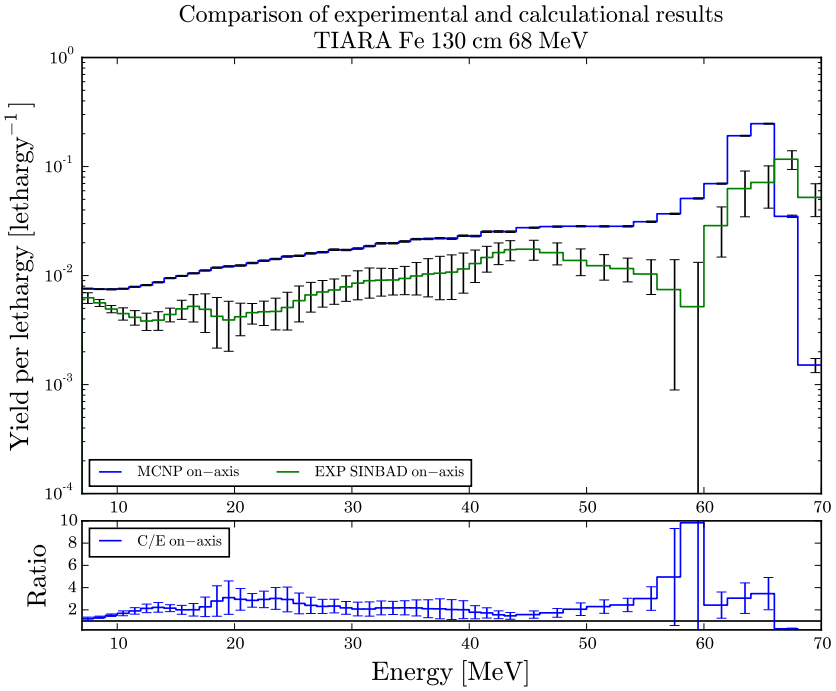

Figure 5.36: 130 cm iron shield, 68 MeV, JEFF-3.3

5.1.1.4 JENDL-4.0u

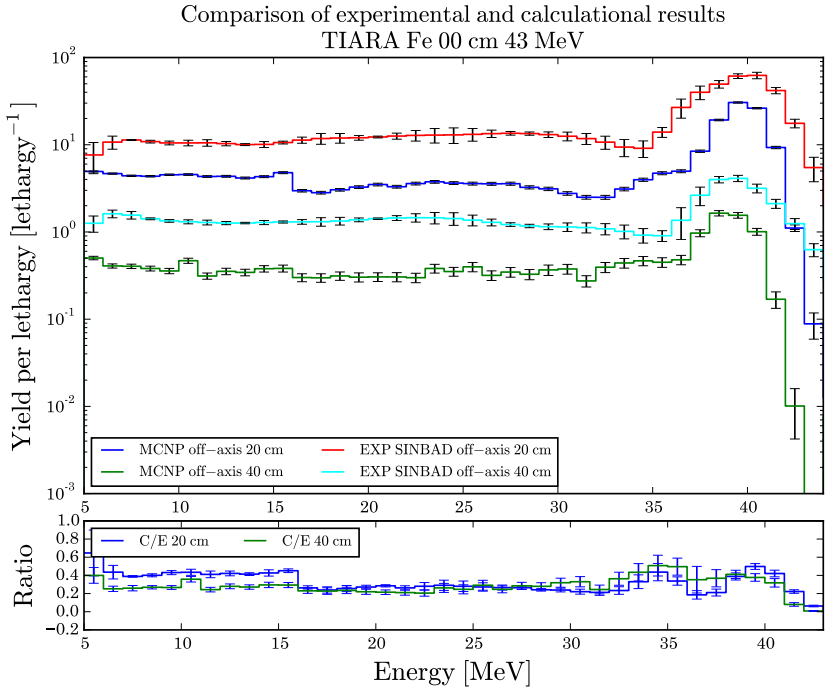

Figure 5.37: 0 cm iron shield, 43 MeV, JENDL-4.0u

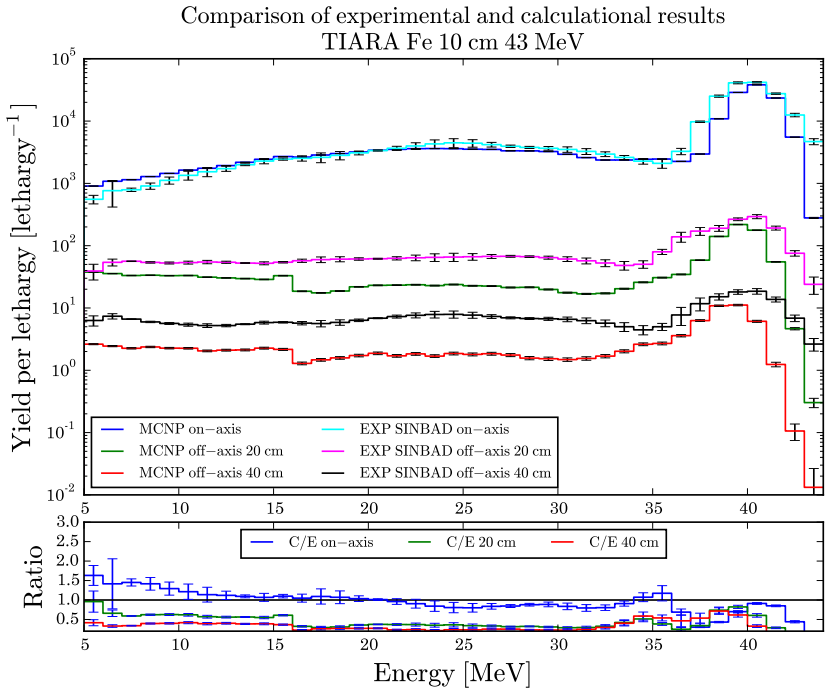

Figure 5.38: 10 cm iron shield, 43 MeV, JENDL-4.0u

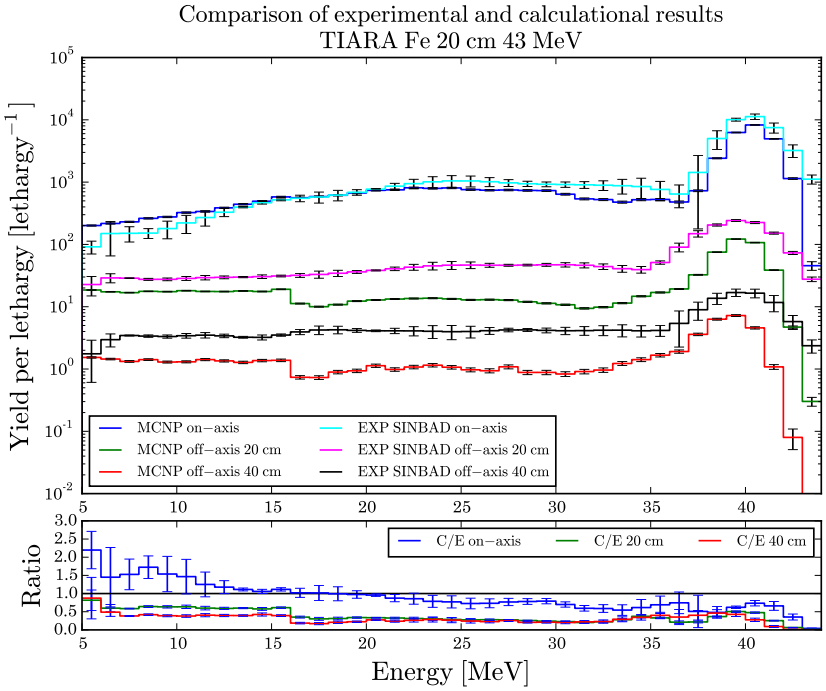

Figure 5.39: 20 cm iron shield, 43 MeV, JENDL-4.0u

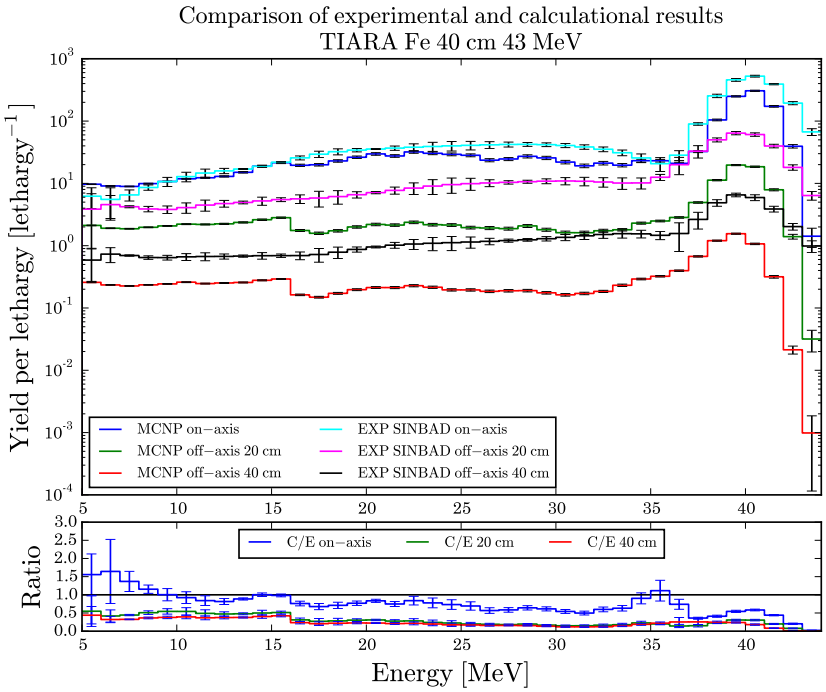

Figure 5.40: 40 cm iron shield, 43 MeV, JENDL-4.0u

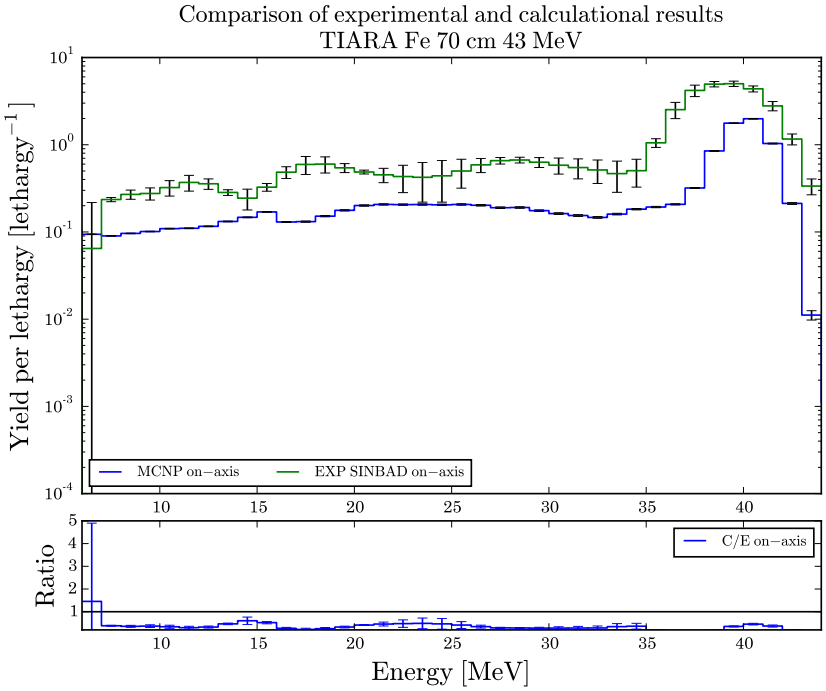

Figure 5.41: 70 cm iron shield, 43 MeV, JENDL-4.0u

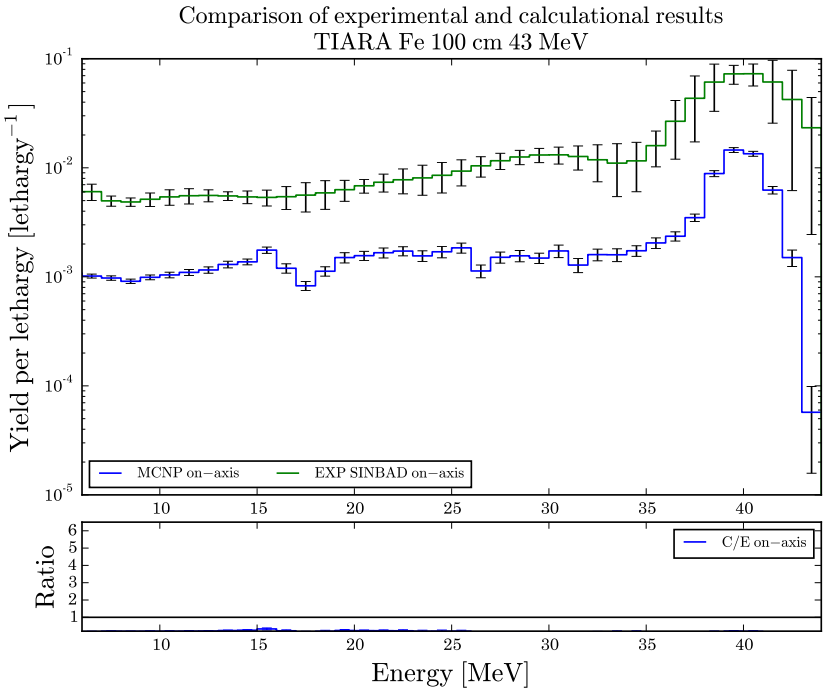

Figure 5.42: 100 cm iron shield, 43 MeV, JENDL-4.0u

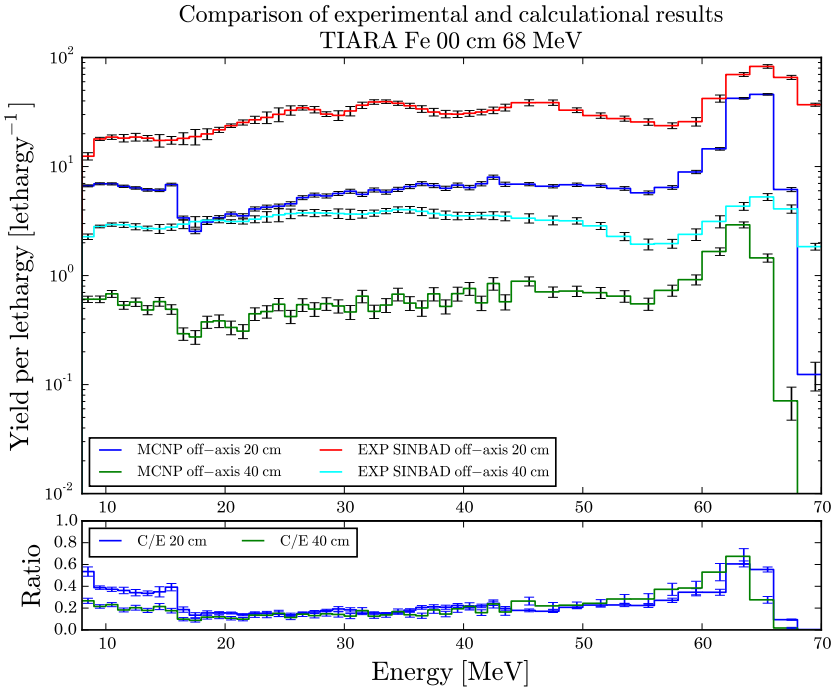

Figure 5.43: 0 cm iron shield, 68 MeV, JENDL-4.0u

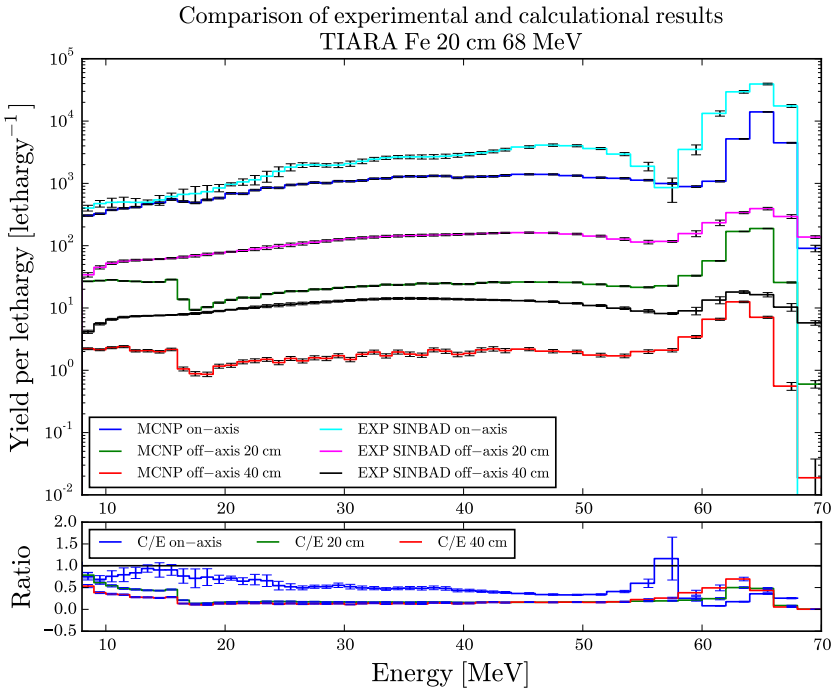

Figure 5.44: 20 cm iron shield, 68 MeV, JENDL-4.0u

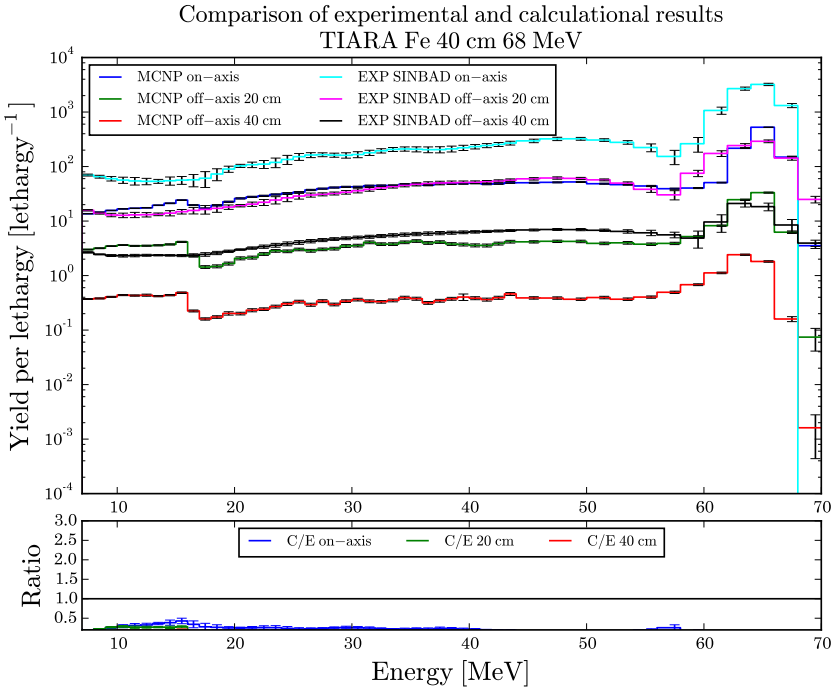

Figure 5.45: 40 cm iron shield, 68 MeV, JENDL-4.0u

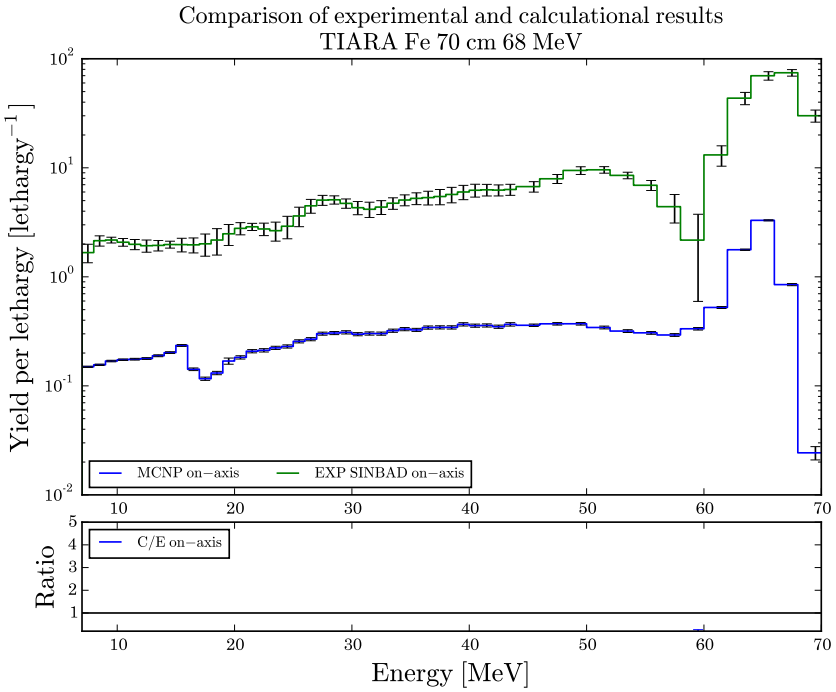

Figure 5.46: 70 cm iron shield, 68 MeV, JENDL-4.0u

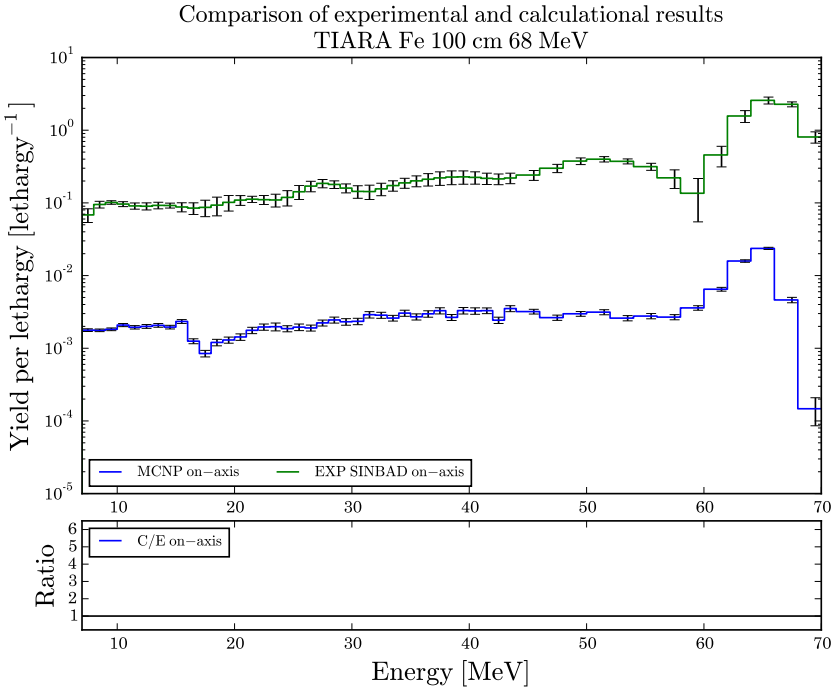

Figure 5.47: 100 cm iron shield, 68 MeV, JENDL-4.0u

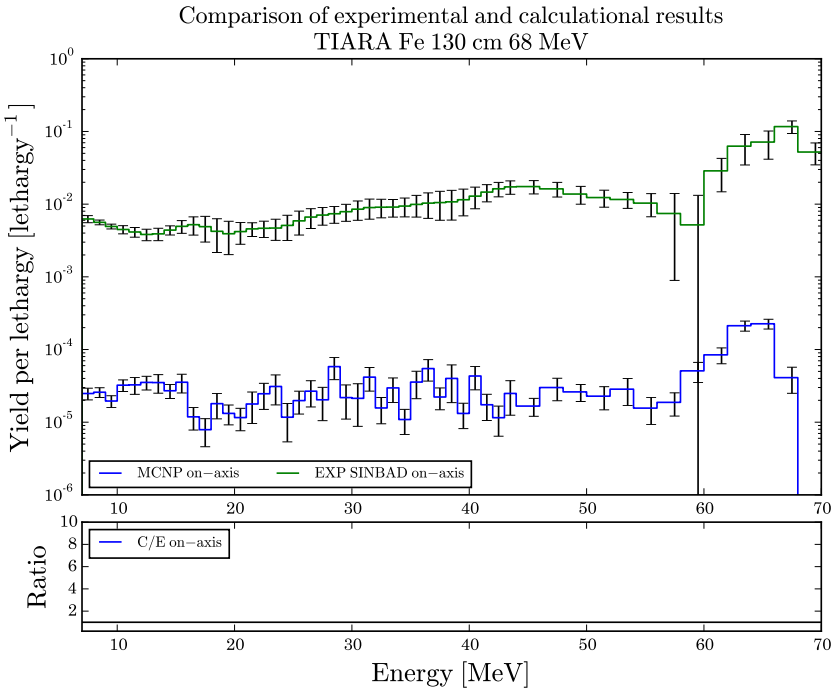

Figure 5.48: 130 cm iron shield, 68 MeV, JENDL-4.0u

5.1.2 Bonner sphere detectors

5.1.2.1 ENDF/B-VII.1

Table 5.1: Bonner sphere detectors, iron shield, 43 MeV, ENDF/B-VII.1 [$\frac{counts}{\mu C}$]

	Experiment			Calculation ENDF/B-VII.1					
Shield t./Polyethylene t.	20 cm	40 cm	100 cm	20 cm		40 cm		100 cm	
				Value	C/E	Value	C/E	Value	C/E
Bare	1.08E+03	2.32E+02	2.29E+01	1.06E+03	0.98	6.53E+02	2.81	4.26E+01	1.86
15 mm	7.71E+03	3.09E+03	1.86E+02	1.12E+04	1.46	5.73E+03	1.85	3.63E+02	1.95
30 mm	2.13E+04	7.54E+03	3.94E+02	1.71E+04	0.80	6.69E+03	0.89	4.73E+02	1.20
50 mm	2.28E+04	9.21E+03	4.72E+02	2.17E+04	0.95	7.49E+03	0.81	4.55E+02	0.96
90 mm	1.79E+04	4.57E+03	1.60E+02	1.23E+04	0.69	3.24E+03	0.71	1.44E+02	0.90

Table 5.2: Bonner sphere detectors, iron shield, 68 MeV, ENDF/B-VII.1 [$\frac{counts}{\mu C}$]

	Experiment			Calculation ENDF/B-VII.1					
Shield t./Polyethylene t.	20 cm	40 cm	100 cm	20 cm		40 cm		100 cm	
				Value	C/E	Value	C/E	Value	C/E
Bare	9.21E+02	4.95E+02	7.24E+01	1.84E+03	2.00	1.33E+03	2.69	9.10E+01	1.26
15 mm	1.09E+04	7.59E+03	6.29E+02	2.03E+04	1.87	1.16E+04	1.53	8.19E+02	1.30
30 mm	3.32E+04	1.86E+04	1.30E+03	3.13E+04	0.94	1.41E+04	0.76	1.09E+03	0.84
50 mm	5.13E+04	2.25E+04	1.34E+03	3.99E+04	0.78	1.61E+04	0.72	1.06E+03	0.79
90 mm	3.85E+04	1.34E+04	5.40E+02	2.31E+04	0.60	7.35E+03	0.55	3.47E+02	0.64

5.1.2.2 ENDF/B-VIII

Table 5.3: Bonner sphere detectors, iron shield, 43 MeV, ENDF/B-VIII [$\frac{counts}{\mu C}$]

	Experiment			Calculation ENDF/B-VIII					
Shield t./Polyethylene t.	20 cm	40 cm	100 cm	20 cm		40 cm		100 cm	
				Value	C/E	Value	C/E	Value	C/E
Bare	1.08E+03	2.32E+02	2.29E+01	1.05E+03	0.97	6.21E+02	2.68	3.89E+01	1.70
15 mm	7.71E+03	3.09E+03	1.86E+02	1.14E+04	1.48	5.41E+03	1.75	3.45E+02	1.86
30 mm	2.13E+04	7.54E+03	3.94E+02	1.74E+04	0.82	6.26E+03	0.83	4.16E+02	1.06
50 mm	2.28E+04	9.21E+03	4.72E+02	2.15E+04	0.95	6.91E+03	0.75	3.95E+02	0.84
90 mm	1.79E+04	4.57E+03	1.60E+02	1.15E+04	0.64	2.84E+03	0.62	1.22E+02	0.76

Table 5.4: Bonner sphere detectors, iron shield, 68 MeV, ENDF/B-VIII [$\frac{counts}{\mu C}$]

	Experiment			Calculation ENDF/B-VIII					
Shield t./Polyethylene t.	20 cm	40 cm	100 cm	20 cm		40 cm		100 cm	
				Value	C/E	Value	C/E	Value	C/E
Bare	9.21E+02	4.95E+02	7.24E+01	1.88E+03	2.04	1.25E+03	2.52	8.14E+01	1.12
15 mm	1.09E+04	7.59E+03	6.29E+02	2.07E+04	1.91	1.10E+04	1.45	7.68E+02	1.22
30 mm	3.32E+04	1.86E+04	1.30E+03	3.23E+04	0.97	1.32E+04	0.71	9.28E+02	0.71
50 mm	5.13E+04	2.25E+04	1.34E+03	4.02E+04	0.78	1.48E+04	0.66	8.78E+02	0.65
90 mm	3.85E+04	1.34E+04	5.40E+02	2.17E+04	0.56	6.37E+03	0.47	2.77E+02	0.51

5.1.2.3 JEFF-3.3

Table 5.5: Bonner sphere detectors, iron shield, 43 MeV, JEFF-3.3 [$\frac{counts}{\mu C}$]

	Experiment			Calculation JEFF-3.3					
Shield t./Polyethylene t.	20 cm	40 cm	100 cm	20 cm		40 cm		100 cm	
				Value	C/E	Value	C/E	Value	C/E
Bare	1.08E+03	2.32E+02	2.29E+01	1.09E+03	1.01	6.69E+02	2.88	4.79E+01	2.09
15 mm	7.71E+03	3.09E+03	1.86E+02	1.16E+04	1.51	6.05E+03	1.96	3.96E+02	2.14
30 mm	2.13E+04	7.54E+03	3.94E+02	1.80E+04	0.85	6.92E+03	0.92	4.80E+02	1.22
50 mm	2.28E+04	9.21E+03	4.72E+02	2.27E+04	1.00	7.71E+03	0.84	4.49E+02	0.95
90 mm	1.79E+04	4.57E+03	1.60E+02	1.25E+04	0.70	3.27E+03	0.72	1.36E+02	0.85

Table 5.6: Bonner sphere detectors, iron shield, 68 MeV, JEFF-3.3 [$\frac{counts}{\mu C}$]

	Experiment			Calculation JEFF-3.3					
Shield t./Polyethylene t.	20 cm	40 cm	100 cm	20 cm		40 cm		100 cm	
				Value	C/E	Value	C/E	Value	C/E
Bare	9.21E+02	4.95E+02	7.24E+01	1.86E+03	2.02	1.26E+03	2.55	9.51E+01	1.31
15 mm	1.09E+04	7.59E+03	6.29E+02	2.03E+04	1.86	1.17E+04	1.55	8.79E+02	1.40
30 mm	3.32E+04	1.86E+04	1.30E+03	3.12E+04	0.94	1.43E+04	0.77	1.11E+03	0.86
50 mm	5.13E+04	2.25E+04	1.34E+03	3.98E+04	0.77	1.63E+04	0.73	1.07E+03	0.80
90 mm	3.85E+04	1.34E+04	5.40E+02	2.27E+04	0.59	7.37E+03	0.55	3.43E+02	0.63

5.1.2.4 JENDL-4.0u

Table 5.7: Bonner sphere detectors, iron shield, 43 MeV, JENDL-4.0u [$\frac{counts}{\mu C}$]

	Experiment			Calculation JENDL-4.0u					
Shield t./Polyethylene t.	20 cm	40 cm	100 cm	20 cm		40 cm		100 cm	
				Value	C/E	Value	C/E	Value	C/E
Bare	1.08E+03	2.32E+02	2.29E+01	9.65E+02	0.89	5.29E+02	2.28	3.32E+01	1.45
15 mm	7.71E+03	3.09E+03	1.86E+02	1.03E+04	1.33	4.71E+03	1.52	2.95E+02	1.59
30 mm	2.13E+04	7.54E+03	3.94E+02	1.58E+04	0.74	5.34E+03	0.71	3.51E+02	0.89
50 mm	2.28E+04	9.21E+03	4.72E+02	1.95E+04	0.86	5.81E+03	0.63	3.25E+02	0.69
90 mm	1.79E+04	4.57E+03	1.60E+02	1.03E+04	0.58	2.33E+03	0.51	9.88E+01	0.62

Table 5.8: Bonner sphere detectors, iron shield, 68 MeV, JENDL-4.0u [$\frac{counts}{\mu C}$]

	Experiment			Calculation JENDL-4.0u					
Shield t./Polyethylene t.	20 cm	40 cm	100 cm	20 cm		40 cm		100 cm	
				Value	C/E	Value	C/E	Value	C/E
Bare	9.21E+02	4.95E+02	7.24E+01	1.47E+03	1.59	8.47E+02	1.71	5.06E+01	0.70
15 mm	1.09E+04	7.59E+03	6.29E+02	1.62E+04	1.49	7.56E+03	1.00	4.75E+02	0.76
30 mm	3.32E+04	1.86E+04	1.30E+03	2.50E+04	0.76	8.55E+03	0.46	5.64E+02	0.43
50 mm	5.13E+04	2.25E+04	1.34E+03	3.08E+04	0.60	9.31E+03	0.41	5.23E+02	0.39
90 mm	3.85E+04	1.34E+04	5.40E+02	1.59E+04	0.41	3.73E+03	0.28	1.59E+02	0.29

5.1.3 Fission cells

5.1.3.1 ENDF/B-VII.1

Table 5.9: Fission cells, iron shield, 43 MeV, ENDF/B-VII.1 [$\frac{n}{\mu C}$]

	Experiment				Calculation ENDF/B-VII.1			
Fission c./Position (shield t., axis offset)	^{238}U		^{232}Th		^{238}U		^{232}Th	
	Value	err. [%]	Value	err. [%]	Value	C/E	Value	C/E
0,0	8.01E-20	0.59	3.27E-20	0.24	6.12E+04	0.76	2.62E+04	0.80
10,0	2.43E-20	1	1.02E-20	0.89	2.09E+04	0.86	8.90E+03	0.87
20,0	5.64E-21	1.8	2.49E-21	0.99	5.47E+03	0.97	2.32E+03	0.93
40,0	2.97E-22	3.4	1.16E-22	3.3	3.11E+02	1.05	1.28E+02	1.10
70,0	6.96E-24	9.8	1.79E-24	28	5.28E+00	0.76	2.05E+00	1.14
0,20	1.00E-22	4.3			2.53E+01	0.25		
10,20	2.47E-22	5.7			2.70E+02	1.09		
20,20	1.95E-22	3.5	6.12E-23	17	2.06E+02	1.06	7.48E+01	1.22
40,20	5.14E-23	5	1.77E-23	14	5.09E+01	0.99	1.92E+01	1.09
70,20	3.61E-24	20	1.53E-24	21	2.50E+00	0.69	9.42E-01	0.62

Table 5.10: Fission cells, iron shield, 68 MeV, ENDF/B-VII.1 [$\frac{n}{\mu C}$]

	Experiment				Calculation ENDF/B-VII.1			
Fission c./Position (shield t., axis offset)	^{238}U		^{232}Th		^{238}U		^{232}Th	
	Value	err.	Value	err.	Value	C/E	Value	C/E
0,0	1.18E-19	0.38	5.71E-20	0.49	9.83E+04	0.83	4.80E+04	0.84
20,0	1.53E-20	0.66	7.70E-21	0.9	1.36E+04	0.89	6.59E+03	0.86
40,0	1.23E-21	2.3	5.47E-22	3.3	1.15E+03	0.93	5.44E+02	0.99
70,0	3.18E-23	7.1	1.08E-23	12	3.66E+01	1.15	1.64E+01	1.52
100,0	2.59E-24	11	8.51E-25	19	1.68E+00	0.65	7.20E-01	0.85
20,20	7.14E-23	4	4.69E-23	4.7	4.27E+02	5.98	1.65E+02	3.51
40,20	1.68E-22	3.4	1.15E-22	4	1.68E+02	1.00	7.10E+01	0.62
70,20	1.58E-23	6	7.12E-24	8.6	1.66E+01	1.05	7.20E+00	1.01
100,20	2.57E-24	9.3	9.07E-25	15	1.13E+00	0.44	4.82E-01	0.53
130,20	1.08E-24	12	4.59E-25	18	7.18E-02	0.07	2.92E-02	0.06

5.1.3.2 ENDF/B-VIII

Table 5.11: Fission cells, iron shield, 43 MeV, ENDF/B-VIII [$\frac{n}{\mu C}$]

	Experiment				Calculation ENDF/B-VIII			
Fission c./Position (shield t., axis offset)	^{238}U		^{232}Th		^{238}U		^{232}Th	
	Value	err. [%]	Value	err. [%]	Value	C/E	Value	C/E
0,0	8.01E-20	0.59	3.27E-20	0.24	6.12E+04	0.76	2.62E+04	0.80
10,0	2.43E-20	1	1.02E-20	0.89	1.92E+04	0.79	8.14E+03	0.80
20,0	5.64E-21	1.8	2.49E-21	0.99	4.68E+03	0.83	1.98E+03	0.80
40,0	2.97E-22	3.4	1.16E-22	3.3	2.28E+02	0.77	9.45E+01	0.81
70,0	6.96E-24	9.8	1.79E-24	28	2.80E+00	0.40	1.09E+00	0.61
0,20	1.00E-22	4.3			2.50E+01	0.25		
10,20	2.47E-22	5.7			2.11E+02	0.86		
20,20	1.95E-22	3.5	6.12E-23	17	1.51E+02	0.78	5.46E+01	0.89
40,20	5.14E-23	5	1.77E-23	14	2.91E+01	0.57	1.10E+01	0.62
70,20	3.61E-24	20	1.53E-24	21	1.17E+00	0.32	4.35E-01	0.28

Table 5.12: Fission cells, iron shield, 68 MeV, ENDF/B-VIII [$\frac{n}{\mu C}$]

	Experiment				Calculation ENDF/B-VII.1			
Fission c./Position (shield t., axis offset)	^{238}U		^{232}Th		^{238}U		^{232}Th	
	Value	err.	Value	err.	Value	C/E	Value	C/E
0,0	1.18E-19	0.38	5.71E-20	0.49	9.83E+04	0.83	4.80E+04	0.84
20,0	1.53E-20	0.66	7.70E-21	0.9	1.13E+04	0.74	5.50E+03	0.71
40,0	1.23E-21	2.3	5.47E-22	3.3	8.15E+02	0.66	3.92E+02	0.72
70,0	3.18E-23	7.1	1.08E-23	12	1.84E+01	0.58	8.41E+00	0.78
100,0	2.59E-24	11	8.51E-25	19	6.14E-01	0.24	2.69E-01	0.32
20,20	7.14E-23	4	4.69E-23	4.7	2.86E+02	4.01	1.08E+02	2.30
40,20	1.68E-22	3.4	1.15E-22	4	1.00E+02	0.60	4.23E+01	0.37
70,20	1.58E-23	6	7.12E-24	8.6	7.54E+00	0.48	3.31E+00	0.46
100,20	2.57E-24	9.3	9.07E-25	15	3.98E-01	0.15	1.71E-01	0.19
130,20	1.08E-24	12	4.59E-25	18	2.14E-02	0.02	8.22E-03	0.02

5.1.3.3 JEFF-3.3

Table 5.13: Fission cells, iron shield, 43 MeV, JEFF-3.3 [$\frac{n}{\mu C}$]

	Experiment				Calculation JEFF-3.3			
Fission c./Position (shield t., axis offset)	^{238}U		^{232}Th		^{238}U		^{232}Th	
	Value	err. [%]	Value	err. [%]	Value	C/E	Value	C/E
0,0	8.01E-20	0.59	3.27E-20	0.24	6.12E+04	0.76	2.62E+04	0.80
10,0	2.43E-20	1	1.02E-20	0.89	2.02E+04	0.83	8.59E+03	0.84
20,0	5.64E-21	1.8	2.49E-21	0.99	5.18E+03	0.92	2.19E+03	0.88
40,0	2.97E-22	3.4	1.16E-22	3.3	2.79E+02	0.94	1.15E+02	0.99
70,0	6.96E-24	9.8	1.79E-24	28	4.18E+00	0.60	1.61E+00	0.90
0,20	1.00E-22	4.3			2.55E+01	0.26		
10,20	2.47E-22	5.7			2.44E+02	0.99		
20,20	1.95E-22	3.5	6.12E-23	17	1.85E+02	0.95	6.64E+01	1.09
40,20	5.14E-23	5	1.77E-23	14	4.12E+01	0.80	1.53E+01	0.86
70,20	3.61E-24	20	1.53E-24	21	1.89E+00	0.52	6.98E-01	0.46

Table 5.14: Fission cells, iron shield, 68 MeV, JEFF-3.3 [$\frac{n}{\mu C}$]

	Experiment				Calculation ENDF/B-VII.1			
Fission c./Position (shield t., axis offset)	^{238}U		^{232}Th		^{238}U		^{232}Th	
	Value	err.	Value	err.	Value	C/E	Value	C/E
0,0	1.18E-19	0.38	5.71E-20	0.49	9.83E+04	0.83	4.80E+04	0.84
20,0	1.53E-20	0.66	7.70E-21	0.9	1.34E+04	0.87	6.54E+03	0.85
40,0	1.23E-21	2.3	5.47E-22	3.3	1.13E+03	0.92	5.44E+02	1.00
70,0	3.18E-23	7.1	1.08E-23	12	3.79E+01	1.19	1.73E+01	1.60
100,0	2.59E-24	11	8.51E-25	19	1.86E+00	0.72	8.22E-01	0.97
20,20	7.14E-23	4	4.69E-23	4.7	4.25E+02	5.95	1.68E+02	3.59
40,20	1.68E-22	3.4	1.15E-22	4	1.78E+02	1.06	7.77E+01	0.68
70,20	1.58E-23	6	7.12E-24	8.6	1.80E+01	1.14	8.00E+00	1.12
100,20	2.57E-24	9.3	9.07E-25	15	1.28E+00	0.50	5.57E-01	0.61
130,20	1.08E-24	12	4.59E-25	18	9.07E-02	0.08	3.86E-02	0.08

5.1.3.4 JENDL-4.0u

Table 5.15: Fission cells, iron shield, 43 MeV, JENDL-4.0u [$\frac{n}{\mu C}$]

	Experiment				Calculation JENDL-4.0u			
Fission c./Position (shield t., axis offset)	^{238}U		^{232}Th		^{238}U		^{232}Th	
	Value	err. [%]	Value	err. [%]	Value	C/E	Value	C/E
0,0	8.01E-20	0.59	3.27E-20	0.24	6.10E+04	0.76	2.62E+04	0.80
10,0	2.43E-20	1	1.02E-20	0.89	1.67E+04	0.69	7.00E+03	0.69
20,0	5.64E-21	1.8	2.49E-21	0.99	3.64E+03	0.64	1.51E+03	0.61
40,0	2.97E-22	3.4	1.16E-22	3.3	1.41E+02	0.47	5.66E+01	0.49
70,0	6.96E-24	9.8	1.79E-24	28	1.11E+00	0.16	4.09E-01	0.23
0,20	1.00E-22	4.3			2.95E+01	0.30		
10,20	2.47E-22	5.7			1.80E+02	0.73		
20,20	1.95E-22	3.5	6.12E-23	17	1.00E+02	0.51	3.33E+01	0.54
40,20	5.14E-23	5	1.77E-23	14	1.44E+01	0.28	4.87E+00	0.27
70,20	3.61E-24	20	1.53E-24	21	3.70E-01	0.10	1.21E-01	0.08

Table 5.16: Fission cells, iron shield, 68 MeV, JENDL-4.0u [$\frac{n}{\mu C}$]

	Experiment				Calculation ENDF/B-VII.1			
Fission c./Position (shield t., axis offset)	^{238}U		^{232}Th		^{238}U		^{232}Th	
	Value	err.	Value	err.	Value	C/E	Value	C/E
0,0	1.18E-19	0.38	5.71E-20	0.49	9.82E+04	0.83	4.80E+04	0.84
20,0	1.53E-20	0.66	7.70E-21	0.9	6.13E+03	0.40	2.86E+03	0.37
40,0	1.23E-21	2.3	5.47E-22	3.3	2.45E+02	0.20	1.10E+02	0.20
70,0	3.18E-23	7.1	1.08E-23	12	1.86E+00	0.06	7.46E-01	0.07
100,0	2.59E-24	11	8.51E-25	19	2.23E-02	0.01	6.21E-03	0.01
20,20	7.14E-23	4	4.69E-23	4.7	1.67E+02	2.33	5.94E+01	1.27
40,20	1.68E-22	3.4	1.15E-22	4	2.49E+01	0.15	9.10E+00	0.08
70,20	1.58E-23	6	7.12E-24	8.6	6.16E-01	0.04	2.17E-01	0.03
100,20	2.57E-24	9.3	9.07E-25	15	1.65E-02	0.01	3.51E-03	0.00
130,20	1.08E-24	12	4.59E-25	18	1.76E-03	0.00	4.16E-05	0.00

5.2 Concrete

The following chapters contain results for the concrete shield cases for the BC 501A liquid scintillator detectors (5.2.2), Bonner sphere detectors (5.2.2) and Fission cells (5.2.3). The sample calculation were performed with the ENDF/B-VII.1, ENDF/B-VIII, JEFF-3.3 and JENDL-4.0u nuclear data libraries.

5.2.1 BC501A liquid scintillation detector

5.2.1.1 ENDF/B-VII.1

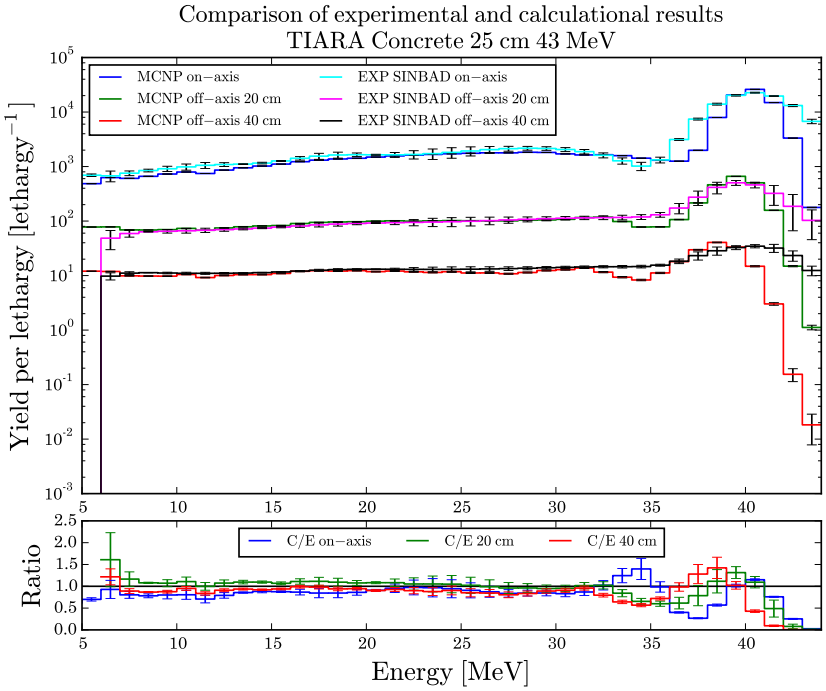

Figure 5.49: 25 cm concrete shield, 43 MeV, ENDF/B-VII.1

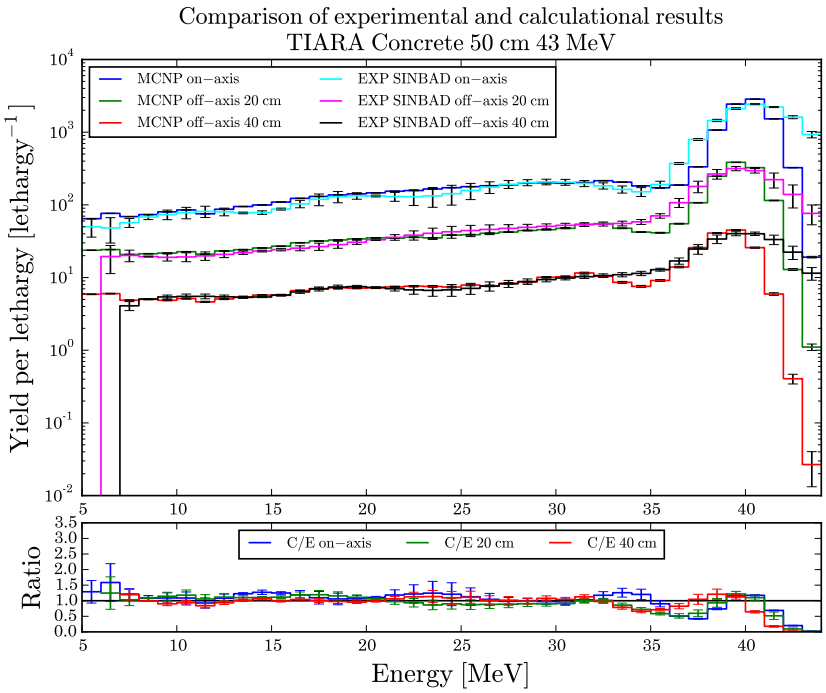

Figure 5.50: 50 cm concrete shield, 43 MeV, ENDF/B-VII.1

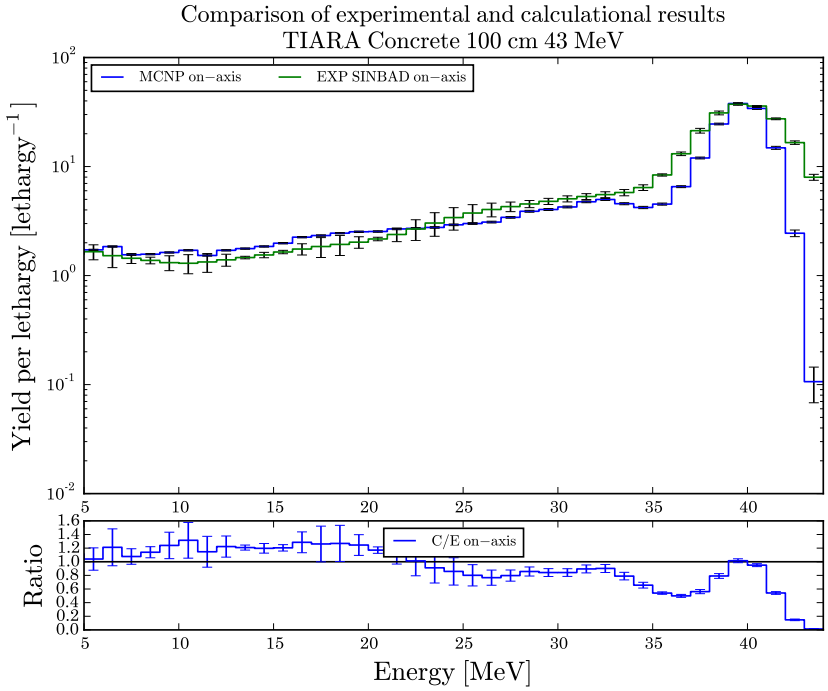

Figure 5.51: 100 cm concrete shield, 43 MeV, ENDF/B-VII.1

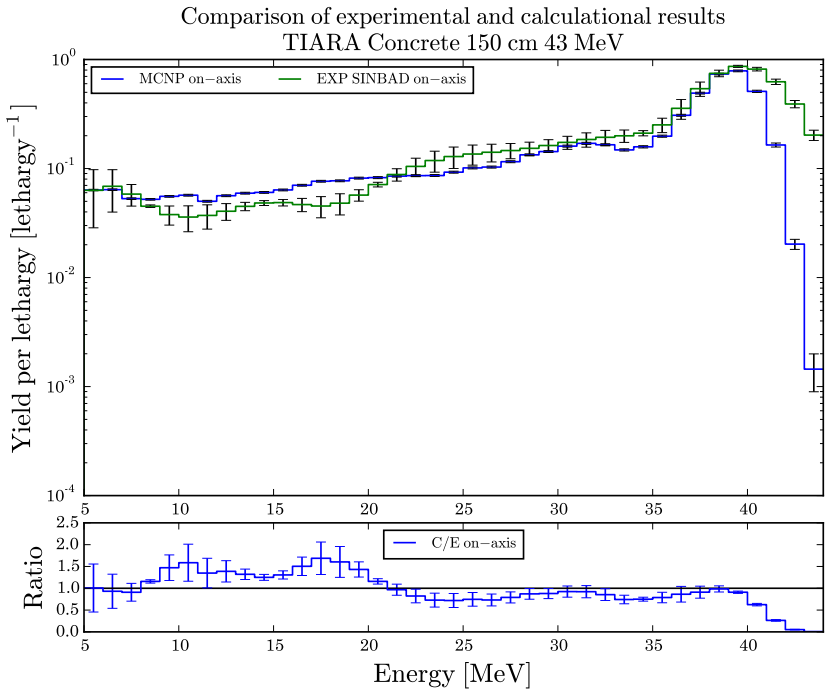

Figure 5.52: 150 cm concrete shield, 43 MeV, ENDF/B-VII.1

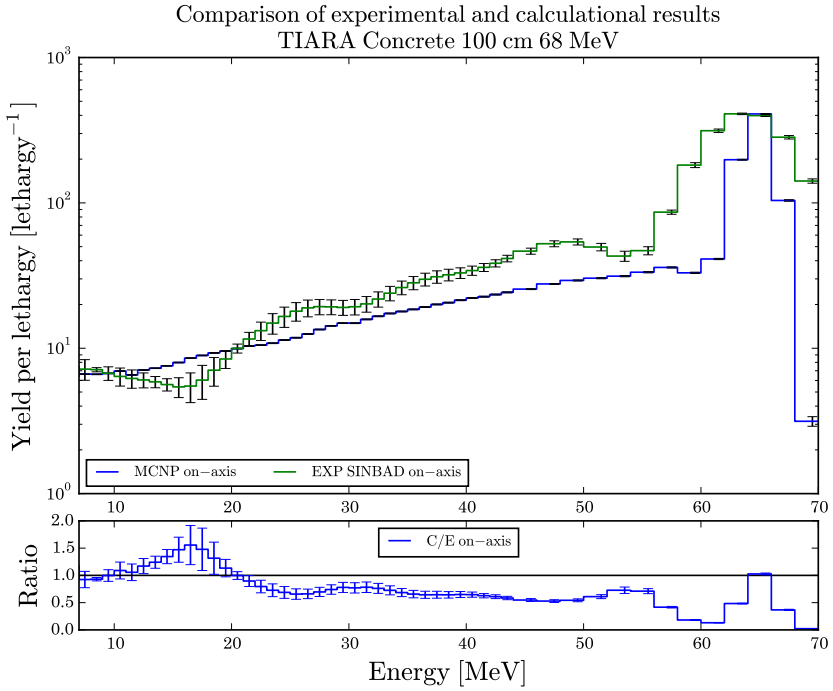

Figure 5.53: 100 cm concrete shield, 68 MeV, ENDF/B-VII.1

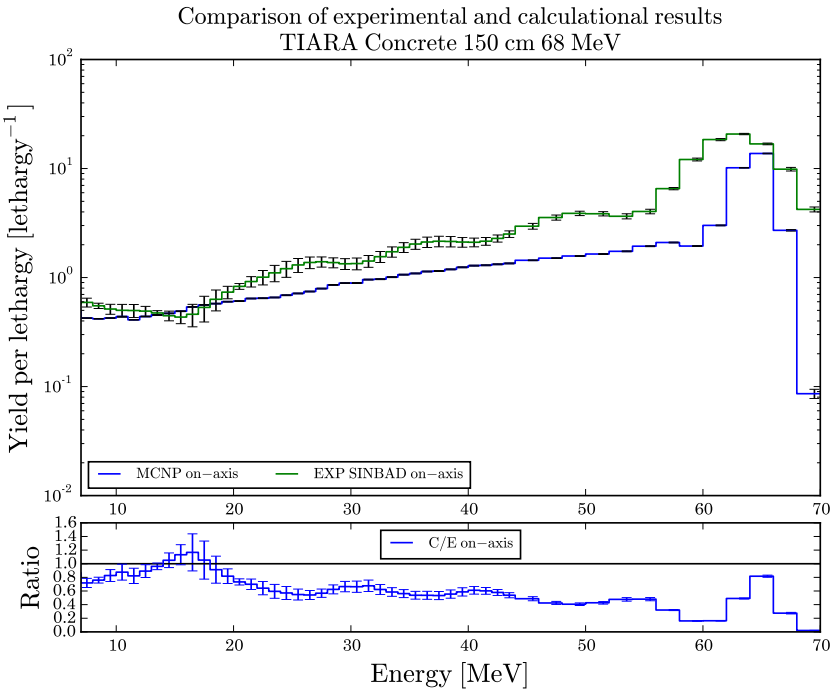

Figure 5.54: 150 cm concrete shield, 68 MeV, ENDF/B-VII.1

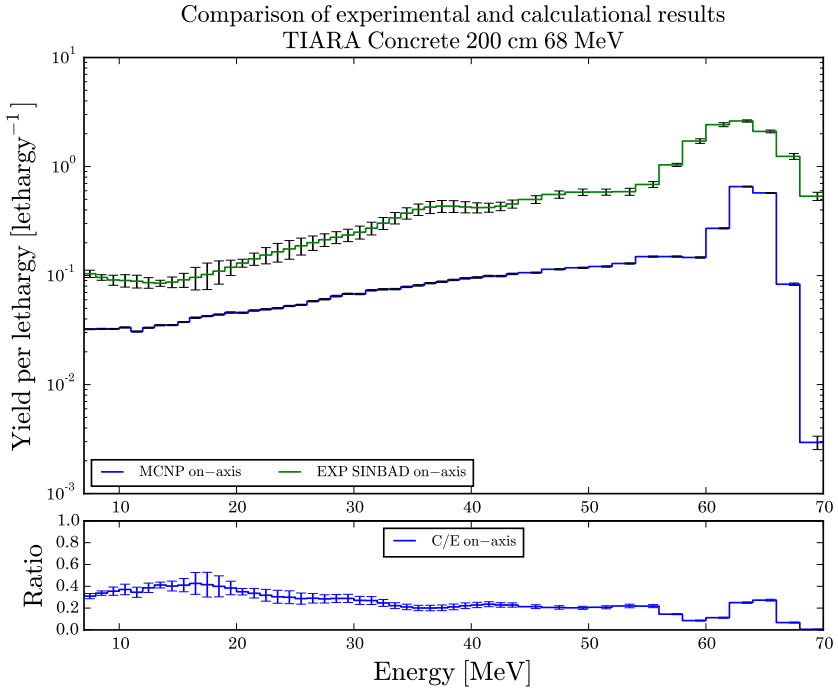

Figure 5.55: 200 cm concrete shield, 68 MeV, ENDF/B-VII.1

5.2.1.2 ENDF/B-VIII

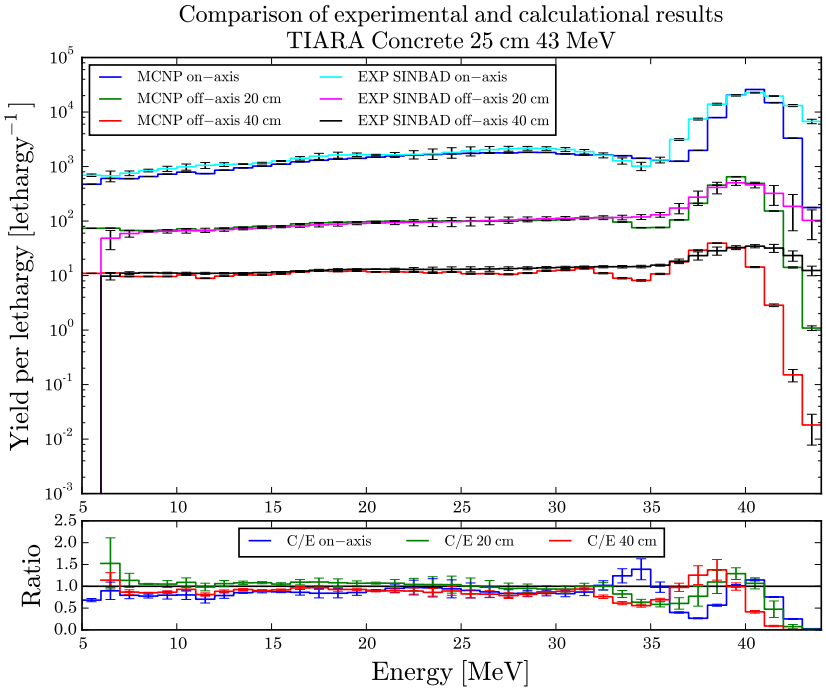

Figure 5.56: 25 cm concrete shield, 43 MeV, ENDF/B-VIII

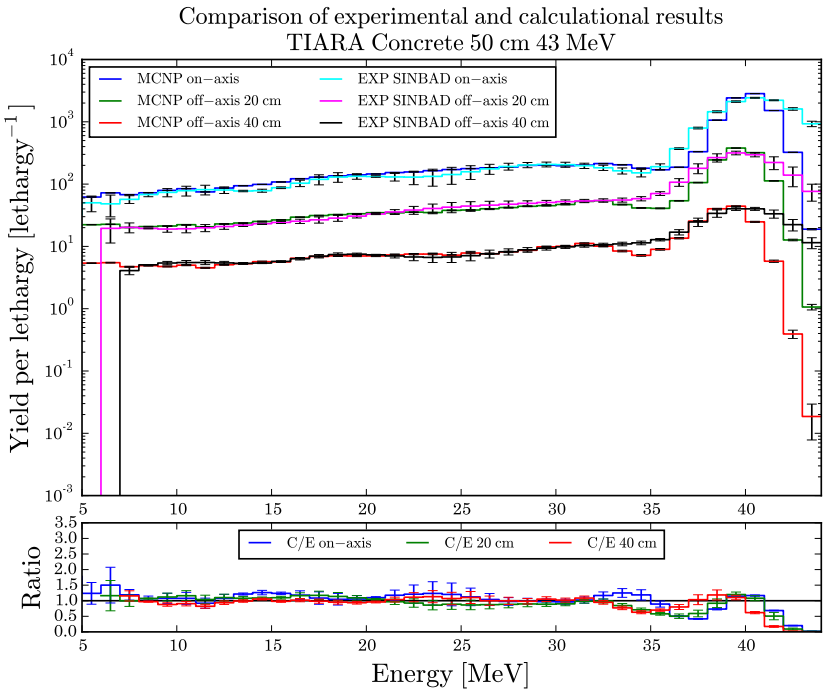

Figure 5.57: 50 cm concrete shield, 43 MeV, ENDF/B-VIII

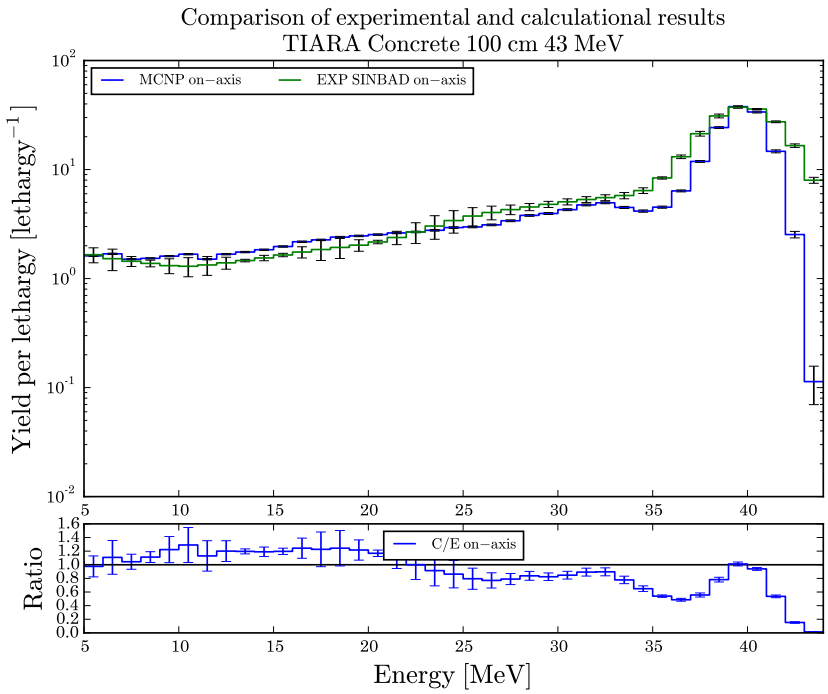

Figure 5.58: 100 cm concrete shield, 43 MeV, ENDF/B-VIII

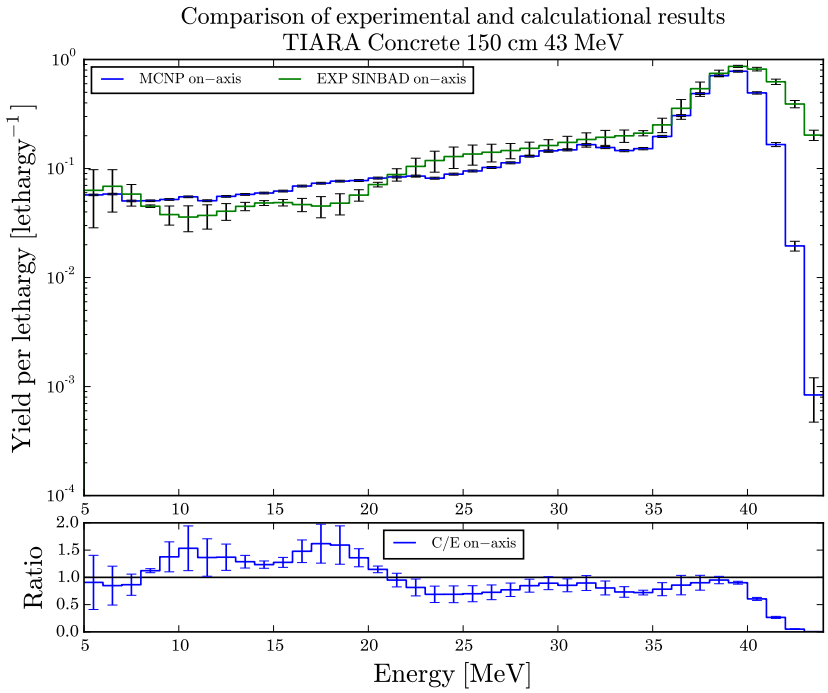

Figure 5.59: 150 cm concrete shield, 43 MeV, ENDF/B-VIII

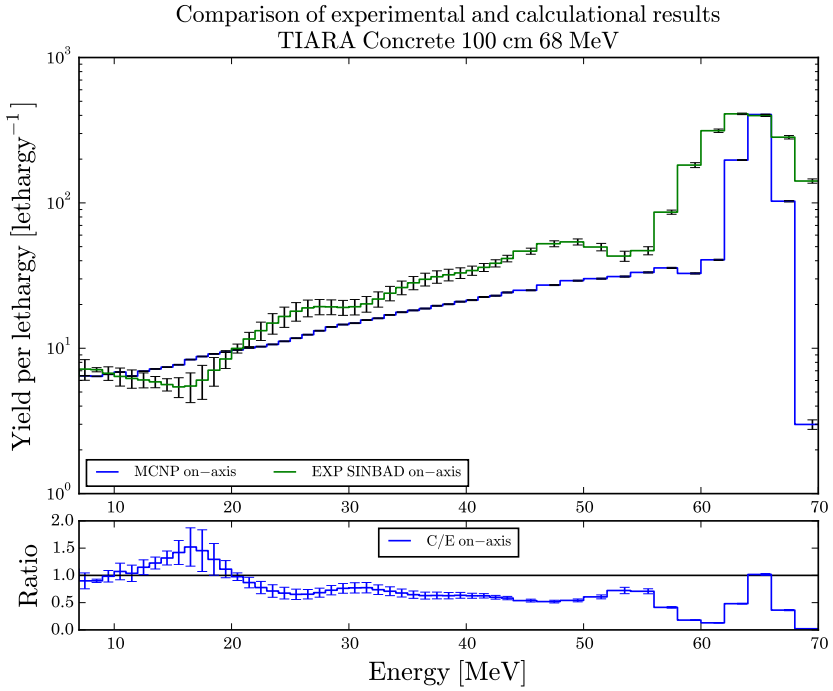

Figure 5.60: 100 cm concrete shield, 68 MeV, ENDF/B-VIII

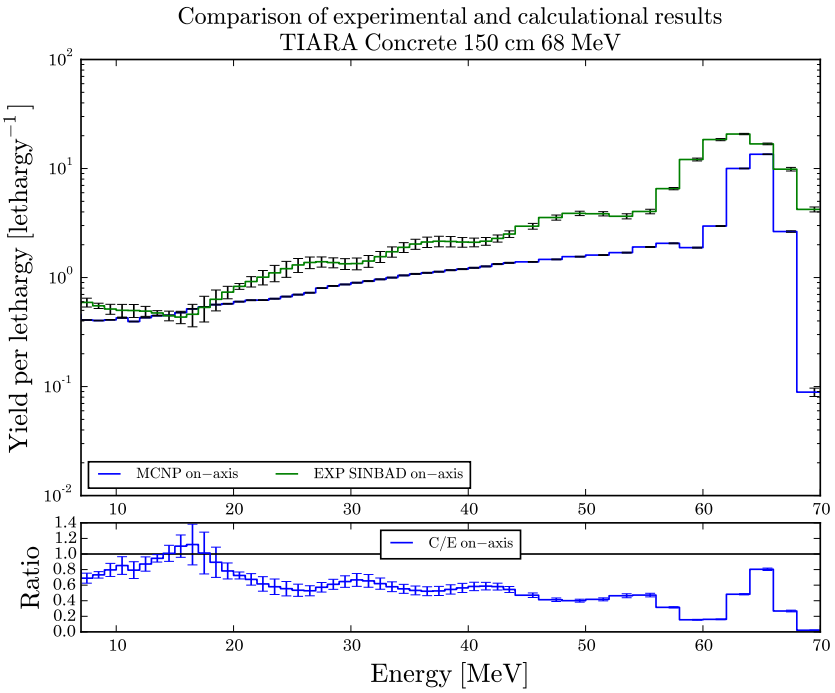

Figure 5.61: 150 cm concrete shield, 68 MeV, ENDF/B-VIII

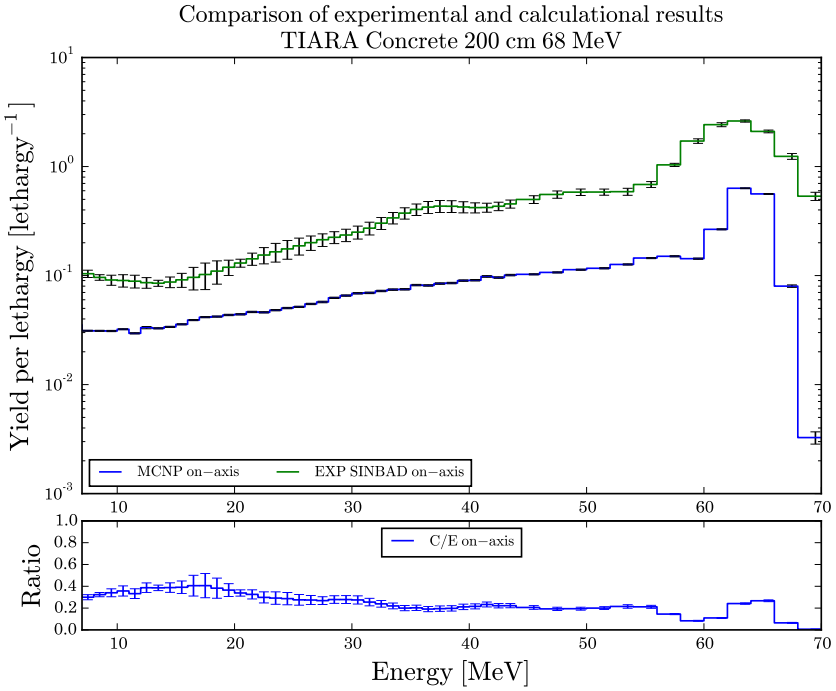

Figure 5.62: 200 cm concrete shield, 68 MeV, ENDF/B-VIII

5.2.1.3 JEFF-3.3

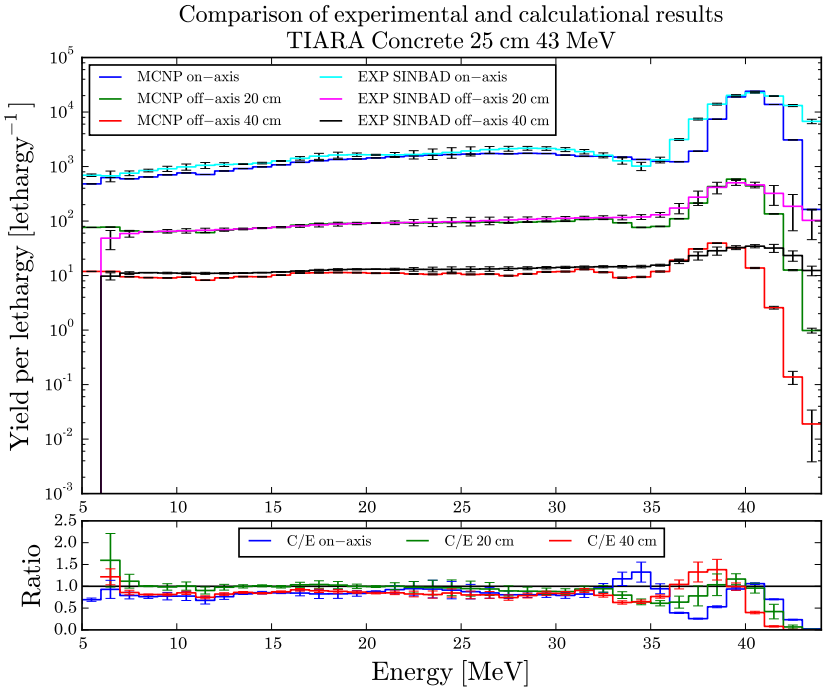

Figure 5.63: 25 cm concrete shield, 43 MeV, JEFF-3.3

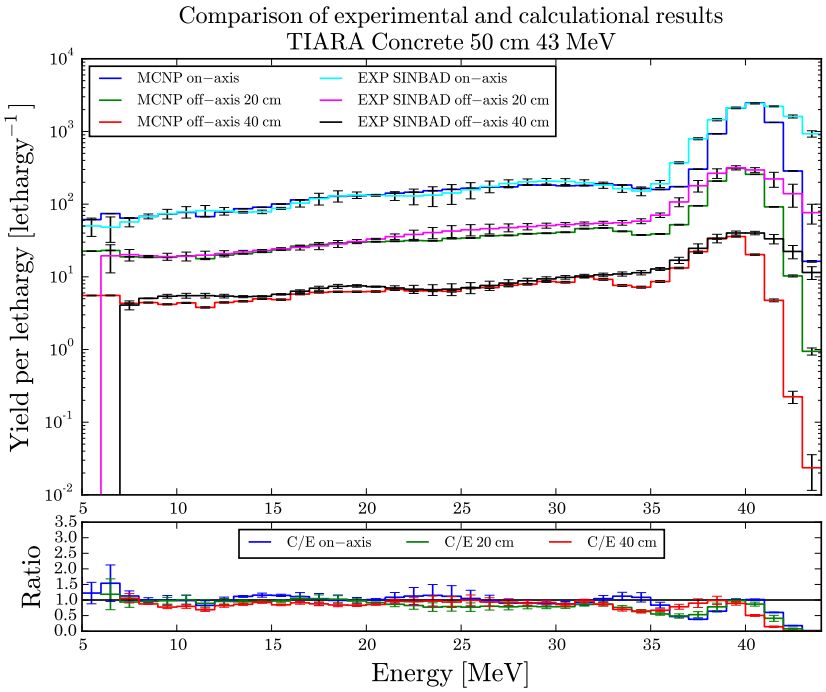

Figure 5.64: 50 cm concrete shield, 43 MeV, JEFF-3.3

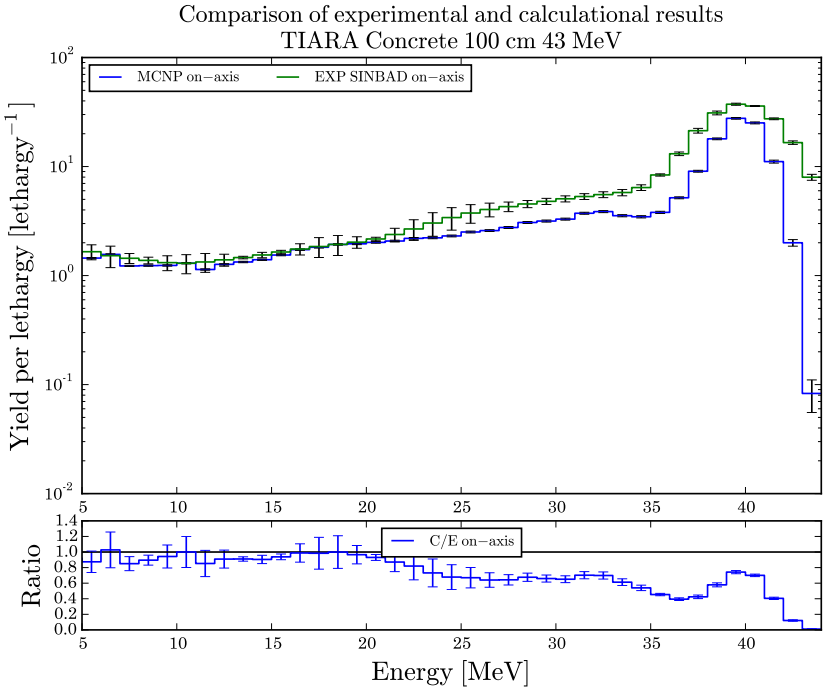

Figure 5.65: 100 cm concrete shield, 43 MeV, JEFF-3.3

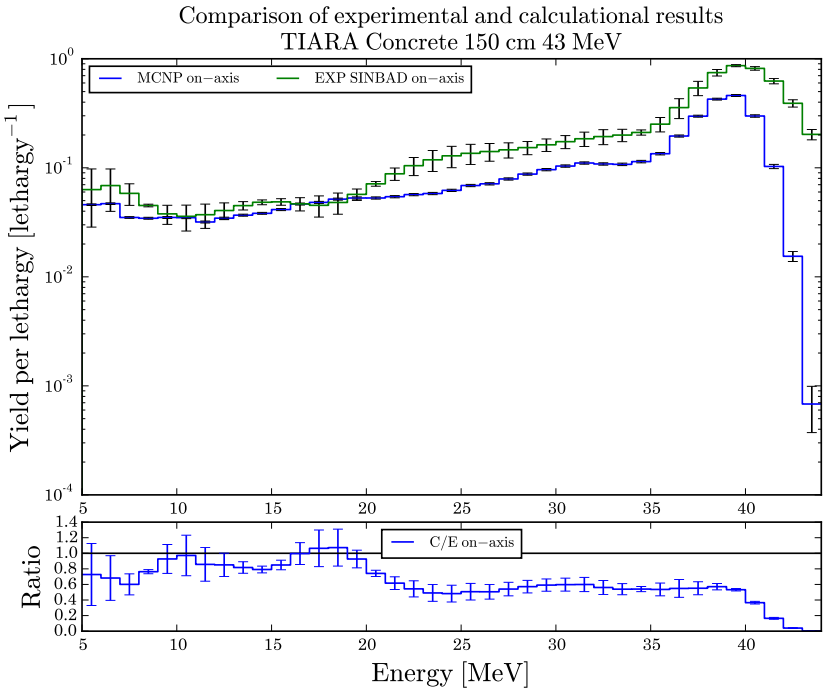

Figure 5.66: 150 cm concrete shield, 43 MeV, JEFF-3.3

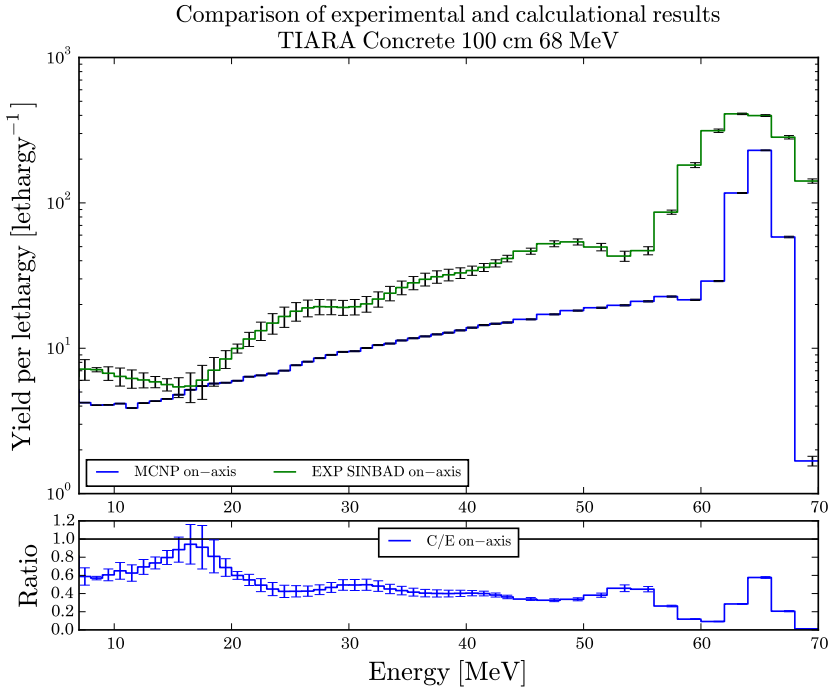

Figure 5.67: 100 cm concrete shield, 68 MeV, JEFF-3.3

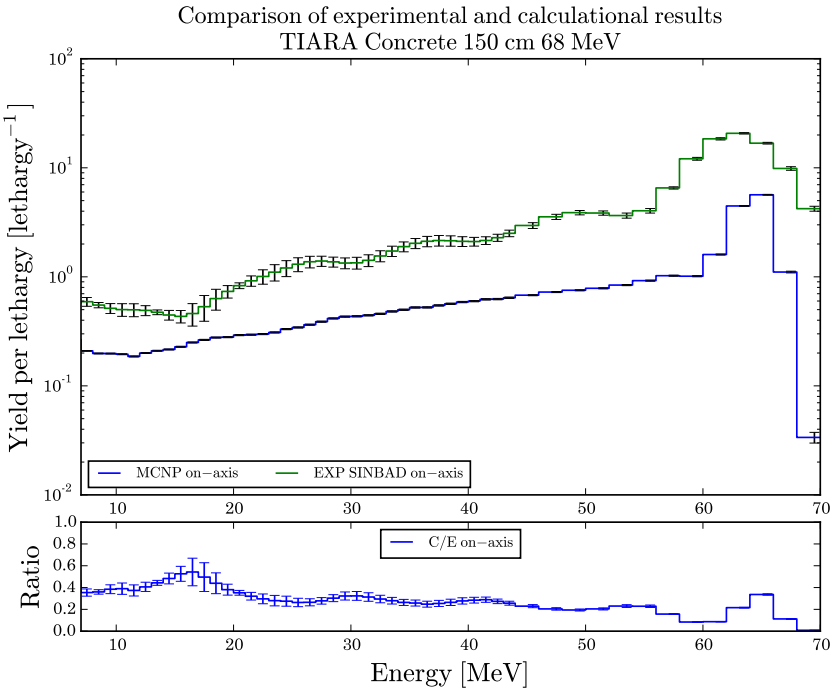

Figure 5.68: 150 cm concrete shield, 68 MeV, JEFF-3.3

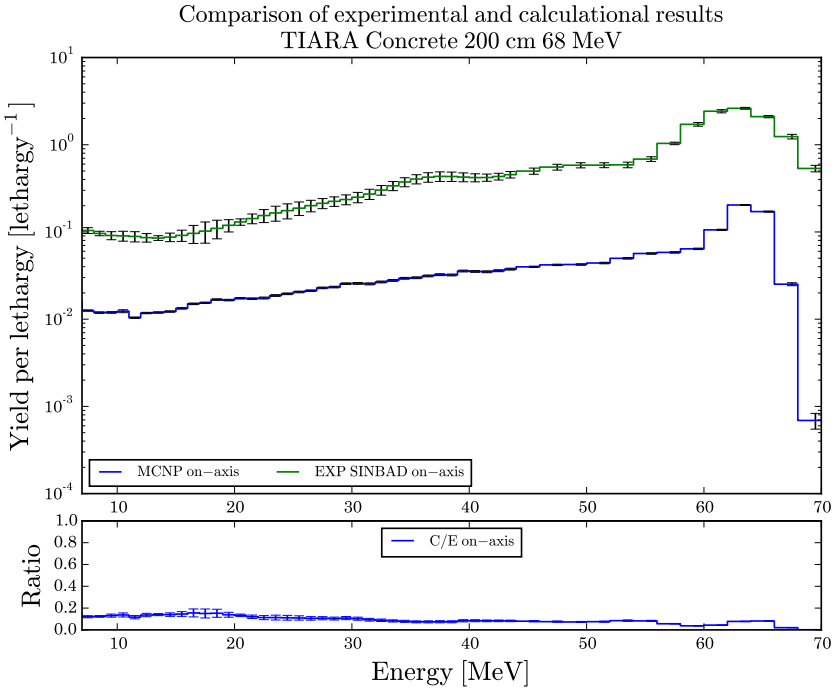

Figure 5.69: 200 cm concrete shield, 68 MeV, JEFF-3.3

5.2.1.4 JENDL-4.0u

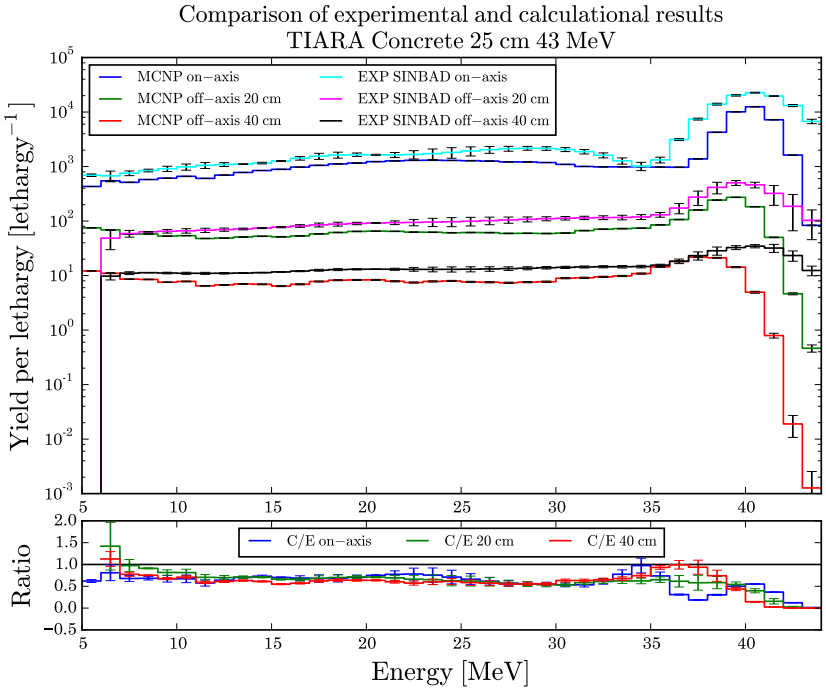

Figure 5.70: 25 cm concrete shield, 43 MeV, JENDL-4.0u

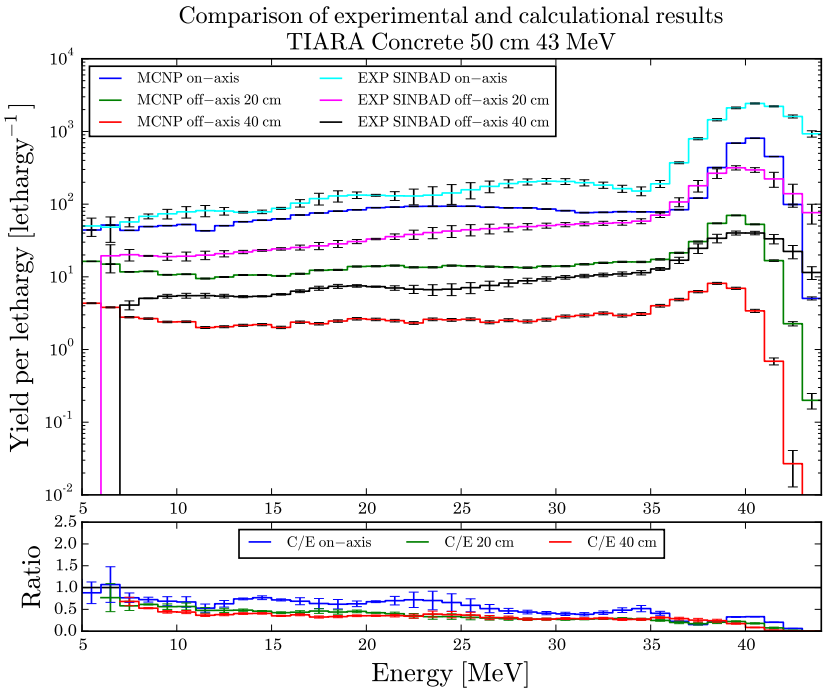

Figure 5.71: 50 cm concrete shield, 43 MeV, JENDL-4.0u

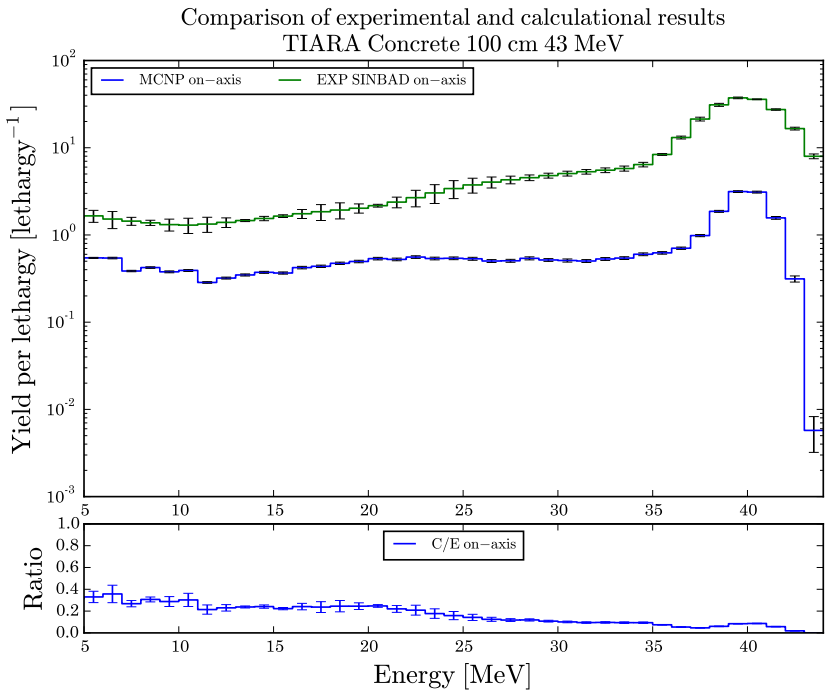

Figure 5.72: 100 cm concrete shield, 43 MeV, JENDL-4.0u

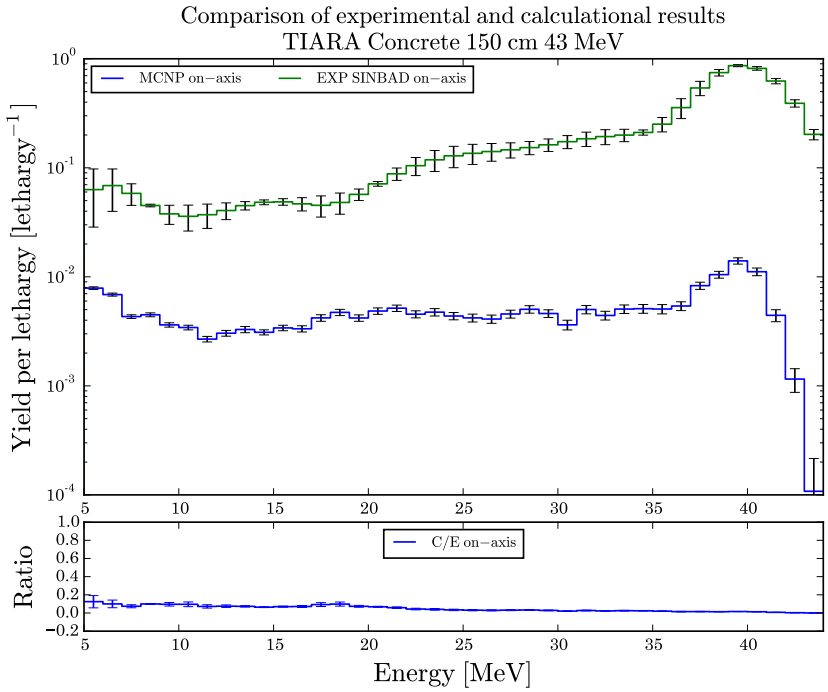

Figure 5.73: 150 cm concrete shield, 43 MeV, JENDL-4.0u

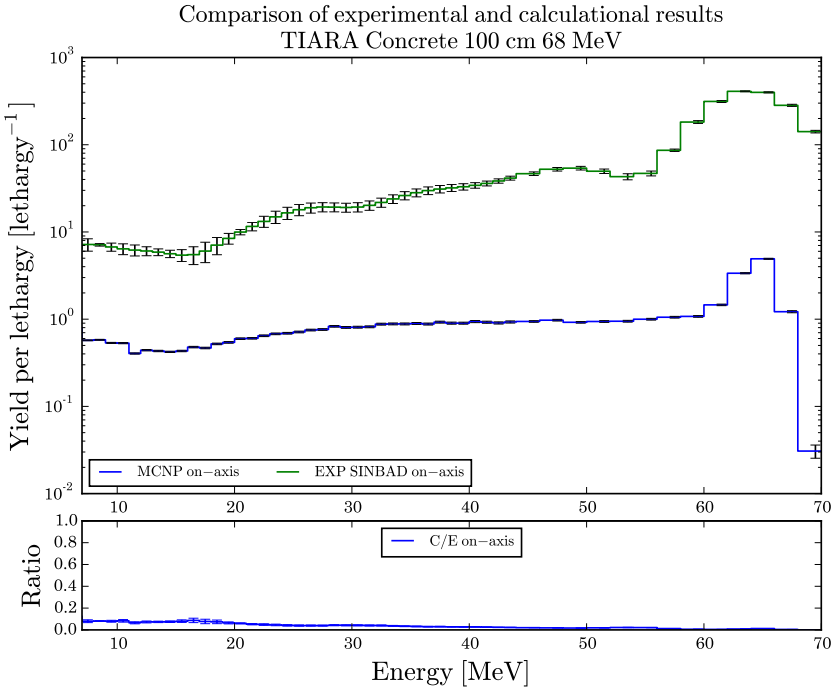

Figure 5.74: 100 cm concrete shield, 68 MeV, JENDL-4.0u

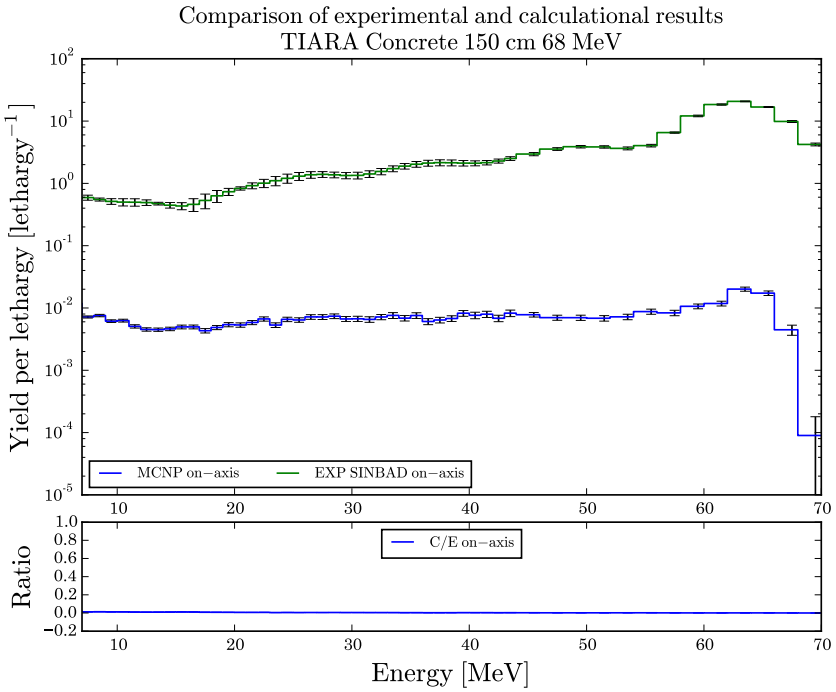

Figure 5.75: 150 cm concrete shield, 68 MeV, JENDL-4.0u

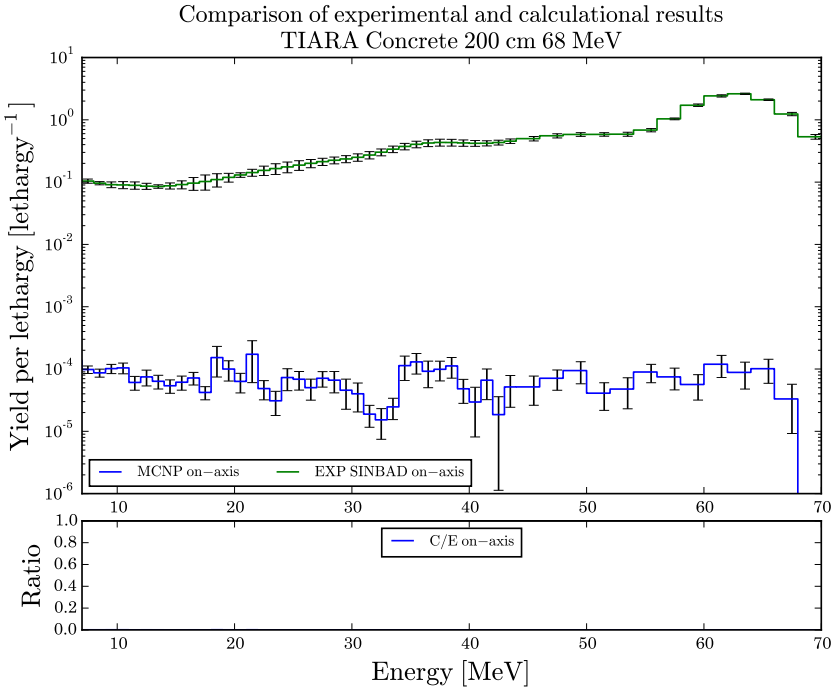

Figure 5.76: 200 cm concrete shield, 68 MeV, JENDL-4.0u

5.2.2 Bonner sphere detectors

5.2.2.1 ENDF/B-VII.1

Table 5.17: Bonner sphere detectors, concrete shield, 43 MeV, ENDF/B-VII.1 [$\frac{counts}{\mu C}$]

	Experiment				Calculation ENDF/B-VII.1							
Shield t./Polyethylene t.	25 cm	50 cm	100 cm	150 cm	25 cm		50 cm		100 cm		150 cm	
					Value	C/E	Value	C/E	Value	C/E	Value	C/E
Bare	5.20E+03	1.32E+03	6.45E+01	2.73E+00	4.34E+03	0.83	1.65E+03	1.25	9.30E+01	1.44	4.17E+00	1.53
15 mm	5.98E+03	1.25E+03	4.84E+01	2.29E+00	3.69E+03	0.62	1.04E+03	0.83	5.03E+01	1.04	2.13E+00	0.93
30 mm	8.94E+04	1.59E+03	6.02E+01	2.89E+00	6.38E+03	0.07	1.39E+03	0.87	5.94E+01	0.99	2.40E+00	0.83
50 mm	1.20E+04	1.90E+03	6.62E+01	3.02E+00	9.09E+03	0.76	1.68E+03	0.88	6.41E+01	0.97	2.53E+00	0.84
90 mm	1.11E+04	1.62E+03	5.27E+01	2.36E+00	8.48E+03	0.76	1.43E+03	0.88	5.04E+01	0.96	1.95E+00	0.83

Table 5.18: Bonner sphere detectors, concrete shield, 68 MeV, ENDF/B-VII.1 [$\frac{counts}{\mu C}$]

	Experiment			Calculation ENDF/B-VII.1					
Shield t./Polyethylene t.	50 cm	100 cm	150 cm	50 cm		100 cm		150 cm	
				Value	C/E	Value	C/E	Value	C/E
Bare	2.04E+03	2.74E+02	1.83E+01	3.53E+03	1.73	3.02E+02	1.10	2.35E+01	1.28
15 mm	2.16E+03	1.44E+02	1.06E+01	2.26E+03	1.04	1.81E+03	12.6	1.43E+02	13.5
30 mm	3.04E+03	3.15E+02	2.42E+01	3.18E+03	1.04	2.25E+02	0.71	1.78E+01	0.74
50 mm	3.72E+03	3.63E+02	2.86E+01	4.00E+03	1.07	2.56E+02	0.71	1.90E+01	0.66
90 mm	3.25E+03	3.08E+02	2.46E+01	3.57E+03	1.10	2.16E+02	0.70	1.53E+01	0.62

5.2.2.2 ENDF/B-VIII

Table 5.19: Bonner sphere detectors, concrete shield, 43 MeV, ENDF/B-VIII [$\frac{counts}{\mu C}$]

	Experiment				Calculation ENDF/B-VIII							
Shield t./Polyethylene t.	25 cm	50 cm	100 cm	150 cm	25 cm		50 cm		100 cm		150 cm	
					Value	C/E	Value	C/E	Value	C/E	Value	C/E
Bare	5.20E+03	1.32E+03	6.45E+01	2.73E+00	4.64E+03	0.89	1.67E+03	1.27	9.47E+01	1.47	3.92E+00	1.44
15 mm	5.98E+03	1.25E+03	4.84E+01	2.29E+00	3.73E+03	0.62	1.05E+03	0.84	4.99E+01	1.03	2.05E+00	0.90
30 mm	8.94E+04	1.59E+03	6.02E+01	2.89E+00	6.33E+03	0.07	1.39E+03	0.88	5.86E+01	0.97	2.33E+00	0.81
50 mm	1.20E+04	1.90E+03	6.62E+01	3.02E+00	9.00E+03	0.75	1.66E+03	0.87	6.30E+01	0.95	2.45E+00	0.81
90 mm	1.11E+04	1.62E+03	5.27E+01	2.36E+00	8.40E+03	0.76	1.42E+03	0.87	4.90E+01	0.93	1.88E+00	0.80

Table 5.20: Bonner sphere detectors, concrete shield, 68 MeV, ENDF/B-VIII [$\frac{counts}{\mu C}$]

	Experiment			Calculation JEFF-3.3					
Shield t./Polyethylene t.	50 cm	100 cm	150 cm	50 cm		100 cm		150 cm	
				Value	C/E	Value	C/E	Value	C/E
Bare	2.04E+03	2.74E+02	1.83E+01	3.41E+03	1.67	3.04E+02	1.11	2.39E+01	1.31
15 mm	2.16E+03	1.44E+02	1.06E+01	2.30E+03	1.06	1.83E+03	12.7	1.42E+02	13.3
30 mm	3.04E+03	3.15E+02	2.42E+01	3.23E+03	1.06	2.24E+02	0.71	1.62E+01	0.67
50 mm	3.72E+03	3.63E+02	2.86E+01	4.00E+03	1.08	2.56E+02	0.71	1.83E+01	0.64
90 mm	3.25E+03	3.08E+02	2.46E+01	3.54E+03	1.09	2.14E+02	0.69	1.48E+01	0.60

5.2.2.3 JEFF-3.3

Table 5.21: Bonner sphere detectors, concrete shield, 43 MeV, JEFF-3.3 [$\frac{counts}{\mu C}$]

	Experiment				Calculation JEFF-3.3							
Shield t./Polyethylene t.	25 cm	50 cm	100 cm	150 cm	25 cm		50 cm		100 cm		150 cm	
					Value	C/E	Value	C/E	Value	C/E	Value	C/E
Bare	5.20E+03	1.32E+03	6.45E+01	2.73E+00	4.63E+03	0.89	1.69E+03	1.29	9.01E+01	1.40	3.08E+00	1.13
15 mm	5.98E+03	1.25E+03	4.84E+01	2.29E+00	3.83E+03	0.64	1.05E+03	0.84	4.52E+01	0.93	1.57E+00	0.69
30 mm	8.94E+04	1.59E+03	6.02E+01	2.89E+00	6.49E+03	0.07	1.36E+03	0.86	5.23E+01	0.87	1.77E+00	0.61
50 mm	1.20E+04	1.90E+03	6.62E+01	3.02E+00	9.03E+03	0.76	1.60E+03	0.84	5.49E+01	0.83	1.83E+00	0.61
90 mm	1.11E+04	1.62E+03	5.27E+01	2.36E+00	8.23E+03	0.74	1.33E+03	0.82	4.13E+01	0.78	1.37E+00	0.58

Table 5.22: Bonner sphere detectors, concrete shield, 68 MeV, JEFF-3.3 [$\frac{counts}{\mu C}$]

	Experiment			Calculation JEFF-3.3					
Shield t./Polyethylene t.	50 cm	100 cm	150 cm	50 cm		100 cm		150 cm	
				Value	C/E	Value	C/E	Value	C/E
Bare	2.04E+03	2.74E+02	1.83E+01	3.12E+03	1.52	2.45E+02	0.90	1.40E+01	0.77
15 mm	2.16E+03	1.44E+02	1.06E+01	2.08E+03	0.96	1.43E+03	9.93	8.55E+01	8.06
30 mm	3.04E+03	3.15E+02	2.42E+01	2.92E+03	0.96	1.64E+02	0.52	9.70E+00	0.40
50 mm	3.72E+03	3.63E+02	2.86E+01	3.53E+03	0.95	1.79E+02	0.49	9.94E+00	0.35
90 mm	3.25E+03	3.08E+02	2.46E+01	3.02E+03	0.93	1.44E+02	0.47	7.79E+00	0.32

5.2.2.4 JENDL-4.0u

Table 5.23: Bonner sphere detectors, concrete shield, 43 MeV, JENDL-4.0u [$\frac{counts}{\mu C}$]

	Experiment				Calculation JENDL-4.0u							
Shield t./Polyethylene t.	25 cm	50 cm	100 cm	150 cm	25 cm		50 cm		100 cm		150 cm	
					Value	C/E	Value	C/E	Value	C/E	Value	C/E
Bare	5.20E+03	1.32E+03	6.45E+01	2.73E+00	5.26E+03	1.01	1.41E+03	1.07	4.03E+01	0.62	7.15E-01	0.26
15 mm	5.98E+03	1.25E+03	4.84E+01	2.29E+00	4.17E+03	0.70	8.41E+02	0.67	1.87E+01	0.39	3.19E-01	0.14
30 mm	8.94E+04	1.59E+03	6.02E+01	2.89E+00	6.55E+03	0.07	1.07E+03	0.67	2.05E+01	0.34	3.19E-01	0.11
50 mm	1.20E+04	1.90E+03	6.62E+01	3.02E+00	8.50E+03	0.71	1.21E+03	0.63	2.05E+01	0.31	2.97E-01	0.10
90 mm	1.11E+04	1.62E+03	5.27E+01	2.36E+00	7.00E+03	0.63	8.76E+02	0.54	1.37E+01	0.26	1.88E-01	0.08

Table 5.24: Bonner sphere detectors, concrete shield, 68 MeV, JENDL-4.0u [$\frac{counts}{\mu C}$]

	Experiment			Calculation JENDL-4.0u					
Shield t./Polyethylene t.	50 cm	100 cm	150 cm	50 cm		100 cm		150 cm	
				Value	C/E	Value	C/E	Value	C/E
Bare	2.04E+03	2.74E+02	1.83E+01	2.58E+03	1.26	7.34E+01	0.27	1.12E+00	0.06
15 mm	2.16E+03	1.44E+02	1.06E+01	1.53E+03	0.71	4.27E+02	2.96	7.07E+00	0.67
30 mm	3.04E+03	3.15E+02	2.42E+01	1.85E+03	0.61	3.65E+01	0.12	6.53E-01	0.03
50 mm	3.72E+03	3.63E+02	2.86E+01	1.97E+03	0.53	3.51E+01	0.10	5.74E-01	0.02
90 mm	3.25E+03	3.08E+02	2.46E+01	1.40E+03	0.43	2.29E+01	0.07	3.82E-01	0.02

5.2.3 Fission cells

5.2.3.1 ENDF/B-VII.1

Table 5.25: Fission cells, concrete shield, 43 MeV, ENDF/B-VII.1 [$\frac{n}{\mu C}$]

	Experiment				Calculation ENDF/B-VII.1			
Fission c./Position (shield t., axis offset)	^{238}U		^{232}Th		^{238}U		^{232}Th	
	Value	err.	Value	err.	Value	C/E	Value	C/E
25,0	1.15E-20	1.4	4.32E-21	4.8	9.63E+03	0.84	4.16E+03	0.96
50,0	1.26E-21	5.6	5.23E-22	4.9	1.00E+03	0.80	4.31E+02	0.82
100,0	1.98E-23	8	7.80E-24	24	1.53E+01	0.77	6.34E+00	0.81
150,0	1.72E-24	17			4.45E-01	0.26		
25,20	4.78E-22	15	1.48E-22	12	3.23E+02	0.68	1.23E+02	0.83
50,20	1.90E-22	8.4	7.58E-23	8.8	1.63E+02	0.86	6.56E+01	0.87
100,20	1.37E-23	17	5.73E-24	27	8.84E+00	0.65	3.57E+00	0.62
150,20	1.33E-24	20			3.58E-01	0.27		

Table 5.26: Fission cells, concrete shield, 68 MeV, ENDF/B-VII.1 [$\frac{n}{\mu C}$]

	Experiment				Calculation ENDF/B-VII.1			
Fission c./Position (shield t., axis offset)	^{238}U		^{232}Th		^{238}U		^{232}Th	
	Value	err.	Value	err.	Value	C/E	Value	C/E
25,0	2.37E-20	1.7	1.41E-20	2.2	2.20E+04	0.93	1.10E+04	0.78
50,0	4.63E-21	1.1	2.43E-21	1.4	3.43E+03	0.74	1.73E+03	0.71
100,0	1.72E-22	4.8	9.23E-23	6.4	1.06E+02	0.61	5.18E+01	0.56
150,0	9.47E-24	7.5	4.93E-24	10	5.15E+00	0.54	2.41E+00	0.49
25,20	1.28E-21	3.9	2.82E-22	8.1	6.04E+02	0.47	2.44E+02	0.87
50,20	7.82E-22	1.9	1.96E-22	3.7	4.16E+02	0.53	1.85E+02	0.95
100,20	8.30E-23	3.3	3.86E-23	4.7	4.88E+01	0.59	2.26E+01	0.59
150,20	7.41E-24	6.7	3.46E-24	9.5	3.87E+00	0.52	1.78E+00	0.51

5.2.3.2 ENDF/B-VIII

Table 5.27: Fission cells, concrete shield, 43 MeV, ENDF/B-VIII [$\frac{n}{\mu C}$]

	Experiment				Calculation ENDF/B-VII.1			
Fission c./Position (shield t., axis offset)	^{238}U		^{232}Th		^{238}U		^{232}Th	
	Value	err.	Value	err.	Value	C/E	Value	C/E
25,0	1.15E-20	1.4	4.32E-21	4.8	9.59E+03	0.83	4.15E+03	0.96
50,0	1.26E-21	5.6	5.23E-22	4.9	9.95E+02	0.79	4.28E+02	0.82
100,0	1.98E-23	8	7.80E-24	24	1.51E+01	0.76	6.26E+00	0.80
150,0	1.72E-24	17			4.30E-01	0.25		
25,20	4.78E-22	15	1.48E-22	12	3.15E+02	0.66	1.21E+02	0.81
50,20	1.90E-22	8.4	7.58E-23	8.8	1.61E+02	0.85	6.49E+01	0.86
100,20	1.37E-23	17	5.73E-24	27	8.70E+00	0.64	3.53E+00	0.62
150,20	1.33E-24	20			3.45E-01	0.26		

Table 5.28: Fission cells, concrete shield, 68 MeV, ENDF/B-VIII [$\frac{n}{\mu C}$]

	Experiment				Calculation ENDF/B-VII.1			
Fission c./Position (shield t., axis offset)	^{238}U		^{232}Th		^{238}U		^{232}Th	
	Value	err.	Value	err.	Value	C/E	Value	C/E
25,0	2.37E-20	1.7	1.41E-20	2.2	2.19E+04	0.92	1.09E+04	0.78
50,0	4.63E-21	1.1	2.43E-21	1.4	3.41E+03	0.74	1.72E+03	0.71
100,0	1.72E-22	4.8	9.23E-23	6.4	1.04E+02	0.60	5.10E+01	0.55
150,0	9.47E-24	7.5	4.93E-24	10	5.05E+00	0.53	2.37E+00	0.48
25,20	1.28E-21	3.9	2.82E-22	8.1	5.87E+02	0.46	2.39E+02	0.85
50,20	7.82E-22	1.9	1.96E-22	3.7	4.11E+02	0.53	1.84E+02	0.94
100,20	8.30E-23	3.3	3.86E-23	4.7	4.78E+01	0.58	2.22E+01	0.58
150,20	7.41E-24	6.7	3.46E-24	9.5	3.75E+00	0.51	1.72E+00	0.50

5.2.3.3 JEFF-3.3

Table 5.29: Fission cells, concrete shield, 43 MeV, JEFF-3.3 [$\frac{n}{\mu C}$]

	Experiment				Calculation ENDF/B-VII.1			
Fission c./Position (shield t., axis offset)	^{238}U		^{232}Th		^{238}U		^{232}Th	
	Value	err.	Value	err.	Value	C/E	Value	C/E
25,0	1.15E-20	1.4	4.32E-21	4.8	9.10E+03	0.79	3.92E+03	0.91
50,0	1.26E-21	5.6	5.23E-22	4.9	8.96E+02	0.71	3.84E+02	0.73
100,0	1.98E-23	8	7.80E-24	24	1.17E+01	0.59	4.84E+00	0.62
150,0	1.72E-24	17			2.88E-01	0.17		
25,20	4.78E-22	15	1.48E-22	12	3.16E+02	0.66	1.20E+02	0.81
50,20	1.90E-22	8.4	7.58E-23	8.8	1.41E+02	0.74	5.59E+01	0.74
100,20	1.37E-23	17	5.73E-24	27	6.66E+00	0.49	2.67E+00	0.47
150,20	1.33E-24	20			2.33E-01	0.17		

Table 5.30: Fission cells, concrete shield, 68 MeV, JEFF-3.3 [$\frac{n}{\mu C}$]

	Experiment				Calculation ENDF/B-VII.1			
Fission c./Position (shield t., axis offset)	^{238}U		^{232}Th		^{238}U		^{232}Th	
	Value	err.	Value	err.	Value	C/E	Value	C/E
25,0	2.37E-20	1.7	1.41E-20	2.2	1.96E+04	0.83	9.71E+03	0.69
50,0	4.63E-21	1.1	2.43E-21	1.4	2.71E+03	0.59	1.36E+03	0.56
100,0	1.72E-22	4.8	9.23E-23	6.4	6.44E+01	0.37	3.12E+01	0.34
150,0	9.47E-24	7.5	4.93E-24	10	2.46E+00	0.26	1.14E+00	0.23
25,20	1.28E-21	3.9	2.82E-22	8.1	5.68E+02	0.44	2.32E+02	0.82
50,20	7.82E-22	1.9	1.96E-22	3.7	3.41E+02	0.44	1.52E+02	0.77
100,20	8.30E-23	3.3	3.86E-23	4.7	2.98E+01	0.36	1.36E+01	0.35
150,20	7.41E-24	6.7	3.46E-24	9.5	1.82E+00	0.24	8.25E-01	0.24

5.2.3.4 JENDL-4.0u

Table 5.31: Fission cells, concrete shield, 43 MeV, JENDL-4.0u [$\frac{n}{\mu C}$]

	Experiment				Calculation ENDF/B-VII.1			
Fission c./Position (shield t., axis offset)	^{238}U		^{232}Th		^{238}U		^{232}Th	
	Value	err.	Value	err.	Value	C/E	Value	C/E
25,0	1.15E-20	1.4	4.32E-21	4.8	6.11E+03	0.53	2.56E+03	0.59
50,0	1.26E-21	5.6	5.23E-22	4.9	4.26E+02	0.34	1.74E+02	0.33
100,0	1.98E-23	8	7.80E-24	24	2.26E+00	0.11	8.62E-01	0.11
150,0	1.72E-24	17			2.15E-02	0.01		
25,20	4.78E-22	15	1.48E-22	12	2.26E+02	0.47	8.13E+01	0.55
50,20	1.90E-22	8.4	7.58E-23	8.8	6.22E+01	0.33	2.29E+01	0.30
100,20	1.37E-23	17	5.73E-24	27	1.12E+00	0.08	4.00E-01	0.07
150,20	1.33E-24	20			1.54E-02	0.01		

Table 5.32: Fission cells, concrete shield, 68 MeV, JENDL-4.0u [$\frac{n}{\mu C}$]

	Experiment				Calculation ENDF/B-VII.1			
Fission c./Position (shield t., axis offset)	^{238}U		^{232}Th		^{238}U		^{232}Th	
	Value	err.	Value	err.	Value	C/E	Value	C/E
25,0	2.37E-20	1.7	1.41E-20	2.2	1.00E+04	0.42	4.75E+03	0.34
50,0	4.63E-21	1.1	2.43E-21	1.4	7.16E+02	0.15	3.28E+02	0.14
100,0	1.72E-22	4.8	9.23E-23	6.4	4.15E+00	0.02	1.73E+00	0.02
150,0	9.47E-24	7.5	4.93E-24	10	3.89E-02	0.00	1.50E-02	0.00
25,20	1.28E-21	3.9	2.82E-22	8.1	3.87E+02	0.30	1.52E+02	0.54
50,20	7.82E-22	1.9	1.96E-22	3.7	1.05E+02	0.13	4.23E+01	0.22
100,20	8.30E-23	3.3	3.86E-23	4.7	2.02E+00	0.02	7.77E-01	0.02
150,20	7.41E-24	6.7	3.46E-24	9.5	2.77E-02	0.00	1.01E-02	0.00

6 Conclusion

The models produced are to our knowledge the most complete set of MCNP input files for the TIARA iron and concrete shielding benchmarks. Previous models were simplified version of the problem which did not include the surrounding structures and more importantly other detector tallies besides the BC 501A liquid scintillator detectors.

The models were developed from scratch starting with CAD models based on original JAERI documentation available in the SINBAD database distribution. CAD models for all shielding material-neutron source-detector combinations were produced.

Based on CAD models the MCNP geometrical models were produced. The material, source and tally (detector) information was taken form the JAERI and SINBAD documentations.

Variance reduction was implemented including a geometrically confined source, simulation energy cut off's and most importantly space and energy dependant weight windows. Weight window variance reduction parameters were produced for most cases whit shielding materials thicker than 40 cm. A speed up of the 100 cm thick iron shield case with the 43 MeV neutron source and the BC 501A liquid scintillator detector was 300, and no bias was introduced to the calculation.

Results simulated using MCNP5 ver 1.6 with the ENDF/B-VII.1, ENDF/B-VIII, JEFF-3.3 and JENDL-4.0u nuclear data libraries were presented. The results for three different detectors were given. The BC 501A liquid scintillator detectors, Bonner sphere detectors and Fission cells. Generally the agreement for the BC 501A detectors are good for the ENDF/B-VII.1, ENDF/B-VIII and JEFF-3.3 libraries, and the JENDL-4.0u library performs worse, especially for the off axis detectors. The simulations with the Bonner sphere detectors generally overestimate the counts with the less moderated spheres (Bare, 15 mm, 30 mm) and underestimate with the more moderated spheres (50 mm, 90 mm). This trend for both shield materials and thicknesses. Generally good

agreement between the calculation and experimental results can be seen for the Fission cells behind thinner iron shields with a slight under prediction of the calculations when using the 43 MeV source. The under prediction is even more obvious when looking at the results with the 68 MeV source. A systematic under prediction is observed when looking at the Fission cell results for the concrete test shields, especially for the thicker shields.

References

[1] Y. Nakane et al. *Neutron Transmission Benchmark Problems for Iron and Concrete Shields in Low, Intermediate and High Energy Proton Accelerator Facilities*. JAERI-Data/Code 96-029. 1996.

[2] I. Kodeli and N. Nakao. *TIARA 43/68 MeV Proton Benchmark*. SINBAD compilation NEA-1552/03. Apr. 2006.

[3] I. Kodeli et al. "20 Years of SINBAD (Shielding Integral Benchmark Archive and Database)". In: *Progress in Nuclear Science and Technology* 4 (2014), pp. 308–311.

[4] X-5 Monte Carlo Team. *MCNP — A General Monte Carlo N-Particle Transport Code, Version 5, Volume I: Overview and Theory*. LA-UR-03-1987. 2003.

[5] S.W. Mosher. *ADVANTG-An Automated Variance Reduction Parameter Generator*. ORNL/TM-2013/416 Rev. 1, Oak Ridge National laboratory. 2015.

[6] Robert McNeel & Associates. *Rhinoceros 5 User's Guide For Windows*. 2004.

[7] B. Kos and L. Snoj. "On using grasshopper add-on for CAD to MCNP conversion". In: *PHYSOR 2016: Unifying Theory and Experiments in the 21st Century*. American Nuclear Society, Inc. 2016.

[8] A.L. Schwarz, R.A. Schwarz, and L.L. Carter. *MCNP/MCNPX Visual Editor Computer Code Manual*. 2008.

[9] A. Trkov et al. "On the Self-Shielding Factors in Neutron Analysis". In: *Nuclear Instruments and Methods in Physics Research* A.610 (2009), pp. 553–565.

[10] J. C. Wagner and S. W. Mosher. *Forward-Weighted CADIS Method for Variance Reduction of Monte Carlo Reactor Analyses*. 2010.

A Sample TIARA iron MCNP input

```
TIARA Fe, 68 MeV, 40 cm shield, 40 cm colimator, B. Kos (bor.kos@ijs.si), 2018
c TIARA Fe, 68 MeV, 40 cm shield, 40 cm colimator
c Bor Kos, JSI, July 2018
c BC501A spectra off-axis
100 6  -2.31      -100:-101:-102 :-103: -104: -105 :(-106 110):
(-110 -109 -106.3 104.1 105.1 111):
(-111  108 -106.3 104.1 105.1 112):
(-112  107 -106.3 104.1 105.1) imp:n=1                $ Concrete structure
101 1  -7.87      -150 151 imp:n=1                     $ Beam dump
102 1  -7.08      -200 201 202 2 imp:n=1               $ Iron filler
c (density is 10 % lower than ordinary iron - original documentation assumes
c a mixutre of iron sand and balls)
103 1  -7.87      -201 2 imp:n=1                     $ Rotary shutter - iron
```

```
104 2  -0.928     -202 2  imp:n=1               $ Rotary shutter - polyethylene
105 3  -2.6989    -210 : -211 : -212 imp:n=1    $ Trolly (aluminium - assumed)
110 1  -7.87      -1000 imp:n=1                            $ Iron test shield
c Detector support table - aluminium assumed -  BC 501A Liquid scintilator off-
axis 20 cm
112 3  -2.6989    -238 : -239 : -240 : -241 : -242 imp:n=1
c BC 501A Liquid scintilator - only dimenssions in benchmark documentation
c - BC 501A off-axis 20 cm
113 4  -0.874     -243 imp:n=1
c Detector support table - aluminium assumed -
c BC 501A Liquid scintilator off-axis 40 cm
114 3  -2.6989    -244 : -245 : -246 : -247 : -248 imp:n=1
c BC 501A Liquid scintilator - only dimenssions in benchmark documentation -
c BC 501A off-axis 40 cm
115 4  -0.874     -249 imp:n=1
500 1  -7.87      -800 2.1 imp:n=1                  $ Additional iron collimator
600 0             -600 #100 #101 #102 #103 #104 -2.2 imp:n=1             $ Void
c Air
700 5 -0.001205   -600 1000 #500 #100 #105 #112 #113 #114 #115 #110 2.2 imp:n=1
601 0              600 imp:n=0                                    $ Outer space

c ------------------------------------------------------------------------------
c         SURFACES
c ------------------------------------------------------------------------------
c Source
1   px    0.0                                                  $ Source plane
c Beam line
2   rcc 0.0 0.0 0.0 396.0 0.0 0.0 5.45
c Concret stucture
100 box -124.0  250.0 -109.0 0.0 0.0 -200.0 0.0 -500.0 0.0 300.0 0.0 0.0
101 box  176.0  250.0 -119.0 0.0 -500.0 0.0 60.0 0.0 0.0 0.0 0.0 -190.0
102 box  716.0 -250.0 -309.0 0.0 0.0 232.65 0.0 500.0 0.0 -480.0 0.0 0.0
103 box  236.0  250.0  -20.0 0.0 -500.0 0.0 160.0 0.0 0.0 0.0 0.0 -56.35
104 box -124.0 -250.0 -119.0 0.0 190.0 0.0 0.0 0.0 399.065125 640.0 0.0 0.0
105 box -124.0  250.0 -119.0 0.0 -190.0 0.0 0.0 0.0 399.065125 640.0 0.0 0.0
106 box  516.0 -60.0    60.0 0.0 120.0 0.0 0.0 0.0 220.065122 -640.0 0.0 0.0
107 p    16020.908203 0.0 16038.62915 2.5053e+6
108 pz   146.558
109 p   -5443.936157 0.0 -5563.590088 -1.5211e+6
110 px   176
111 px   129.637
```

```
112 px   9.65524
c Beam dump
150 box 236.0 -20.0 -119.0 -60.0 0.0 0.0 0.0 40.0 0.0 0.0 0.0 99.0
151 box 206.0 -20.0 -89.0 0.0 40.0 0.0 -30.0 0.0 0.0 0.0 0.0 50.0
c Iron filler (iron balls and iron sand)
200 box 176.0 60.0 60.0 0.0 0.0 -80.0 0.0 -120.0 0.0 220.0 0.0 0.0
c Rotary shutter - iron
201 rcc 183 0 9.08 100.0 0.0 0.0 21.8
c Rotary shutter - polyethylene
202 rcc 283 0 9.08 50.0 0.0 0.0 21.8
c Trolly
210 box 398.5 -60.0 -60.0 0.0 0.0 -10.0 0.0 120.0 0.0 120.0 0.0 0.0
211 rcc 409.718 -60.0 -70.0 0.0 120.0 0.0 6.35
212 rcc 503.650752 -60.0 -70.0 0.0 120.0 0.0 6.35
c BC 501A Liquid scintilator - off-axis 20 cm
c Detector support table - aluminium assumed
238 box 481.0 -10.0 -6.350 0.0 0.0 -1.000 0.0 -20.0 0.0 40.0 0.0 0.0
239 rcc 482.0 -11.0 -7.350 0.0 0.0 -52.65 0.99
240 rcc 482.0 -29.0 -7.350 0.0 0.0 -52.65 0.99
241 rcc 520.0 -11.0 -7.350 0.0 0.0 -52.65 0.99
242 rcc 520.0 -29.0 -7.350 0.0 0.0 -52.65 0.99
c Liquid Scintilator BC 501A off-axis 20 cm
243 rcc 481.0 -20.0  0.0  12.7 0.0   0.0  6.350
c BC 501A Liquid scintilator - off-axis 40 cm
c Detector support table - aluminium assumed
244 box 481.0 -30.0 -6.350 0.0 0.0 -1.000 0.0 -20.0 0.0 40.0 0.0 0.0
245 rcc 482.0 -31.0 -7.350 0.0 0.0 -52.65 0.99
246 rcc 482.0 -49.0 -7.350 0.0 0.0 -52.65 0.99
247 rcc 520.0 -31.0 -7.350 0.0 0.0 -52.65 0.99
248 rcc 520.0 -49.0 -7.350 0.0 0.0 -52.65 0.99
c Liquid Scintilator BC 501A off-axis 40 cm
249 rcc 481.0 -40.0  0.0  12.7 0.0   0.0  6.350
c Outside world
600 box -130 -252 -315 850 0.0 0.0 0.0 504.0 0.0 0.0 0.0 600.0
c Additional iron colimator
800 box 401.0 -60 -60 40.0 0.0 0.0 0.0 120.0 0.0 0.0 0.0 120.0
c Shield
1000 box 441.0 -60 -60 40.0 0.0 0.0 0.0 120.0 0.0 0.0 0.0 120.0

c ------------------------------------------------------------------------
c         MATERIALS
```

```
c -------------------------------------------------------------------------
c Iron shield - atom density, Density ( g /cm3 )= 7.87.
c Naturan iron from benchmark documetation - Table 1.2 JAERI-Data/Code 96-
029
m1   26054. 4.9605E-03
26056. 7.7869E-02
26057. 1.7983E-03
26058. 2.3933E-04
c Polyethylene - atom density, Density ( g /cm3 )= 0.928,
c Reference: http://physics.nist.gov/PhysRefData/XrayMassCoef/tab2.html
m2    1001. 0.079855
6000. 0.039929
c Aluminum - atom density, Density ( g /cm3 )= 2.6989
m3   13027. 0.060238
c Liquid scintillator - atom density, Density ( g /cm3 )= 0.874
c "https://www.crystals.saint-gobain.com/sites/
c imdf.crystals.com/files/documents/sgc-bc501-501a-519-data-sheet_69711.pdf"
m4    1001. 0.0482
6000. 0.0398
c Dry Air - atom density, Density ( g /cm3 )= 0.001205
m5    6000. 7.4919E-09
7014. 3.8987E-05
7015. 1.4243E-07
8016. 1.0487E-05
8017. 3.9948E-09
18036. 7.8407E-10
18038. 1.4726E-10
18040. 2.3208E-07
c Concrete from benchmark documentation
c (per nuclide definition) - atom desnity, Density ( g /cm3 )= 2.31
m6    1001. 1.49783E-02
1002. 1.72270E-06
8016. 4.18641E-02
8017. 1.59471E-05
11023. 1.23000E-03
12024. 4.89740E-04
12025. 6.19982E-05
12026. 6.82614E-05
13027. 3.12000E-03
14028. 1.02368E-02
14029. 5.20043E-04
```

```
14030. 3.43204E-04
19039. 3.54381E-04
19040. 4.44605E-08
19041. 2.55745E-05
20040. 4.16846E-03
20042. 2.78219E-05
20043. 5.80511E-06
20044. 8.96994E-05
20046. 1.72004E-07
20048. 8.04130E-06
26054. 8.24154E-05
26056. 1.29373E-03
26057. 2.98785E-05
26058. 3.97622E-06
c -------------------------------------------------------------------------
c         SOURCE
c -------------------------------------------------------------------------
c --- Point isotropic neutron source collimated into an -x cone.
c Particles are confined to a (+x axis) cone whose half-angle
c is acos(0.99990531) = 0.7788 degrees about the x-axis.
c Angles are with respect to the vector specified by VEC
c
sdef cell=600 pos=0 0 0 erg=d1 par=1 vec=1 0 0 dir=d2
si2 -1  0.99990531  1          $ histogram for cosine bin limits
sp2  0  0.99995265  0.00004735 $ frac. solid angle for each bin
sb2  0. 0.          1.         $ source bias for each bin
si1 H    0.0
5.5  6.5  7.5  8.5  9.5 10.5 11.5 12.5 13.5 14.5
15.5 16.5 17.5 18.5 19.5 20.5 21.5 22.5 23.5 24.5
25.5 26.5 27.5 28.5 29.5 30.5 31.5 32.5 33.5 34.5
35.5 36.5 37.5 38.5 39.5 40.5 41.5 42.5 43.5 44.5
45.5 46.5 47.5 48.5 49.5 50.5 51.5 52.5 53.5 54.5
55.5 56.5 57.5 58.5 59.5 60.5 61.5 62.5 63.5 64.5
65.5 66.5 67.5 68.5 69.5 70.5 71.5 72.5
sp1   0.0      0.
2.373E-2 2.373E-2 2.395E-2 2.440E-2 2.508E-2
2.569E-2 2.533E-2 2.592E-2 2.678E-2 2.714E-2
2.788E-2 2.795E-2 2.855E-2 2.954E-2 3.100E-2
3.149E-2 3.334E-2 3.383E-2 3.528E-2 3.624E-2
3.669E-2 3.841E-2 3.806E-2 3.927E-2 3.845E-2
3.875E-2 3.857E-2 3.878E-2 3.762E-2 3.702E-2
```

```
3.716E-2 3.656E-2 3.615E-2 3.399E-2 3.345E-2
3.324E-2 3.340E-2 3.137E-2 3.211E-2 3.103E-2
3.102E-2 3.160E-2 3.086E-2 3.003E-2 2.856E-2
2.804E-2 2.656E-2 2.505E-2 2.391E-2 2.177E-2
1.959E-2 1.604E-2 1.281E-2 1.088E-2 9.010E-3
7.428E-3 8.095E-3 4.701E-2 2.104E-1 3.614E-1
2.765E-1 8.202E-2 8.896E-3 1.074E-3 4.013E-4
4.973E-4 1.324E-4
c -------------------------------------------------------------------------
c         TALLIES
c -------------------------------------------------------------------------
c Absolute normalization of results 1.56368E+11 (=2.61*4770000000*4*3.14=peak
c to continuum from SINBAD html note, peak flux of neutrons in SINBAD html,
c solid angle (4 pi))
F14:n 113
FC14 BC 501A Liquid scintilator - off-axis 20 cm
FM14 1.56368E+11
E14    6  7  8  9 10 11 12 13 14 15 16 17 18 19 20 21 22 23 24 25 26 27
28 29 30 31 32 33 34 35 36 37 38 39 40 41 42 43 44 46 48 50 52 54
56 58 60 62 64 66 68 70
F24:n 115
FC24 BC 501A Liquid scintilator - off-axis 40 cm
FM24 1.56368E+11
E24    6  7  8  9 10 11 12 13 14 15 16 17 18 19 20 21 22 23 24 25 26 27
28 29 30 31 32 33 34 35 36 37 38 39 40 41 42 43 44 46 48 50 52 54
56 58 60 62 64 66 68 70
print
NPS 1e6
cut:n j 5.0
c * added by ADVANTG
wwp:n 5.0 j 100 j -1 0 4.008745734e+00
```

B Sample TIARA concrete MCNP input

```
TIARA Concrete, 68 MeV, 50 cm shield, 80 cm col., B. Kos (bor.kos@ijs.si), 2018
c TIARA Concrete, 68 MeV, 50 cm shield, 80 cm additional iron colimator
c Bor Kos, JSI, July 2018
c BC501A spectra on-axis, off-axis 20 cm, 40 cm
100 6  -2.31      -100:-101:-102 :-103: -104: -105 :(-106 110):
(-110 -109 -106.3 104.1 105.1 111):
(-111  108 -106.3 104.1 105.1 112):
```

```
(-112  107 -106.3 104.1 105.1) imp:n=1          $ Concrete structure
101 1  -7.87      -150 151 imp:n=1              $ Beam dump
102 1  -7.08      -200 201 202 2 imp:n=1        $ Iron filler
103 1  -7.87      -201 2 imp:n=1                $ Rotary shutter - iron
104 2  -0.928     -202 2  imp:n=1               $ Rotary shutter - polyethylene
105 3  -2.6989    -210 : -211 : -212 imp:n=1    $ Trolly (aluminium - assumed)
110 3  -2.6989    -232 : -233 : -234 : -235 : -236 imp:n=1  $ Det. support table
111 4  -0.874     -237 imp:n=1  $ BC 501A Liquid scintilator - BC 501A on axis
112 3  -2.6989    -238 : -239 : -240 : -241 : -242 imp:n=1  $ Det. support table
113 4  -0.874     -243 imp:n=1  $ BC 501A Liquid scintilator off-axis 20 cm
114 3  -2.6989    -244 : -245 : -246 : -247 : -248 imp:n=1  $ Det. support table
115 4  -0.874     -249 imp:n=1  $ BC 501A Liquid scintilator off-axis 40 cm
109 6  -2.31      -1000 imp:n=1                   $ Concrete test shield
500 1  -7.87      -800 2.1 imp:n=1                $ Additional iron collimator
600 0             -600 #100 #101 #102 #103 #104 -2.2 imp:n=1            $ void
700 5  -0.001205  -600 1000 #500  #100 #105 #110 #111 #112 #113 #114 #115
                   2.2 imp:n=1        $ air
601 0              600 imp:n=0        $ Outer space

c ------------------------------------------------------------------------------
c         SURFACES
c ------------------------------------------------------------------------------
c Source
1   px    0.0                                                  $ Source plane
c Beam line
2   rcc 0.0 0.0 0.0 396.0 0.0 0.0 5.45
c Concret stucture
100 box -124.0  250.0 -109.0 0.0 0.0 -200.0 0.0 -500.0 0.0 300.0 0.0 0.0
101 box  176.0  250.0 -119.0 0.0 -500.0 0.0 60.0 0.0 0.0 0.0 0.0 -190.0
102 box  716.0 -250.0 -309.0 0.0 0.0 232.65 0.0 500.0 0.0 -480.0 0.0 0.0
103 box  236.0  250.0  -20.0 0.0 -500.0 0.0 160.0 0.0 0.0 0.0 0.0 -56.35
104 box -124.0 -250.0 -119.0 0.0 190.0 0.0 0.0 0.0 399.065125 640.0 0.0 0.0
105 box -124.0  250.0 -119.0 0.0 -190.0 0.0 0.0 0.0 399.065125 640.0 0.0 0.0
106 box  516.0 -60.0    60.0 0.0 120.0 0.0 0.0 0.0 220.065122 -640.0 0.0 0.0
107 p    16020.908203 0.0 16038.62915 2.5053e+6
108 pz   146.558
109 p   -5443.936157 0.0 -5563.590088 -1.5211e+6
110 px   176
111 px   129.637
112 px   9.65524
c Beam dump
```

```
150 box 236.0 -20.0 -119.0 -60.0 0.0 0.0 0.0 40.0 0.0 0.0 0.0 99.0
151 box 206.0 -20.0 -89.0 0.0 40.0 0.0 -30.0 0.0 0.0 0.0 0.0 50.0
c Iron filler (iron balls and iron sand)
200 box 176.0 60.0 60.0 0.0 0.0 -80.0 0.0 -120.0 0.0 220.0 0.0 0.0
c Rotary shutter - iron
201 rcc 183 0 9.08 100.0 0.0 0.0 21.8
c Rotary shutter - polyethylene
202 rcc 283 0 9.08 50.0 0.0 0.0 21.8
c Trolly
210 box 398.5 -60.0 -60.0 0.0 0.0 -10.0 0.0 120.0 0.0 120.0 0.0 0.0
211 rcc 409.718 -60.0 -70.0 0.0 120.0 0.0 6.35
212 rcc 503.650752 -60.0 -70.0 0.0 120.0 0.0 6.35
c BC 501A Liquid scintilator - on-axis
c Detector support table - aluminium assumed
232 box 531.0 10.0 -6.351 0.0 0.0 -0.999 0.0 -20.0 0.0 40.0 0.0 0.0
233 rcc 532.0  9.0 -7.350 0.0 0.0 -52.65 0.99
234 rcc 532.0 -9.0 -7.350 0.0 0.0 -52.65 0.99
235 rcc 560.0  9.0 -7.350 0.0 0.0 -52.65 0.99
236 rcc 560.0 -9.0 -7.350 0.0 0.0 -52.65 0.99
237 rcc 531.0  0.0  0.0  12.7 0.0   0.0  6.350 $ Liquid Scintilator BC 501A on-
axis
c BC 501A Liquid scintilator - off-axis 20 cm
c Detector support table - aluminium assumed
238 box 531.0 -10.0 -6.351 0.0 0.0 -0.999 0.0 -20.0 0.0 40.0 0.0 0.0
239 rcc 532.0 -11.0 -7.350 0.0 0.0 -52.65 0.99
240 rcc 532.0 -29.0 -7.350 0.0 0.0 -52.65 0.99
241 rcc 560.0 -11.0 -7.350 0.0 0.0 -52.65 0.99
242 rcc 560.0 -29.0 -7.350 0.0 0.0 -52.65 0.99
c Liquid Scintilator BC 501A off-axis 20 cm
243 rcc 531.0 -20.0  0.0  12.7 0.0   0.0  6.350
c BC 501A Liquid scintilator - off-axis 40 cm
c Detector support table - aluminium assumed
244 box 531.0 -30.0 -6.351 0.0 0.0 -0.999 0.0 -20.0 0.0 40.0 0.0 0.0
245 rcc 532.0 -31.0 -7.350 0.0 0.0 -52.65 0.99
246 rcc 532.0 -49.0 -7.350 0.0 0.0 -52.65 0.99
247 rcc 560.0 -31.0 -7.350 0.0 0.0 -52.65 0.99
248 rcc 560.0 -49.0 -7.350 0.0 0.0 -52.65 0.99
c Liquid Scintilator BC 501A off-axis 40 cm
249 rcc 531.0 -40.0  0.0  12.7 0.0   0.0  6.350
c Outside world
600 box -130 -252 -315 850 0.0 0.0 0.0 504.0 0.0 0.0 0.0 600.0
```

```
c Additional iron colimator
800  box 401.0 -60 -60 80.0 0.0 0.0 0.0 120.0 0.0 0.0 0.0 120.0
c Shield
1000 box 481.0 -60 -60 50.0 0.0 0.0 0.0 120.0 0.0 0.0 0.0 120.0

c -------------------------------------------------------------------------
c         MATERIALS
c -------------------------------------------------------------------------
c Iron shield - atom density, Density ( g /cm3 )= 7.87. Naturan iron from benchmark
c documetation - Table 1.2 JAERI-Data/Code 96-029
m1   26054. 4.9605E-03
26056. 7.7869E-02
26057. 1.7983E-03
26058. 2.3933E-04
c Polyethylene - atom density, Density ( g /cm3 )= 0.928,
c Reference: http://physics.nist.gov/PhysRefData/XrayMassCoef/tab2.html
m2    1001. 0.079855
6000. 0.039929
c Aluminum - atom density, Density ( g /cm3 )= 2.6989
m3   13027. 0.060238
c Liquid scintillator - atom density, Density ( g /cm3 )= 0.874
c "https://www.crystals.saint-gobain.com/sites/imdf.crystals.com
c /files/documents/sgc-bc501-501a-519-data-sheet_69711.pdf"
m4    1001. 0.0482
6000. 0.0398
c Dry Air - atom density, Density ( g /cm3 )= 0.001205
m5    6000. 7.4919E-09
7014. 3.8987E-05
7015. 1.4243E-07
8016. 1.0487E-05
8017. 3.9948E-09
18036. 7.8407E-10
18038. 1.4726E-10
18040. 2.3208E-07
c Concrete from benchmark documentation (per nuclide definition) -
c atom desnity, Density ( g /cm3 )= 2.31
m6    1001. 1.49783E-02
1002. 1.72270E-06
8016. 4.18641E-02
8017. 1.59471E-05
11023. 1.23000E-03
```

```
12024. 4.89740E-04
12025. 6.19982E-05
12026. 6.82614E-05
13027. 3.12000E-03
14028. 1.02368E-02
14029. 5.20043E-04
14030. 3.43204E-04
19039. 3.54381E-04
19040. 4.44605E-08
19041. 2.55745E-05
20040. 4.16846E-03
20042. 2.78219E-05
20043. 5.80511E-06
20044. 8.96994E-05
20046. 1.72004E-07
20048. 8.04130E-06
26054. 8.24154E-05
26056. 1.29373E-03
26057. 2.98785E-05
26058. 3.97622E-06
c ---------------------------------------------------------------------------
c         SOURCE
c ---------------------------------------------------------------------------
c --- Point isotropic neutron source collimated into an -x cone.
c Particles are confined to a (+x axis) cone whose half-angle
c is acos(0.99990531) = 0.7788 degrees about the x-axis.
c Angles are with respect to the vector specified by VEC
c
sdef cell=600 pos=0 0 0 erg=d1 par=1 vec=1 0 0 dir=d2
si2 -1  0.99990531  1          $ histogram for cosine bin limits
sp2  0  0.99995265  0.00004735 $ frac. solid angle for each bin
sb2  0. 0.          1.         $ source bias for each bin
si1 H    0.0
5.5  6.5  7.5  8.5  9.5 10.5 11.5 12.5 13.5 14.5
15.5 16.5 17.5 18.5 19.5 20.5 21.5 22.5 23.5 24.5
25.5 26.5 27.5 28.5 29.5 30.5 31.5 32.5 33.5 34.5
35.5 36.5 37.5 38.5 39.5 40.5 41.5 42.5 43.5 44.5
45.5 46.5 47.5 48.5 49.5 50.5 51.5 52.5 53.5 54.5
55.5 56.5 57.5 58.5 59.5 60.5 61.5 62.5 63.5 64.5
65.5 66.5 67.5 68.5 69.5 70.5 71.5 72.5
sp1   0.0      0.
```

```
2.373E-2 2.373E-2 2.395E-2 2.440E-2 2.508E-2
2.569E-2 2.533E-2 2.592E-2 2.678E-2 2.714E-2
2.788E-2 2.795E-2 2.855E-2 2.954E-2 3.100E-2
3.149E-2 3.334E-2 3.383E-2 3.528E-2 3.624E-2
3.669E-2 3.841E-2 3.806E-2 3.927E-2 3.845E-2
3.875E-2 3.857E-2 3.878E-2 3.762E-2 3.702E-2
3.716E-2 3.656E-2 3.615E-2 3.399E-2 3.345E-2
3.324E-2 3.340E-2 3.137E-2 3.211E-2 3.103E-2
3.102E-2 3.160E-2 3.086E-2 3.003E-2 2.856E-2
2.804E-2 2.656E-2 2.505E-2 2.391E-2 2.177E-2
1.959E-2 1.604E-2 1.281E-2 1.088E-2 9.010E-3
7.428E-3 8.095E-3 4.701E-2 2.104E-1 3.614E-1
2.765E-1 8.202E-2 8.896E-3 1.074E-3 4.013E-4
4.973E-4 1.324E-4
c -------------------------------------------------------------------------
c         TALLIES
c -------------------------------------------------------------------------
c Absolute normalization of results 1.56368E+11 (=2.61*4770000000*4*3.14=peak
c to continuum from SINBAD html note, peak flux of neutrons in SINBAD html,
c solid angle (4 pi))
F14:n 111
FC14 BC 501A Liquid scintilator - on-axis
FM14 1.56368E+11
E14    6  7  8  9 10 11 12 13 14 15 16 17 18 19 20 21 22 23 24 25 26 27
28 29 30 31 32 33 34 35 36 37 38 39 40 41 42 43 44 46 48 50 52 54
56 58 60 62 64 66 68 70
F24:n 113
FC24 BC 501A Liquid scintilator - off-axis 20 cm
FM24 1.56368E+11
E24    6  7  8  9 10 11 12 13 14 15 16 17 18 19 20 21 22 23 24 25 26 27
28 29 30 31 32 33 34 35 36 37 38 39 40 41 42 43 44 46 48 50 52 54
56 58 60 62 64 66 68 70
F34:n 115
FC34 BC 501A Liquid scintilator - off-axis 40 cm
FM34 1.56368E+11
E34    6  7  8  9 10 11 12 13 14 15 16 17 18 19 20 21 22 23 24 25 26 27
28 29 30 31 32 33 34 35 36 37 38 39 40 41 42 43 44 46 48 50 52 54
56 58 60 62 64 66 68 70
print
NPS 1e8
cut:n j 5.0
```

C List of all appended MCNP input files and WW files

Format of the MCNP input files names (tiara-fe/cc-xx-xx-BC/FC/BS.i):

- tiara - name of experiment
- fe or cc - name of shielding material; fe = iron, cc = concrete
- first two digit number - shield thickness
- second two digit number - additional collimator thickness
- BC, FC or BS - name of detector tally; BC = BC501A liquid scintillator, FC fission cells, BS = Bonner sphere detectors (optionally thickness of polyethylene around the Bonner spheres in millimetres)

The weight window file names correspond to the MCNP file names, but the suffix (file name extension) is *.wwinp .

```
tiara-cc-43-25-00_FC.i
tiara-cc-43-25-40_BC.i
tiara-cc-43-25-40_BS_all.i
tiara-cc-43-50-00_FC.i
tiara-cc-43-50-40_BC.i
tiara-cc-43-50-40_BS_all.i
tiara-cc-43-100-00_BC.i
tiara-cc-43-100-00_BS_all.i
tiara-cc-43-100-00_FC.i
tiara-cc-43-150-00_BC.i
tiara-cc-43-150-00_BS_all.i
tiara-cc-68-25-00_FC.i
tiara-cc-68-25-80_BC.i
tiara-cc-68-50-00_BS_all.i
tiara-cc-68-50-00_FC.i
tiara-cc-68-50-80_BC.i
tiara-cc-68-100-00_BC.i
tiara-cc-68-100-00_BS_all.i
tiara-cc-68-100-00_FC.i
tiara-cc-68-150-00_BC.i
tiara-cc-68-150-00_BS_30_50_90mm.i
tiara-cc-68-150-00_BS_bare_15mm.i
tiara-cc-68-150-00_FC.i
tiara-cc-68-200-00_BC.i
tiara-fe-43-00-00_FC.i
tiara-fe-43-00-80_BC.i
```

```
tiara-fe-43-10-00_BC.i
tiara-fe-43-10-00_FC.i
tiara-fe-43-10-70_BC.i
tiara-fe-43-20-00_BC.i
tiara-fe-43-20-00_BS_all.i
tiara-fe-43-20-00_FC.i
tiara-fe-43-20-60_BC.i
tiara-fe-43-40-00_BC.i
tiara-fe-43-40-00_BS_all.i
tiara-fe-43-40-00_FC.i
tiara-fe-43-40-40_BC.i
tiara-fe-43-70-00_BC.i
tiara-fe-43-70-00_FC.i
tiara-fe-43-100-00_BC.i
tiara-fe-43-100-00_BS_all.i
tiara-fe-68-00-00_FC.i
tiara-fe-68-00-80_BC.i
tiara-fe-68-20-00_BC.i
tiara-fe-68-20-00_BS_all.i
tiara-fe-68-20-00_FC.i
tiara-fe-68-20-60_BC.i
tiara-fe-68-40-00_BC.i
tiara-fe-68-40-00_BS_all.i
tiara-fe-68-40-00_FC.i
tiara-fe-68-40-40_BC.i
tiara-fe-68-70-00_BC.i
tiara-fe-68-70-00_FC.i
tiara-fe-68-100-00_BC.i
tiara-fe-68-100-00_BS_all.i
tiara-fe-68-100-00_FC.i
tiara-fe-68-130-00_BC.i
tiara-fe-68-130-00_FC.i
tiara-cc-43-100-00_BC.wwinp
tiara-cc-43-100-00_FC.wwinp
tiara-cc-43-150-00_BC.wwinp
tiara-cc-43-150-00_BS_all.wwinp
tiara-cc-68-100-00_BC.wwinp
tiara-cc-68-100-00_FC.wwinp
tiara-cc-68-150-00_BC.wwinp
tiara-cc-68-150-00_BS_bare_15mm.wwinp
tiara-cc-68-150-00_FC.wwinp
```

```
tiara-cc-68-200-00_BC.wwinp
tiara-fe-43-40-00_BC.wwinp
tiara-fe-43-40-40_BC.wwinp
tiara-fe-43-70-00_BC.wwinp
tiara-fe-43-70-00_FC.wwinp
tiara-fe-43-100-00_BC.wwinp
tiara-fe-68-40-00_BC.wwinp
tiara-fe-68-40-40_BC.wwinp
tiara-fe-68-70-00_BC.wwinp
tiara-fe-68-70-00_FC.wwinp
tiara-fe-68-100-00_BC.wwinp
tiara-fe-68-100-00_FC.wwinp
tiara-fe-68-130-00_BC.wwinp
tiara-fe-68-130-00_FC.wwinp
```

Nuclear Data Section
International Atomic Energy Agency
Vienna International Centre, P.O. Box 100
A-1400 Vienna, Austria

E-mail: nds.contact-point@iaea.org
Fax: (43-1) 26007
Telephone: (43-1) 2600 21725
Web: http://www-nds.iaea.org